Nitric Oxide and the Endothelium: Characterisation of *in vitro* Nitric Oxide Detection Techniques and an *ex vivo* Method of Measuring Endothelial Function.

by
Dirk Jacobus Loubser

Thesis presented in fulfilment of the requirements for the degree of Master of Science in Medical Sciences in the Faculty of Medicine and Health Sciences at Stellenbosch University

Supervisor: Prof. Hans Strijdom

April 2014

Declaration

By submitting this thesis electronically, I declare that the entirety of the work contained therein is my own, original work, that I am the sole author thereof (save to the extent explicitly otherwise stated), that reproduction and publication thereof by Stellenbosch University will not infringe any third party rights and that I have not previously in its entirety or in part submitted it for obtaining any qualification.

April 2014

i

Abstract

Introduction: Nitric oxide (NO) is an important chemical messenger in the cardiovascular system. Despite considerable progress in this field, there remains an on-going need for affordable and user-friendly NO measurement techniques. Therefore, in this study we aimed to develop and characterise NO-detection techniques not previously used in our laboratory, and, in addition, characterise an *ex vivo* method to measure the functional effects of the endothelium and NO production in the vasculature.

Methods: Three different NO-detection techniques were compared: (i) **Amperometric NO sensors.** Here, NO-increasing effects of known NO synthase (NOS) activators were investigated (insulin, acetylcholine and biosynthetic human insulin). Three different NO sensors were evaluated on cultured endothelial cells and aortic tissue. Putative NO-increasing effects of shear stress were also investigated; (ii) **Nitrite (NO_2^-) + nitrate (NO_3^-) sensors.** Here, I aimed to measure NO release from cultured endothelial cells; (iii) **Colorimetric NO_2^- measurement assay with the Griess reagent.** Here, NO_2^- production by endothelial cells was measured with a plate reader.

In the second part of the study an organ bath - isometric tension technique was established to measure endothelium-dependent function of aortic rings. Functional differences in aortic rings isolated from diet-induced obese rats compared to lean rats were investigated. Ring contraction was induced with phenylephrine and relaxation with acetylcholine. These investigations were further supported by western blot analyses of selected critical proteins. Lastly, the effects of perivascular adipose tissue (PVAT) on contraction and relaxation were investigated in endothelium-containing or denuded aortic ring segments.

ii

Results: Although some success was achieved with the amperometric sensors regarding calibration, any experimental results obtained were difficult to repeat due to instability of the sensors. With the NO_2^-/NO_3^- sensor we were not able to carry out any planned experiments due to failure to properly calibrate and standardise the sensors. Success was achieved with the Griess method. All the drugs used as positive controls (DEA/NO, fenofibrate, oleanolic acid and IL-1ß) proved to be potent inducers of NO_2^- release from endothelial cells.

Interestingly, the isometric tension studies showed a higher % relaxation in high fat (HF) diet aortic rings compared to those from lean animals. Western blot data showed downregulation of eNOS activation and iNOS expression in obese groups, which was suggestive of endothelial dysfunction. Interestingly, proteins associated with oxidative stress (p22phox and nitrotyrosine) were downregulated in obese groups. The presence of PVAT exerted anti-contractile effects on the rings from HF rats, however in denuded aortic rings, PVAT showed a significant pro-contractile response in both lean and HF groups. PVAT also exerted anti-relaxation effects in aortic rings from both lean and HF rats.

Conclusion: We managed to successfully establish two new techniques for our laboratory (Griess method and the organ bath – isometric tension method) which can complement the more established techniques in our laboratory in order to aid us in future vascular research. Finally, the isometric tension technique used in the obese rat studies generated interesting data, which further assisted in characterising the diet-induced obesity rat model in our laboratory.

Opsomming

Inleiding: Stikstofoksied (NO) is 'n belangrike chemiese boodskapper in die kardiovaskulêre sisteem. Ondanks vordering in die veld, bestaan daar 'n aangaande behoefte aan bekostigbare en gebruikersvriendelike NO-metingstegnieke. Gevolglik het ons in hierdie studie daarna gemik om NO-metingstegnieke wat nie vantevore in ons laboratorium beskikbaar was nie, te ontwikkel en karakteriseer. Verder het ons ten doel gehad om 'n *ex vivo* model te karakteriseer om die funksionele effekte van vaskulêre endoteel en NO produksie te meet.

Metodes: Drie verskillende NO-metingstegnieke was ondersoek: (i) **Amperometriese NO sensors.** Hier het ons die verhogende effekte op NO van bekende aktiveerders van NO sintetase (NOS) ondersoek (Insulien, asetielcholien en biosintetiese menslike insulien). Drie verskillende NO-sensors was ge-evalueer in gekultuurde endoteelselle en aortaweefsel. Die vermeende NO verhogende effekte van die wrywingskragte opgewek deur laminêre vloei ("shear stress") is ook ondersoek. (ii) **Nitriet (NO_2^-) + nitraat (NO_3^-) sensors.** Hier het ons beplan om NO-vrystelling deur gekultuurde endoteelselle te meet. (iii) **Kolorimetriese meting van NO_2^- met die Griess reagens.** Hier het ons m.b.v. 'n mikroplaat leser die NO_2^- - vrystelling deur endoteelselle gemeet.

In die tweede deel van die studie het ons 'n orgaan bad–isometriese spanningstegniek opgestel om endoteelafhanklike funksie van aortaringe te meet. Funksionele verskille in aortaringe van vetsugtige rotte is vergelyk met kontrole rotte. Ringkontraksie is met fenielefrien geïnduseer en verslapping met asetielcholien. Hierdie ondersoeke is verder ondersteun deur Western blot analises van sleutelproteïene in die aortaweefsel.

Laastens het ons die effekte van perivaskulêre vetweefsel (PVAT) op kontraksie en verslapping in aortaringe met of sonder intakte endoteel ondersoek.

Resultate: Alhoewel 'n mate van sukses behaal was met die kalibrasie van die amperometriese sensors, was eksperimentele resultate moeilik om te herhaal a.g.v. sensor-onstabiliteit. Geen eksperimente kon met die NO_2^-/NO_3^- sensors uitgevoer word nie weens 'n onvermoë om ordentlike kalibrasie en standardisering uit te voer. Ons het egter wel sukses behaal met die Griess-metode. Al die middels wat as positiewe kontroles gebruik was (DEA/NO, fenofibraat, oleanoliese suur and IL-1ß) het geblyk kragtige induseerders van NO_2^- produksie vanaf endoteelselle te wees.

Die isometriese spanningsstudies het 'n hoër % verslapping getoon in die hoë vet (HF) dieet aortaringe in vergelyking met die kontroles. Western blot data het 'n afregulering van eNOS en iNOS getoon in die HF diere, wat aanduidend is van endoteel disfunksie, terwyl proteïene geassosieer met oksidatiewe stress (p22phox en nitrotirosien) afgereguleer was in die HF groep. Die aanwesigheid van PVAT het 'n anti-kontraktiele effek gehad op die ringe van die HF groep. Toe die endoteel egter verwyder was, het PVAT in beide kontrole en HF ringe 'n beduidende pro-kontraktiele effek gehad. Verder het PVAT ook anti-verslappingseffekte op aortaringe beide kontrole en HF rotte uitgeoefen.

Gevolgtrekking: Ons het daarin geslaag om twee nuwe tegnieke vir ons laboratorium suksesvol te vestig (Griess metode en die orgaanbad-isometriese spanningstegniek) wat in die toekoms die meer gevestigde tegnieke in ons laboratorium kan komplementeer. Laastens het die isometriese spanningstegniek wat in die dieëtstudies

gebruik is, data opgelewer wat ons verder sal help om die vetsug model in ons laboratorium te karakteriseer.

This dissertation is dedicated to my parents:

Herman and Annemarie Loubser

For their unconditional love and support

Acknowledgements

I would like to express my sincere gratitude and appreciation to the following persons for their assistance to the successful completion of this study:

Table of Contents

List of Figures

List of Tables

Chapter 1

Review of the literature

1.1) Nitric oxide (NO)

One of the big breakthroughs in vascular research was made in 1987 when Ignarro *et al.* showed that endothelium derived relaxation factor (EDRF), the substance released from vascular tissue, was in fact NO. By this time NO was already known as a potent vasodilator, as it was described by Grueter *et al.* in 1976, but after the work of Ignarro *et al.* (1987), it was also widely accepted to be a naturally occurring vasodilator in mammalian cells. They found that both EDRF and NO showed similar increases in cyclic GMP in perfused bovine pulmonary arteries and veins. Furthermore, cyclic GMP release was decreased in both NO and EDRF models after treatment with substances such as oxyhaemoglobin and methylene blue. Finally EDRF was chemically identified as NO firstly by showing that, like NO, EDRF secreted from isolated aortic endothelial cells yielded nitrosylhaemoglobin when reacting with haemoglobin. Secondly, NO and EDRF yielded the same product after reacting with N-(1-naphtyl)-ethylenediamine. The year 1987 proved to be a prosperous year for NO as another researcher and his team showed that when stimulating bovine endothelial cells in culture with either bradykinin or exogenous NO, the adhesion of human platelet cells was greatly reduced (Radomski *et al.,* 1987). This reduction was abolished when inhibiting NO with haemoglobin. These results pointed towards a role for NO in the reduction of platelet aggregation in the vascular system. Other ground-breaking studies, such as the one by Bult *et al.* in 1990, showed that a vasorelaxant factor was released after stimulation of non-cholinergic non-

1

adrenergic nerves. After use of inhibitors such as N-nitro-L-arginine and inactivators like haemoglobin, Bult and his colleagues proved that the vasorelaxant factor was indeed NO, indicating a further role for NO as a neurotransmitter.

To understand the theory behind NO measurement, it might be helpful to first discuss the NO molecule itself as well as the synthesis thereof *in vivo*. NO is a hydrophobic, gaseous molecule synthesized by the guanidino nitrogen from L-Arginine and molecular oxygen (Archer, 1993) that can cross lipid membranes with ease and has a short half-life (5-40 seconds) and high reactivity due to the presence of an unpaired electron in a 2p-π anti-bonding orbital.
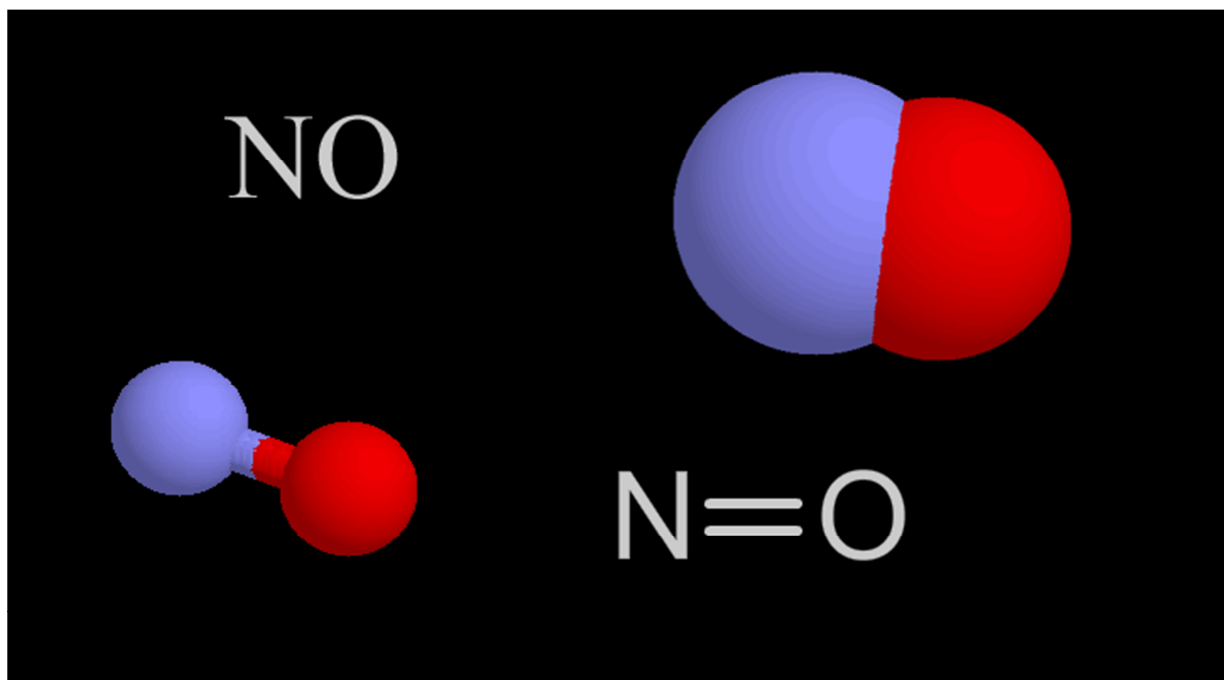
Figure 1: nitric oxide molecule. (Randy Russell, 2006)

NO is produced by one of three isoforms of an enzyme known as nitric oxide synthase (NOS). The three isoforms are endothelial NOS (eNOS), inducible NOS (iNOS) and neuronal NOS (nNOS), with eNOS believed to be the isoform that produces most NO

(Förstermann and Münzel, 2006). The NOS molecule consists of two monomers, both containing a reductase domain on its C-terminus and an oxygenase domain on its N-terminus (Fig. 2). The reductase domain on the C-terminus binds nicotinamide adenine dinucleotide phosphate (NADPH), flavin mononucleotide (FMN) and flavin adenine dinucleotide (FAD) and is linked to the oxygenase domain on the N-terminus of the second NOS monomer. Under normal physiological conditions, eNOS oxidizes its substrate, L-Arginine, to L-Citrulline and NO. For this to happen, the dimerization of eNOS is required, as well as the presence of a naturally occurring co-factor (6R)-5,6,7,8-tetrahydro-L-biopterin (BH_4) that binds to the reductase domain on the C-terminus of eNOS together with molecular oxygen. It is believed that BH_4 is influential in eNOS activity and that eNOS becomes uncoupled in the absence of BH_4 (Crabtree *et al.*, 2008). Dimerization is thus not possible when BH_4 is absent. The actual production of NO is a complex two-step process where, firstly, L-Arginine is hydroxylized by NOS to N-hydroxy-L-arginine. In the second step NOS oxidises N-hydroxy-L-arginine to L-Citrulline and NO (Förstermann and Münzel, 2006).
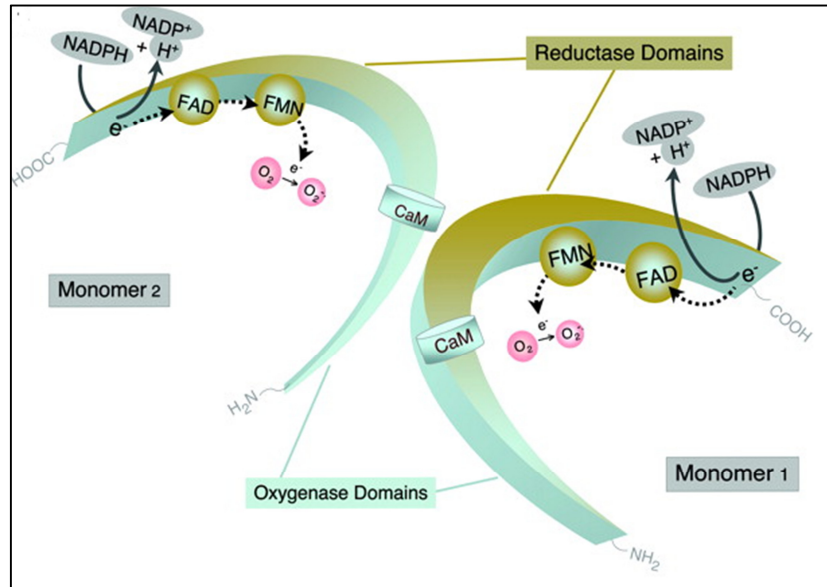
Figure 2: A diagrammatic presentation of the NOS molecule (Förstermann and Münzel, 2006) showing the reductase domain on the C-terminal and the oxygenase domain on the N-terminal.

Figure 3: The protein structure of a NOS molecule

(http://www.rcsb.org/pdb/explore.do?structureId=1m9m)

1.2) NO-measurement techniques

The desire to measure NO in physiological systems increased rapidly after the discovery that NO was in fact an endogenously produced molecule (Ignarro *et al.*, 1987). This, along with other findings mentioned earlier, such as the work by Radomski (1987) and Bult (1990), further supported the growth in interest in studying the effects of, as well as measuring NO within physiological systems.

In addition to its role as an important mediator of vascular homeostasis, a number of other reasons exist why measuring NO in a physiological system is deemed important. One of the reasons stems from the existence of multiple endothelium derived vasodilators (Archer, 1993) such as prostacyclin, which was shown to induce vasodilatation via potassium sensitive ATP channels (Jackson *et al.*, 1993) or endothelium derived hyperpolarizing factor (EDHF) that is released via the muscarinic receptors on the endothelium and induces vasodilatation through an increase in K^+ conductance in smooth muscle cells (Komori and Vanhoutte, 1990). It is thus necessary in experimental models to distinguish between NO and other endothelium-derived vasodilators. Another reason why it is important to measure NO in physiological systems is that inhibitors of NO synthesis, such as L–NG-nitroarginine methyl ester (L-NAME) and L-NG-nonomethylarginine (L-NMMA), were found to have effects on intracellular iron containing systems in addition to their inhibitory effects on NO production (Peterson *et al.*, 1992). Arginine analogues (e.g. L-NAME and L-NMMA) are however widely used to inhibit the function of NOS, as this targets the site of NO production, while inhibition of soluble guanylate cyclase by use of methylene blue is used to inhibit vasodilatation caused by NO (Masaki *et al.*, 1999). Although this might

prove successful, the assumption cannot be made that NO is the only vasodilator present in a given experimental model. Therefore, whether using an arginine analog or inhibiting downstream targets of NO production, the direct measurement of NO is important to either validate the effects of a NOS inhibitor on NO production or, to show that, even in the absence of NO, other factors may also contribute to vasodilatation.

Even though the field of NO research has grown substantially over the past 25 years, the short half-life of NO, together with the small amounts of NO produced, makes it difficult to measure and quantify NO in physiological systems (Xian *et al.*, 2000). Furthermore, NO is easily oxidized to nitrite (NO_2^-) and nitrate (NO_3^-), adding to the challenges of direct NO measurement (Tang *et al.*, 2011). NO_2^- and NO_3^- are stable products of NO metabolism, and techniques do exist to measure NO_2^- and NO_3^-, albeit an indirect assessment of NO levels. This will be discussed in more detail later. Schmidt *et al.* (1996) proposed that the NOS molecule might produce the nitroxyl anion (NO^-) instead of NO, due to the fact that they failed to detect NO production from isolated NOS. The direct measurement of NO in physiological systems has subsequently received little attention until recent years, with most research focusing on the measurement of NO metabolites in studies investigating the enzymatic function of NOS. Zhang *et al.* reported in 2004 that direct measurement of NO made up a mere 10% of NO research at that time. Techniques that are most frequently used to measure NO include chemiluminescence, paramagnetic resonance imaging, spectrophotometry and bioassays. These methods, however, have significant limitations such as poor sensitivity, or as in the case of paramagnetic resonance imaging, high costs.

Furthermore, some of these techniques do not allow for measurement of NO release in real time and quantification of NO is limited.

1.2.1) Amperometric detection of NO
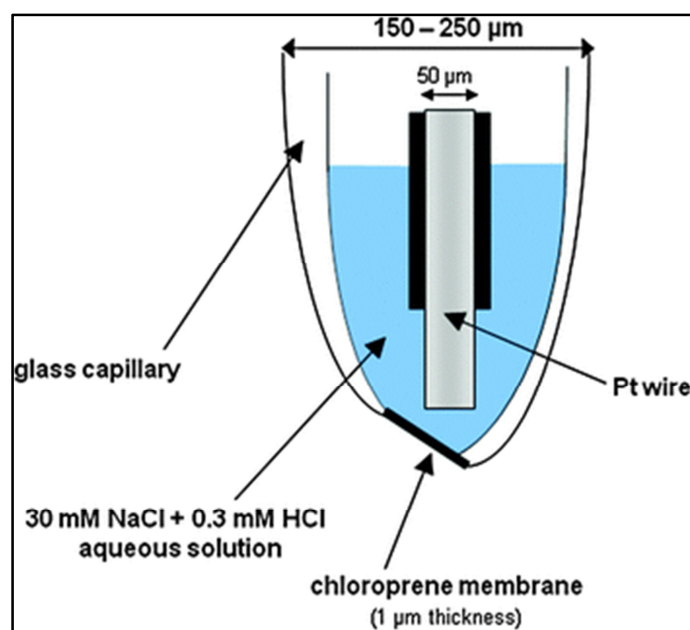
Figure 4: The Clark-type NO sensor developed by Shibuki (Bedioui and Villeneuve, 2002).

Direct amperometric NO sensing is an electrochemical detection technique that first came to the fore in 1992 when World Precision Instruments (WPI) developed a commercially available NO sensor (Zhang, X., 2004). The first types of amperometric NO sensors were designed on the same principles as the Clark-type sensors. The Clark-type sensor was developed in 1954 by Leland Clark after he had built one of the first blood oxygenators to be used in animal cardiac surgery. He could, however, not publish his work as the editor of *Science* demanded that he measured the oxygen levels in the blood. This inspired Clark to develop an oxygen-sensor (Severinghaus, 2002).

The development of the Clark-type NO sensor was based on its oxygen sensor predecessor (Fig. 4). The NO sensor consists of two electrodes, namely the platinum electrode and the silver electrode. The platinum electrode acts as the working electrode and the silver electrode acts as a reference electrode that is set at a fixed or poised voltage potential. The oxidation of NO then proceeds through an electrochemical reaction where one electron from NO is transferred at the working electrode, leading to the formation of a cation:

$$NO\text{-}e \rightarrow NO^+$$
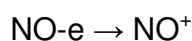
Next a chemical reaction takes place where NO^+ is converted to nitrite (NO_2^-) in the presence of OH^-:

$$NO^+ + OH^- \rightarrow HNO_2 \rightarrow H^+ + NO_2^-$$

Further oxidation of nitrite can take place to form nitrate. The sensor then works on the principle that one can measure very small changes in a redox current that is generated when NO is oxidized on the working electrode (Zhang *et al*., 2004). The electrodes of the Clark-type sensor are usually encased in a glass pipette and sealed with a NO-selective membrane. The pipette is also filled with an electrolyte solution, most commonly consisting of 30mM NaCl and 0.3mM HCl (Zhang *et al*., 2004).

NO-sensors were later modified in order to be more selective when used in experiments. These sensors incorporated the use of a carbon fiber electrode. The biggest modification however was the introduction of metal porphyrins to coat the carbon fiber electrode. These sensors work on the same principle as the Clark-type electrode, meaning that it is dependent on the oxidation of NO on the metal porphyrin

8

surface and subsequent measurement of the change in current generated (Zhang, 2004). The sensor tip is covered with Nafion, which is a synthetic polymer with ionic properties that acts, in the case of the sensor, as a selectively permeable membrane for NO. A shortcoming of these sensors however, is that their sensitivity differs between each individual sensor and selectivity is a problem due to the interference of other biological species (Zhang *et al.*, 2004).

Further developments of NO-sensors made use of a combination of carbon fiber as a working electrode and a separate integrated Ag/AgCl reference electrode, which is then covered with a proprietary gas permeable selective membrane mixture developed by WPI. Furthermore, a Faraday-shielded layer was applied to the outer surface of the sensor in order to minimize environmental noise (Zhang *et al.*, 2004).

As briefly mentioned earlier, NO can be oxidized to form NO_2^- and oxidation of NO_2^- further leads to NO_3^- formation. These inorganic anions have, as of late, received a lot of attention in biomedical research focusing on dietary intake of NO_2^- and NO_3^- and the impact they have on NO levels in the physiological system. These findings seem to suggest that the intake of nitrate-containing food such as green, leafy vegetables can be a significant role player in maintaining nitrite and nitric oxide levels in the physiological system (Tang *et al*, 2011).

With amperometric sensing being a direct and fast (millisecond to second range) method to measure NO concentration, it can potentially be of great use when aiming to solve certain controversies and uncertainties surrounding the signaling functions and regulation of NO (Zhang, X. 2004).

In 2001, Porterfield *et al.* measured the NO fluxes from individual macrophages by making use of an amperometric NO detection technique. After stimulation of the macrophages by interferon γ, they observed high NO produced by iNOS. They also succeeded in measuring the diffusion range of NO by measuring NO levels at distances ranging from 100um to 500um from cells. The presence of L-Arginine was required for NO fluxes and these fluxes were decreased in the presence of hemoglobin, a known NO scavenger, and the NOS inhibitor, L-NAME. Fluxes of NO were also found to be highest when the probe was placed closer to the cells. Porterfield and colleagues thus provided the scientific community with greater insight into not only the amount of NO produced by macrophages after stimulation, but also showed the effective range of the release of NO from macrophages using amperometric NO detection techniques.

A nickel-porphyrin and nafion-based sensor was used in 2001 by Kanai *et al.* to solve the uncertainty with regards to NO production in mitochondria isolated from cardiomyocytes. In previous studies, fluorescent dye techniques, such as diaminofluorescein (DAF) -derived probes, were able to demonstrate the presence of NO in the mitochondria. It could not however, conclusively demonstrate that the NO was produced by the mitochondria or whether it was derived from other biological sources (López-Figueroa *et al.*, 2000). Kanai *et al.* (2001) made use of dystrophin deficient (mdx) mice that have previously been shown, by the same group, to be deficient of caveolar eNOS. This was therefore a good model to use when trying to measure isolated NO production from the mitochondria alone.

It would thus seem that the amperometric NO sensor technique has the potential to be of great value to the cardiovascular research field, as it provides the researcher with

real-time and quantitative results regarding NO production. Most alternative NO detection techniques, as mentioned earlier, use indirect methods to obtain an estimate of NO levels. Many of these techniques rely on measuring secondary species of NO metabolism, such as cGMP or L-citrulline. Amperometric detection of NO does, however, also have a number of shortcomings. For example, Bedioui *et al*. (2003) reported that cellular adhesion and fibrous formations on the sensor along with interferences from enzyme activity could interfere with the reading of NO sensors. Furthermore, mechanical disturbances and temperature changes, both *in vitro* and *in vivo*, can lead to false readings from the sensor. Finally, the quick conversion of NO to nitrate due to it reacting with oxygen further complicates readings and might lead to inconsistent readings between samples.

1.2.2) *Measurement of nitrite (NO_2^-) and nitrate (NO_3^-) levels*

It was not until recently that the NO-NO_2^-/NO_3^- metabolic pathway was better understood and that NO_2^- and NO_3^- were no longer considered as mere inert end-products of NO metabolism. Physiological effects of NO_2^-/NO_3^- have been shown to include an increase in blood flow at low levels and thereby increasing oxygen delivery to hypoxic tissue. This is mainly due to the fact that NO_2^- can be reduced to NO. Therefore, NO_2^-, and not S-nitrosothiols, can be regarded as a major storage pool of NO in the biological system. This statement was made by Cosby *et al*. in 2003 when they observed an increase in the nitrite levels and not the S-nitrothiol levels of human subjects following the inhalation of NO gas.

Measurement of NO_2^- and NO_3^- in a physiology laboratory by making use of a sensor is not widely used. Nitrite and nitrate sensors are mostly used in water research such as in

a study by Larsen *et al.* (1999) where a biosensor was used to measure nitrite and nitrate levels in an activated sludge plant. This particular biosensor was based on diffusion of nitrite and nitrate through a membrane and into a mass of bacteria where the ions get converted into NO and subsequently measured electrochemically.

NO_3^- and NO_2^- however, accumulates in extracellular fluids and cell culture media and can serve as valuable indicators of NO that was produced under a given circumstance (Boo *et al.* 2006). Bovine cell cultures were used by Boo *et al.* (2006) to successfully measure NO levels within the culture medium using the AmiNO700 NO selective sensor from Innovative Instruments Inc. The nitrites and nitrates in the culture medium were reduced to NO in an acidic iodide bath while NO levels were being measured. With this method they succeeded in quantitatively measuring basal and stimulated NO.
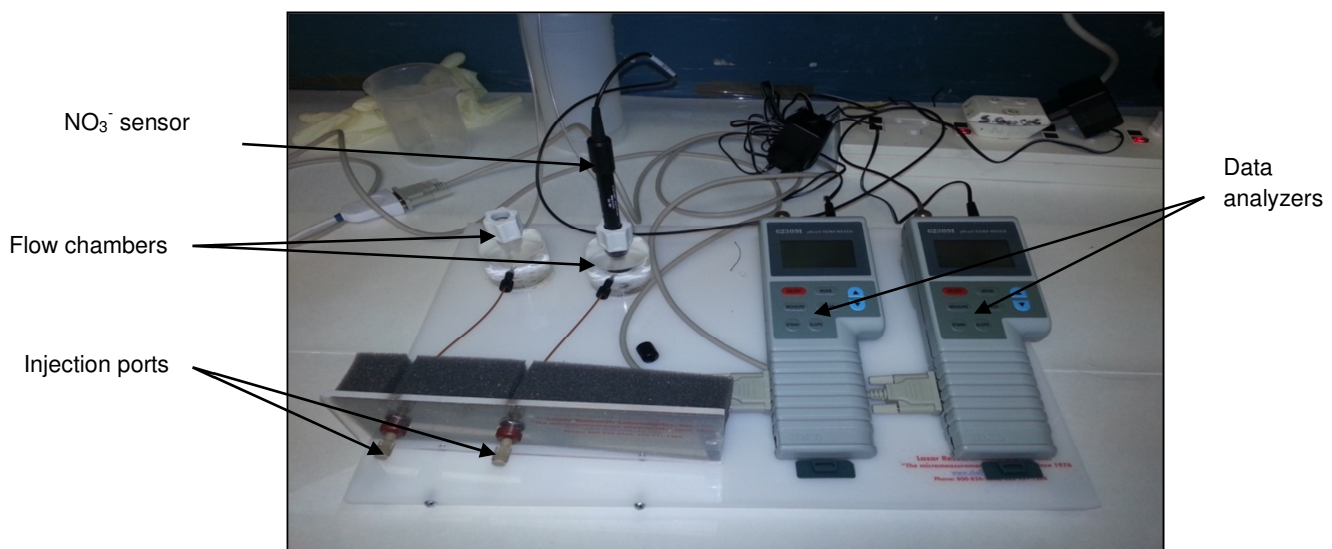
Figure 5: ArrowSTRAIGHT NO_2^-/NO_3^- sensor purchased for the current study.

The fact that NO_2^- and NO_3^- can be used as an indicator of NO production, together with the higher stability of NO_2^- and NO_3^- in a fluid compared to NO, suggest that the

measurement of NO_2^- and NO_3^- levels can possibly be a reliable method in determining the NO levels in an experiment (Boo *et al.*, 2006). Nitric oxide measurement systems that employ the measurement of NO_2^- and NO_3^-, such as the ArrowSTRAIGHT™ used in the present study (Fig. 5), consist of two ion-selective sensors. These sensors are placed inside flow chambers to minimize the sample volume needed (±200 ul) to take an accurate reading. An electrode potential develops when the sensor comes in contact with an analyte containing solution. This potential is measured against a constant reference potential with a digital mV/pH meter. The higher the mV reading, the lower the concentration will be. Lazar Research Laboratories Inc. claims that the sensitivity of these sensors range from 10 uM to about 10 mM when using demineralized water with 10% nitrate buffer solution. The sum of the NO_2^- and NO_3^- concentrations resulting from measurement are then taken as an indication of the NO concentration. Research using the NO_2^-/NO_3^- sensor in physiological studies are however extremely limited, but similar sensors have been used in studies that measured sodium and chlorine in plant material (Ellis *et al.*, 1999) and dissolved inorganic carbon in photochemistry studies involving microbial mats (Cockell *et al.*, 1999) among others.

A 2013 publication by Spark *et al.* mentions the intention to use the ArrowSTRAIGHT™ NO_2^-/ NO_3^- biosensor system to analyze blood serum from human subjects that underwent a 12 week period where fish oil supplementation was given to their diet. This however, is still an ongoing study and no results have been made available as of yet.

1.2.3) The Griess Method

One of the oldest and most widely used methods used to detect NO_2^- is known as the Griess reaction that was first described in 1879 (Griess, 1879). This is a

spectrophometric assay that operates on the basis of NO_2^- reacting with sulfanilamine under acidic conditions and subsequently revealed by producing a colour after diazotization with N-(1-naphtyl)ethylenediamine (NED) (Giustarini *et al.*, 2008) (Fig. 6). NO_3^- can also be measured with this reaction but it must first be converted into NO_2^- via either an enzymatic reductase reaction or by metallic reduction (Giustarini *et al.*, 2008).

This conversion of NO_3^- into NO_2^- not only gives a more accurate indication of NO initially produced, but also increases the amount of product that can be analyzed in the Griess reaction and thereby increasing the ease of use of the method (Miranda *et al.*, 2001). As mentioned above, the conversion step can either be carried out through metallic reduction via use of cadmium or through enzymatic reduction of nitrates. Reduction of nitrate with cadmium is however time consuming due to an extra conversion step and is also dangerous as cadmium is a hazardous metal. Enzymatic conversion of NO_3^- into NO_2^- also has a drawback in the form of NADPH/NADP$^+$ interference with the Griess reaction.

Miranda *et al* (2001) however showed that when reducing nitrate with vanadium(III), the reduction of NO_3^- and subsequent measuring of NO_2^- with the Griess reaction, can be carried out in one step. This is due to the fact that vanadium(III) does not have to be removed before the Griess reaction is carried out, thus greatly reducing the time of the experiment.
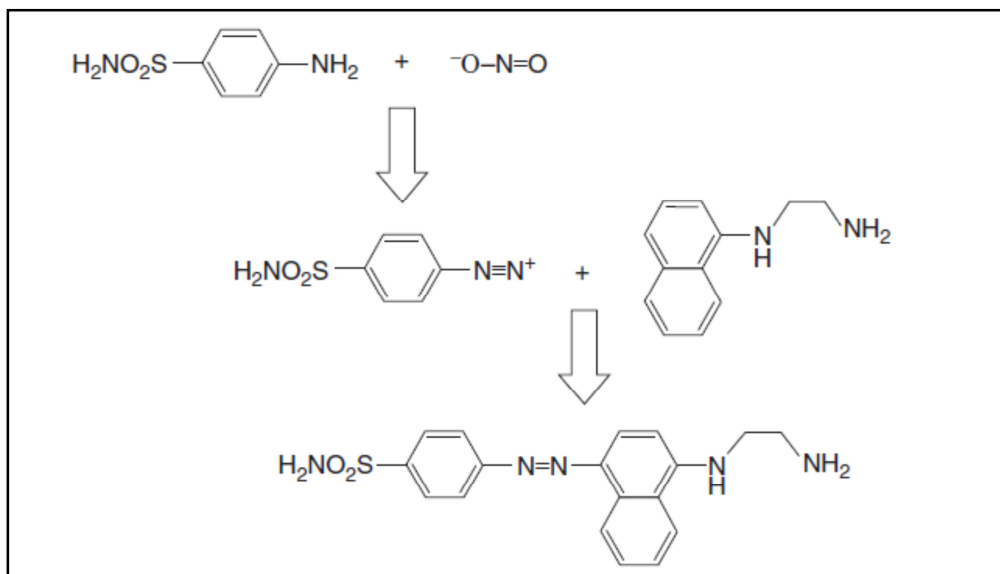
Figure 6: The reaction of NO_2^- with sulfinilamine and subsequent binding to NED to form a chromophoric substance that absorbs strongly at 540nm. (Giustarini *et al.*, 2008)

The fact that NO_3^- can be converted into NO_2^- and then measured using the Griess reaction, means that NO measurements can be carried out in the laboratory using the Griess reagent since both NO_2^- and NO_3^- are oxidized forms of NO and serve as an indication of the amount of NO that was present or produced under a given circumstance. This is of importance since NO_2^- will always be found in aqueous and plasma solution due to oxidation of NO and in blood NO_2^- reacts with oxyhaemoglobin to produce NO_3^- and methaemoglobin (Schultz *et al.*, 1999).

1.2.4.) Fluorescence-based NO detection assays: diaminofluorescein-diacetate (DAF-2/DA)

In order to obtain direct evidence of NO production and function, Kojima *et al* (1998) designed and synthesized diaminofluorescein (DAF) as a novel fluorescent indicator of NO. Prior to the development of DAF, the bioimaging of NO had already been

demonstrated via the use of chemiluminescence by Leone *et al* (1996) when they visualized nitric oxide production from activated macrophages. This model however has disadvantages regarding the analysis of NO such as low special resolution as well as the need to administer cytotoxic H_2O_2 as part of the protocol (Kojima *et al*., 1998). The intracellular detection of NO using 2,7-dichlorofluoroscein was used prior to the development of DAF, but the probe was not able to distinguish between NO and reactive oxygen species and the detection limit was only 16 µM (Kojima *et al*., 1998).

The chemical transformation of DAF in order to fluoresce is based on the reactivity of aromatic vicinal diamines in the structure of DAF with N_2O_3, which is formed in a reaction involving NO and O_2. This reaction is known as the N-nitrosation of DAF and yields a highly green-fluorescent form of DAF called Triazolofluorescein (DAF-2T). In order for DAF to cross membranes however it first needs to be converted to a membrane permeable form known as DAF diacetate (DAF-2/DA) (Fig. 7). The ability of DAF-2/DA to cross membrane means that it can thus be used in conjunction with fluorescent microscopy or a flow cytometer in order to analyze and quantify intracellular NO production (Tarpey *et al*., 2004).

Our own laboratory has previously successfully established a flow cytometry-based method to detect intracellular NO-production in isolated cells, including adult rat cardiomyocytes and cardiac endothelial cells (Strijdom *et al*., 2004; Strijdom *et al*., 2006).
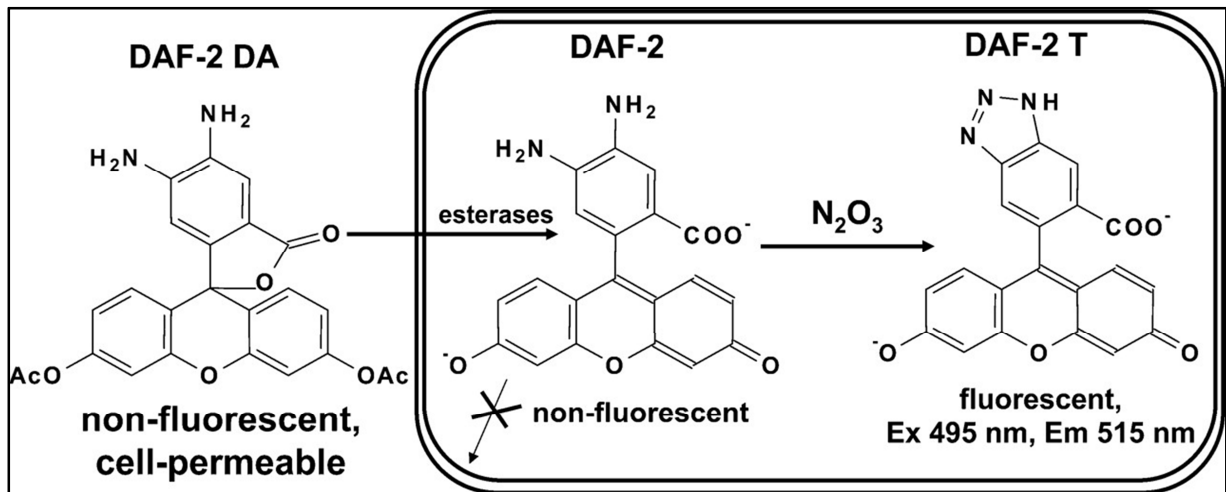
Figure 7: Diagrammatic presentation of DAF-2DA moving across a membrane where it is intracellularly converted to DAF-2 and subsequently reacts with N_2O_3 to yield the fluorescent DAF-2T (Tarpey *et al.*, 2004).

1.3) The vascular endothelium
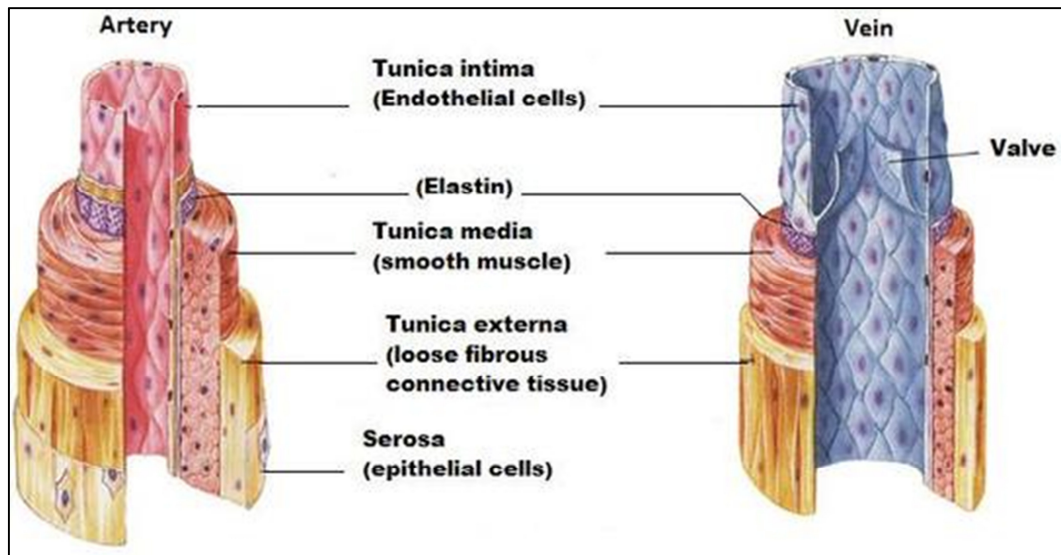
Figure 8: Composition of bloodvessels (Fox; Human Physiology 4th edition; Brown Publishers)

The endothelium is an important role player in maintaining vascular homeostasis and the days of the endothelium being regarded as a mere physical barrier between the vascular wall and the vessel lumen are long gone. The vascular endothelium has a large secretory capacity and endothelium-derived factors are known to regulate a number of processes such as platelet aggregation, coagulation, fibrinolysis, inflammation and vessel diameter (Avogaro and de Kreutzenberg, 2005). The endothelium can regulate vascular tone by either mediating vasoconstriction through secretion of endothelin-1 and thromboxane A2 or it can induce vasodilatation by release of NO, prostacyclin and EDHF (Vallance, 2001). Mediation of vascular tone is thus a balancing act mediated in most part by the vascular endothelium.

Endothelial dysfunction, also referred to as impaired endothelium-dependent vasodilation, has been shown in experimental and human models to be associated with

hypercholesterolemia, chronic heart failure, atherosclerosis and hypertension (Vallance, 2001). Although impaired endothelial function due to a decreased bioavailability of NO is an underlying cause of these disease states, the restoration of endothelial function and vascular homeostasis could potentially reduce cardiovascular risks (Bignornio *et al.*, 2010).

Levels of NO and impaired vascular function can thus serve as warning signals of cardiovascular risks. It is thus important to be able to measure NO in a biological system and also to be able to assess endothelium-dependent vascular function under experimental circumstances in order to gain greater understanding into the link between the relative endothelial health and cardiovascular disease. This can then serve as a basis for the development of therapeutic tools to attempt to restore vascular homeostasis and reduce cardiovascular risks.

1.3.1) Obesity and the vascular endothelium

Obesity is a recognised cardiovascular risk factor and has previously been shown to be associated with the development of endothelial dysfunction. Endothelial dysfunction, defined as the reduced ability of an artery to dilate due to a decreased bioavailbility of NO, is an early precursor of atherosclerosis and coronary artery disease (Deanfield *et al.*, 2007). A number of factors exist in an obese individual that can contribute to endothelial dysfunction. These include hypertension, high cholesterol and triglycerides, insulin resistance and a general proinflammatory state (Falaschetti *et al.*, 2010). Endothelial dysfunction can thus not be explained by only one factor and an understanding of all factors is critical in the understanding of endothelial dysfunction.

Obesity increases blood pressure and this in turns activates the Renin-Angiotensin-Aldosterone System (RAAS). A major role-playing hormone in this system is Angiotensin II which is known to affect eNOS activity and subsequently lower NO production (Bruyndonckx *et al.*, 2013). As mentioned above, lipids also play a role in NO production in obese individuals who typically possess low levels of high density lipoprotein (HDL) cholesterol and high levels of low density lipoprotein (LDL) cholesterol. These respective levels are well documented to be cardiovascular risk factors (Barter *et al.*, 2007; Grundy *et al.*, 2005). LDL can decrease NO availability and decrease eNOS activation and this effect can become more significant when LDL is taken up by macrophages and subsequently oxidized to form oxidized-LDL (Steinberg *et al.*, 2002). HDL on the other hand can decrease hypertension by increasing NO bioavailability (Mineo *et al.*, 2006). Furthermore, obesity is associated with a low grade inflammatory status (Visser *et al.*, 1999). Endothelial cells express adhesion molecules in response to an inflammatory insult that result in the adhesion of leukocytes and subsequently further activation of a cascade of inflammatory reactions. High levels of inflammatory cytokines, such as C-reactive protein (CRP) and tumour necrosis factor – α (TNFα), are associated with cardiovascular risk and endothelial dysfunction (Yudkin *et al.*, 2003). Interleukin-6 (IL-6) has also been shown by Yudkin *et al* (2000) to be a mediator of inflammation in obese individuals. Insulin resistance is a well-known result of obesity and causal factor of endothelial dysfunction (Kim *et al.*, 2006). Under normal physiological conditions, insulin acts as a vasodilator by stimulating NO production via the PI3K/Akt pathway, but under conditions of insulin resistance, this is not the case.

Insulin is still however able to activate the ERK1/2 pathway, leading to production of endothelin 1 and subsequently to vasoconstriction (Kim *et al.*, 2006).

Although obesity is associated with increased risk of cardiovascular dysfunction, studies such as the one by Bigornia *et al.* (2010) have shown a decrease in LDL cholesterol, blood glucose levels as well as CRP. They also showed increased endothelium-dependent brachial artery vasodilatation in subjects who have lost weight. These data suggest that weight loss can lead to a decrease in cardiovascular risk and thus improve vascular function. Obesity is therefore not an irreversible terminal state and studies into the mechanisms of endothelial function and dysfunction are of importance in order to possibly develop therapeutic interventions where exercise or surgical intervention might not be an option for the obese individual.

1.3.2) Perivascular adipose tissue (PVAT) and vascular function

The effect of PVAT on vascular tone has been a topic of interest in recent literature. More specifically, it has been shown that PVAT secretes one or more factors that attenuate the vascular response to a wide range of vasoconstrictors (Brandes, 2007). One such substance is referred to as the adipose derived relaxation factor (ADRF), although its chemical nature has not yet been confirmed. A number of candidate molecules have been proposed to be ADRF, most notably H_2S and H_2O_2. The former is a known endogenous opener of K_{ATP}-channels that can lead to vascular smooth muscle cell hyperpolarization and subsequently result in vascular relaxation (Zhao *et al.*, 2001). H_2O_2 has in turn been proposed by Gao *et al.* (2007) to illicit vascular relaxation via an endothelial-independent activation of soluble guanylate cyclase (sGC).
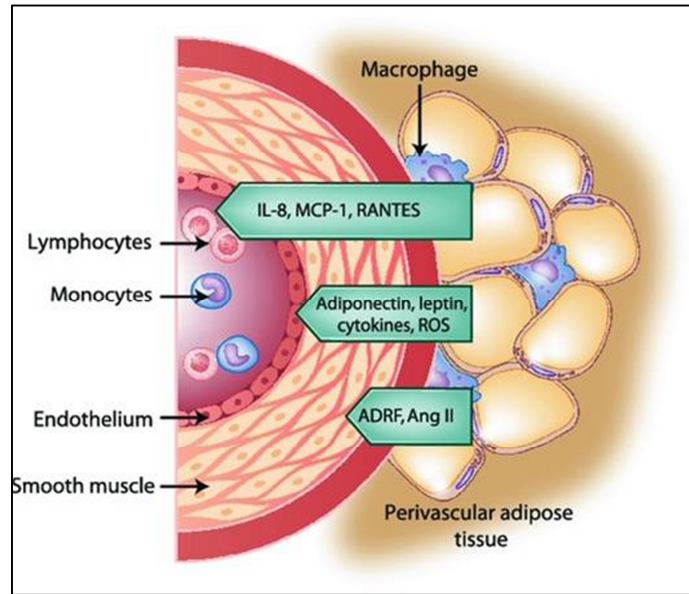
Figure 9: Diagrammatic representation of the position of PVAT and some of its secreted products. (Szasz *et al.*, 2013)

There is still considerable debate surrounding the physiological effects of PVAT. ADRF has yet to be identified, and some authors are questioning whether the factors released by PVAT exert sufficiently large enough effects on vascular function *in vivo,* as autocoids present in the vascularized adipose tissue are rapidly washed away by the bloodstream and so far no study has been able to show conclusive effects of PVAT *in vivo* (Brandes, 2007). It also would seem from the literature that more than one type of potassium channel is involved in the vasodilatory effects of PVAT and that different results are being produced by different vascular beds as well as between different species (Brandes, 2007; Gao *et al.*, 2007).

A number of changes in PVAT are associated with obesity (Szasz and Webb, 2012). These include a change in adipocyte type, cell size, inflammatory cell infiltration, extracellular matrix remodelling and structural changes, all of which is naturally followed

22

by functional changes of PVAT (Szasz and Webb, 2012). In obese humans, an increase in PVAT mass has been observed that correlated negatively with insulin sensitivity and was also associated with an attenuation of the anti-contractile effects of PVAT (Greenstein *et al.*, 2009). Similar observations were also made in obese animal studies using Wistar rats (Szasz and Webb, 2012). In 2010, Ma *et al.* observed an improvement in endothelial dysfunction *ex vivo,* when removing PVAT from aortas of rats fed with a high fat diet. In addition, they observed a decrease in eNOS and AMPK activation and an upregulation of mTOR in vascular tissue from the high fat diet rats. From the literature it seems thus that PVAT is altered, both physically and functionally, by obesity.

Even though many uncertainties regarding the exact vascular effects of PVAT exist, it has to be borne in mind that investigations into PVAT and its secretory profile are only in their beginning stages. The role of PVAT therefore is an important research topic to pursue in order to gain greater clarity on the mechanisms of vascular homeostasis as well as therapeutic interventions into vascular disease, particularly in view of the increasing prevalence of obesity.

1.3.3) Ex vivo measurement of endothelial function in aortic ring segments: Isometric tension studies

Assessment of the functional vascular effects of NO via aortic ring contraction and relaxation measurements is a recognised and established technique (Cordaillat *et al.*, 2006; Dhanakoti *et al.*, 2000; Streefkerk, 2002).

The aorta ring contraction/relaxation model serves as a useful tool when attempting to measure and quantify endothelial function/dysfunction by means of isometric tension

studies. These models usually involve the removal of a section of the aorta from laboratory animals such as rats. Once the aortic ring segment is mounted in an organ bath, contraction is usually by the α_1-agonist, phenylephrine, after which endothelium-dependent relaxation, usually with the administration of acetylcholine, is measured and compared to controls. With this technique, one can assess the impact of acute drug treatment on the ring segment *ex vivo,* or evaluate the effects of *in vivo* interventions on aortic function, such as those performed in the current study.

The isometric tension technique was successfully applied in a study by Cordaillat *et al.* (2006). Fifty male Sprague-Dawley rats were randomly assigned into either a control diet or high sodium (HS) diet group. After removal, aortic rings were pre-treated with phenylephrine, KCl and caffeine, where after contraction and acetyl-induced relaxation was measured. They found a higher contraction in the HS groups compared to controls. Furthermore, they found a higher percentage of acetylcholine induced relaxation in the HS groups, associated with greater activation of the repolarizing BK_{Ca}-channels.

Figure 10: The Isometric tension apparatus. *Left:* Organ bath and force transducer. *Right:* The 4-channel data analyser.

Similarly, Owu *et al.* (2013) compared the contraction and relaxation of aortic rings isolated from rats with streptozotocin-induced type 1 diabetes compared to aortic rings from age matched Wistar controls, citrate buffer controls and Goto Kakizaki (GK) rats, known to develop type 2 diabetes mellitus early in their lives. Streptozotocin groups showed a significant increase in maximum phenylephrine induced contractile force compared to age-matched and GK groups. The GK groups in turn showed a significant decrease in contraction compared to Wistar controls. Potency to acetylcholine induced relaxation was significantly decreased in the streptozotocin group compared to citrate buffer controls. GK rats also showed decreased potency compared to Wistar controls.

In another study, Ma *et al.* (2010) made use of the aortic ring model technique to investigate the effects of perivascular fat on vascular function in a model of high fat diet rats that were compared to age matched controls. Results showed an increase in phenylephrine induced contraction in the high fat diet group, especially in the presence of perivascular fat, compared to controls. The high fat diet group also showed a decreased response to acetylcholine induced relaxation only in the presence of perivascular fat.

In view of the above, the aortic ring model has proven itself as a useful tool to observe real-time physiological effects on the endothelial function of either drug or diet induced changes in animal models.

1.4.) Motivation and rationale of the study

The composition of arteries and veins changes throughout the vascular tree, ranging from the large arteries, consisting of smooth muscle tissue, elastic tissue, connective

tissue and finally an endothelial cell layer that forms the inner most lining, right down to the smaller arterioles, venules and capillaries made up of only an endothelial cell layer. Even though there is substantial variability with regard to the composition of the vessel walls in the vascular system, the endothelium is the one layer that is ubiquitously present in all vessels, suggesting an important role for the endothelium in cardiovascular physiology and pathophysiology.

The vascular endothelium was originally thought to play a primary role as a selectively permeable membrane for molecules between the vascular lumen and the interstitial space (Münzel et al., 2005). Since the discovery by Furchgott and Zawadski (1980) of the role of the endothelium in regulating vascular tone however, many more studies emerged pointing to the importance of the endothelium in the vascular system. Along with the control of permeation of various gasses, metabolites and molecules, the vascular endothelium possess over auto- and paracrine factors that aid in the regulatory role of the vascular endothelium (Münzel et al., 2005; Resnick et al., 2003). Some of these regulatory roles include: (i) The secretion of von Willebrand factor to aid release of platelets and lead to coagulation of blood; (ii) The involvement in adhesion of macrophages during the inflammatory response; (iii) Regulation of angiogenesis and controlling blood pressure by regulating smooth muscle tone in response to hormonal and mechanical demands, such as shear stress, in blood vessels by secreting NO (Pan, 2009). Similar to the role of the endothelium in the vascular system, cardiac endothelial cells have been shown to play an important regulatory role in the function of cardiomyocytes (Brutsaert, 2002). Cardiac endothelial cells, similarly to vascular endothelial cells, secrete a number of factors such as nitric oxide, prostaglandin I_2,

endothelin and angiotensin II, all of which influence cardiac metabolism (Brutsaert, 2002).

The vascular endothelium today is thus seen as a biologically active cell layer that is influenced by different stimuli that determine the physiological, as well as the pathological state, of the cardiovascular system. One of the molecules that has been shown to be intrinsically linked to the function of the endothelium is NO. Numerous studies have shown the involvement of NO as a regulator in a wide range of processes within the physiological system. This makes the study and the measurement of this molecule extremely relevant.

NO is notoriously difficult to measure and quantify in the laboratory setting, mainly due to its reactivity, gaseous nature and relatively short half-life (Xian *et al.*, 2000; Zhang, 2004). The most reliable commercially available techniques are simply too expensive for the average laboratory (e.g. electron spin resonance spectroscopy); therefore many researchers make use of indirect measurement tools, such as the measurement of stable metabolic breakdown products of NO, such as nitrites (NO_2^-) and nitrates (NO_3^-) (Tang *et al.*, 2011). Our own laboratory pioneered the detection of fluorescently labelled intracellular NO in isolated rat cardiomyocytes (Strijdom *et al.,* 2004), and subsequently in cardiac endothelial cells (Strijdom *et al.*, 2006). This technique involves the administration of the NO-specific fluorescent probe, diaminofluorescein diacetate (DAF-2/DA), to the cells, and after reacting with NO, the fluorescence intensity is detected and quantified by a flow cytometer.

27

Although this method is useful when comparing NO release under different circumstances, actual quantification of NO generation is not possible, and the investigator is restricted to expressing the data as relative changes in fluorescence intensity between experimental groups. Furthermore, from our research group's unique perspective, the flow cytometry unit is located a fair distance from our laboratory, with the result that the samples must be transferred to the flow cytometry unit, during which time the cells are possibly and unintentionally exposed to light, air and other environmental factors that could affect the fluorescence reactions. In addition, the very nature of flow cytometry analyses requires that the cells are enzymatically isolated by the process of trypsinization after experimental interventions, followed by a centrifugation-washing process, all of which can be regarded as stressful to the cells. Such robust interventions can affect NO-levels and thus DAF-2/DA fluorescence intensity in the cells.

After years of making use exclusively of the DAF-2/DA-flow cytometry technique to measure NO production in our laboratory, it was decided to explore other measurement techniques, which could be utilised to complement the DAF-flow technique. In order to achieve this we purchased an amperometric NO sensor apparatus and a NO_2^-/NO_3^- measurement system to test on cell cultures. Finally, we incorporated the use of the Griess method, which will be optimised for measurement of the colorimetric reactions by a plate reader. The ease of use, reproducibility of results as well as the finances for operation of these techniques were all factors that had to be taken into consideration.

Due to the fact that the endothelium is exposed to harmful circulating stimuli and other haemodynamic factors such as high blood pressure and elevated lipid levels, the role of

the endothelium in controlling vascular homeostasis can be disturbed (Bruyndonckx *et al*., 2013). This is for example evident in obese individuals. Body mass index (BMI) is often used in studies to determine health risks associated with overweight (25-30 kg/m^2) and obese (<30 kg/m^2) individuals. Although there is mostly an increase in the mortality risk with a higher BMI, the exact BMI value where this occurs differ between studies with some studies finding no risk of mortality in the overweight BMI range (Lewis *et al*., 2009). These conclusions have caused confusion and some studies in the literature have interpreted the data to mean that being overweight is not detrimental to one's health (Campos *et al*., 2006) Obesity is, however, well documented to have adverse effects to an individual's health and according to the World Health Organization (WHO) obesity has nearly doubled worldwide between 1980 (www.who.int/gho/ncd/risk factors/obesity text/en) , with 10% of men and 14% of women being obese in 2008. In South Africa alone 31.3% of the upper middle class population was obese in 2008 (http://www.who.int/nmh/countries/zaf_en.pdf). Research into endothelial dysfunction due to obesity is thus extremely relevant both locally and internationally. Therefore, in the second part of this study, our laboratory acquired a new apparatus, which allows the investigator to measure endothelium-dependent effects on vascular function in an *ex vivo* model of rat aortic ring segments. The isometric tension apparatus provides an opportunity to evaluate whether endothelial dysfunction is present, and to this end we evaluated whether endothelial function was compromised in obese animals.

1.5.) Aims of the study:

In view of the above, the aims of the study were as follows:

- To set up and standardize techniques that allow for direct, quantifiable measurements of NO, namely: (i) amperometric NO detection; (ii) electrochemical determination of NO_2^- and NO_3^- levels with biosensors; and (iii) colorimetric NO detection assay (Griess reagent).

- To set up and standardize an organ bath based vascular contraction/relaxation technique that enables the user to perform isometric tension studies on adult rat aortic ring segments.

- After establishing the organ bath technique, we aim to compare the endothelial function of aortic rings isolated from diet-induced obese and age-matched control rats. Underlying mechanisms will be evaluated by Western blotting analyses of aortic tissue harvested from the rats.

Chapter 2:

Methods

2.1) Evaluation of different NO-measurement techniques

2.1.1) Amperometric measurement of NO

2.1.1.1) ISO-NOP Stainless steel sleeve sensor: CMECs

Initially, the ISO-NOP stainless steel NO sensor from World Precision Instruments (WPI) was used together with an Apollo 1000 data analyzer and DataTrax™ data capturing software (Fig. 11 and 12). Before calibration procedures could be carried out, the sensor had to be polarized by placing the sensor tip in a 0.1 M KI/H_2SO_4 solution (solution#1) prepared by pouring 20 ml of 0.1 M H_2SO_4 (Merck; Darmstadt, Germany) into a glass vial, and adding 0.33 g of KI (Sigma Aldrich; St. Louis, Missouri, USA). Once the sensor was placed in the solution, the poise voltage was set to 865 mV and the sensor was allowed to polarize for at least 12 hours in order for the baseline reading to stabilize in the 1000-8000 pico-ampere (pA) range. The pA measurements constitute the raw sensor recordings, which are eventually converted to nanoMolar values through the calibration process. According to the instructions from the suppliers, the 1000–8000 pA range is the optimal working current of the sensor. Any baseline reading below or above this range could indicate malfunction of the sensor.
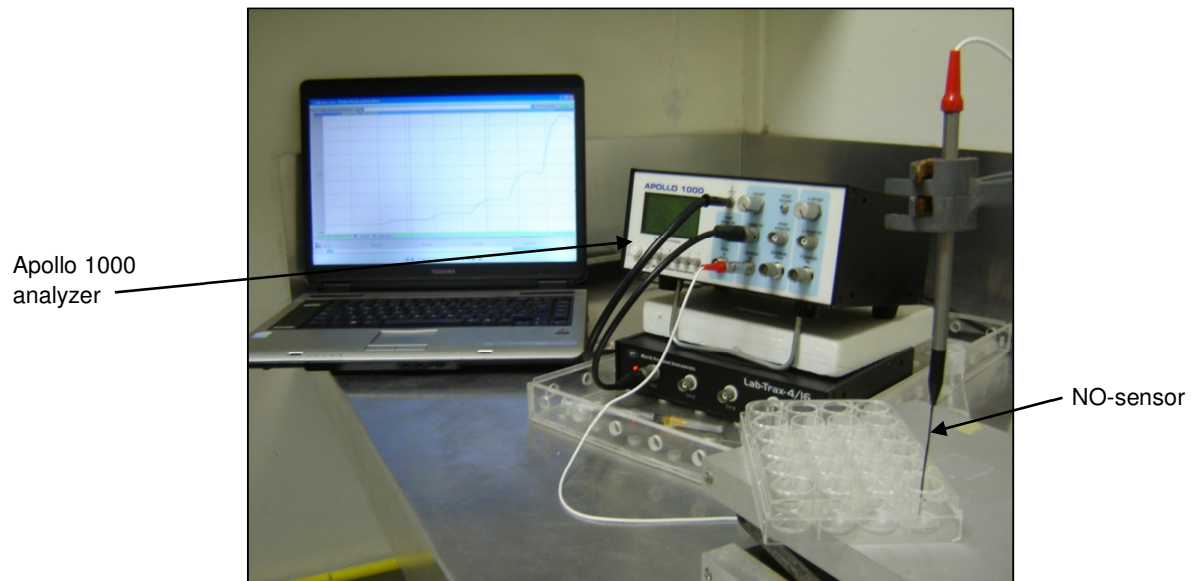
Figure 11: The Apollo 1000 analyzer and NO-sensor.
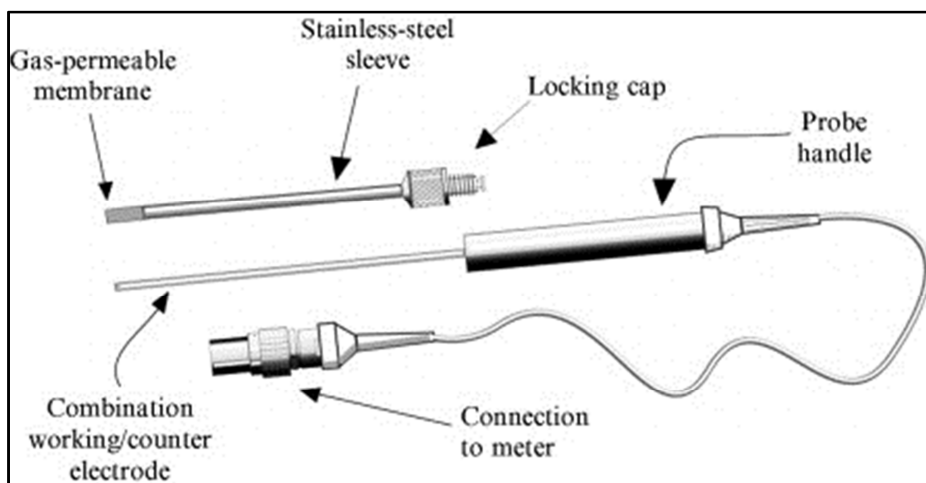
Figure 12: The stainless steel sleeve sensor from WPI (Zhang, 2004)

Calibration of the ISO-NOP sensor was carried out in solution#1 with cumulative additions of 3 aliquots of a 50 uM $NaNO_2$ (Sigma Aldrich, St. Louis, Missouri, USA) solution (solution#2). $NaNO_2$ serves as a NO - donor due to the reaction with solution #1 which generates NO on a mole-to-mole basis as per the following equation:

$$2 \, KI + \mathbf{2 \, NaNO_2} + 2 \, H_2SO_4 = I_2 + \mathbf{2 \, NO} + K_2SO_4 + Na_2SO_4 + 2 \, H_2O$$
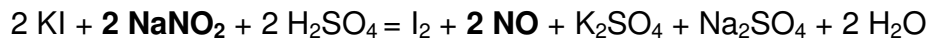
Three aliquots of increasing volumes of solution #2 were added, namely 50 ul, 100 ul and 200 ul. These volumes translated into 125 nM, 248 nM and 491 nM of NO respectively. The resulting pA response reading was then plotted on a standard curve against the [NO] in nM. We used commercially purchased adult rat cardiac microvascular endothelial cells of the 3rd or 4th generation (Rensselaer, NY, USA) in these experiments.
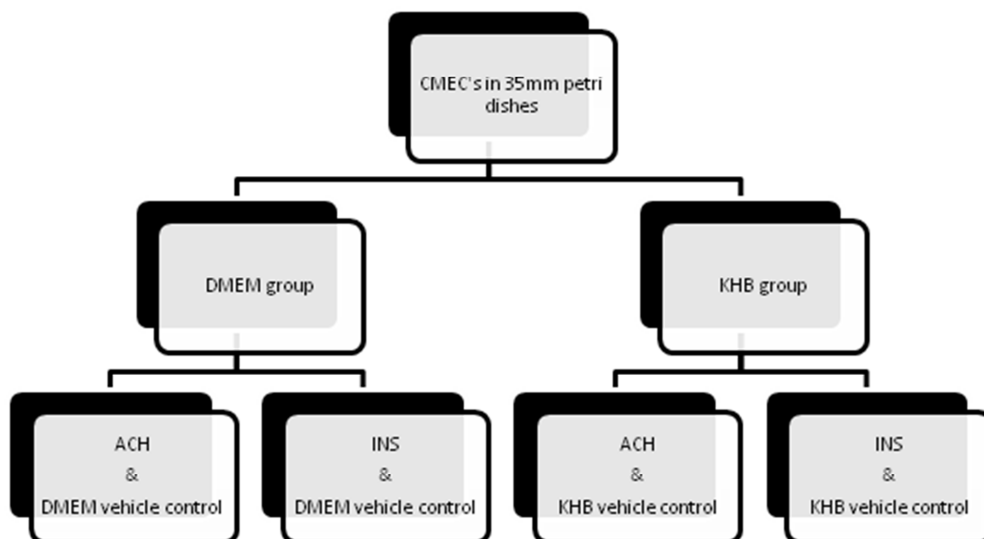
Figure 13: Diagram of the experimental groups for the ISO-NOP stainless steel sleeve sensor studies (DMEM = Dulbecco's Modified Eagle Medium; ACH = Acetylcholine; INS = Insulin; KHB = Krebs-Henseleit Buffer).

Initial experiments were carried out on CMECs cultured in 35 mm petri dishes. CMECs were incubated in either standard growth medium (Dulbecco's modified eagle medium (DMEM); Sigma-Aldrich, St Louis, MA, USA) or Krebs-Henselheit buffer (KHB) containing in mM: 119.0 NaCl; 25.0 $NaHCO_3$; 4.75 KCl; 1.2 KH_2PO_4; 0.6 $MgSO_4.7H2O$; 0.6 Na_2SO_4; 1.25 $CaCl_2.H_2O$; 10.0 Glucose. Different incubation media were used in order to test whether the chemical compositions of these media might affect the sensor readings. These groups were further subdivided into an acetylcholine (ACH; Sigma Aldrich; St. Louis, MA, USA) and an insulin (INS; Sigma Aldrich; St. Louis, MA, USA) group. Acetylcholine was administered with a micropipette in close proximity to the cells and the sensor tip in order to stimulate NO release from the cells at concentrations of 100 µM and 300 µM. Acetylcholine increases intracellular inositol triphosphate (IP_3) which leads to an increase in intracellular Ca^{2+}, with subsequent activation of calmodulin and eNOS respectively, ultimately resulting in increased NO production. A vehicle control (either DMEM or KHB) of the same volume as the acetylcholine aliquots (60 ul) was included to exclude vehicle effects on the readings. Similarly, for the insulin subgroup, insulin was administered using a micropipette in three aliquots to reach final concentrations of 10 nM, 30 nM and 70 nM respectively. Insulin induces NO release via activation of phosphoinositol 3-kinase (PI3-K) which in turn activates protein kinase B (PKB/Akt). PKB/Akt is an upstream activator of eNOS which results in increased NO-production. Again a vehicle control (24 ul) of either DMEM or KHB was used depending on the group.

The instability of the ISO-NOP stainless steel sleeve sensor during experiments as well as difficulty to repeat successful polarization and calibration hampered further experimentation with the ISO-NOP senor. This will be discussed later.

2.1.1.2) ISO-NOPF carbon fiber tip NO-sensor

The manufacturers claim that the carbon fiber tip sensor (Fig. 14) has many advantages compared to other sensor types. Apart from increased sensitivity, the detection area of the sensor is also increased due to a larger area of the sensor area being exposed to the sample compared to the stainless steel tip sensor. There is also no need to exchange membranes from time to time as in the case of the stainless steel tip sensor. The overall ease of use is also increased with no need for a filling solution that has to be injected into a sensor sleeve, as was the case with the stainless steel sensor.

Figure 14: The ISO-NOPF carbon fiber tip NO-sensor (WPI ISO-NOPF500 Instruction manual).

As was the case with the ISO-NOP sensor, polarization of the carbon fiber tip sensor is a requirement. For these types of sensors a 0.1 M $CuCl_2$ solution (solution#1) was used. To make up this solution, 0.268 g of $CuCl_2$ (Sigma Aldrich; St.Louis, Missouri,

USA) was added to 20 ml of distilled H_2O. The sensor was immersed into solution #1 and left until a stable baseline reading was achieved, ranging between 500-8000 pA.

For calibration of the ISO-NOPF sensor a standard solution containing S-Nitroso-N-acetyl-DL-penicillamine (SNAP) (Sigma Aldrich; St. Louis, Missouri, USA) is used (solution #2). SNAP is a well-known NO donor. For this solution 5.6 mg of SNAP is added to 250 ml of distilled H_2O along with 5.0 mg of EDTA. EDTA acts as a binding agent and binds to unwanted metals in the solution and subsequently greatly diminishes the reactivity of the unwanted metals. While the sensor was immersed in solution#1, and the solution was stirred at a constant rate using a magnetic stirrer, five aliquots of solution#2 were added to solution#1 (2 ul, 4 ul, 8 ul, 16 ul and 32 ul). These volumes equated to 6 nM, 12 nM, 24 nM, 47.97 nM and 95.79 nM of NO. A standard curve was thus generated by plotting the pA readings against the known concentrations.

2.1.1.2.1) ISO-NOPF carbon fiber tip sensor: CMECs in 35mm petri dishes

Investigations were carried out on two groups namely CMEC's incubated in phosphate buffered saline (PBS) or DMEM respectively. We changed from KHB to PBS at this point due to the fact that KHB caused instability in the readings in previous experiments as well as the fact that KHB contains glucose that might affect insulin signalling in the insulin treatment groups. In the current series of experiments, cells were treated with insulin or acetylcholine in order to stimulate NO release. CMECs cultured in 35 mm petri dishes were used in these experiments and insulin treatments were administered with a micropipette at 10 nM (6 ul), 20 nM (12 ul) and 40 nM (24 ul) with either PBS or DMEM used as vehicle controls at the same volumes as the treatments. Acetylcholine was administered using a micropipette at 100 μM (60 ul) and 200 μM (120 ul) and either

PBS or DMEM, depending on the group, was administered as vehicle controls at the same volumes.

Humulin (synthetic human insulin) (Eli Lilly; Indianapolis, IN, USA), was also tested on CMECs and aortic endothelial cells (AECs). Humulin was dissolved in distilled H_2O and administered by use of a micropipette. These experiments were later compared to experimental groups where we dissolved Humulin in endothelial cell basal growth medium-2 (EBM-2; Lonza, Walkersville, Maryland, USA)
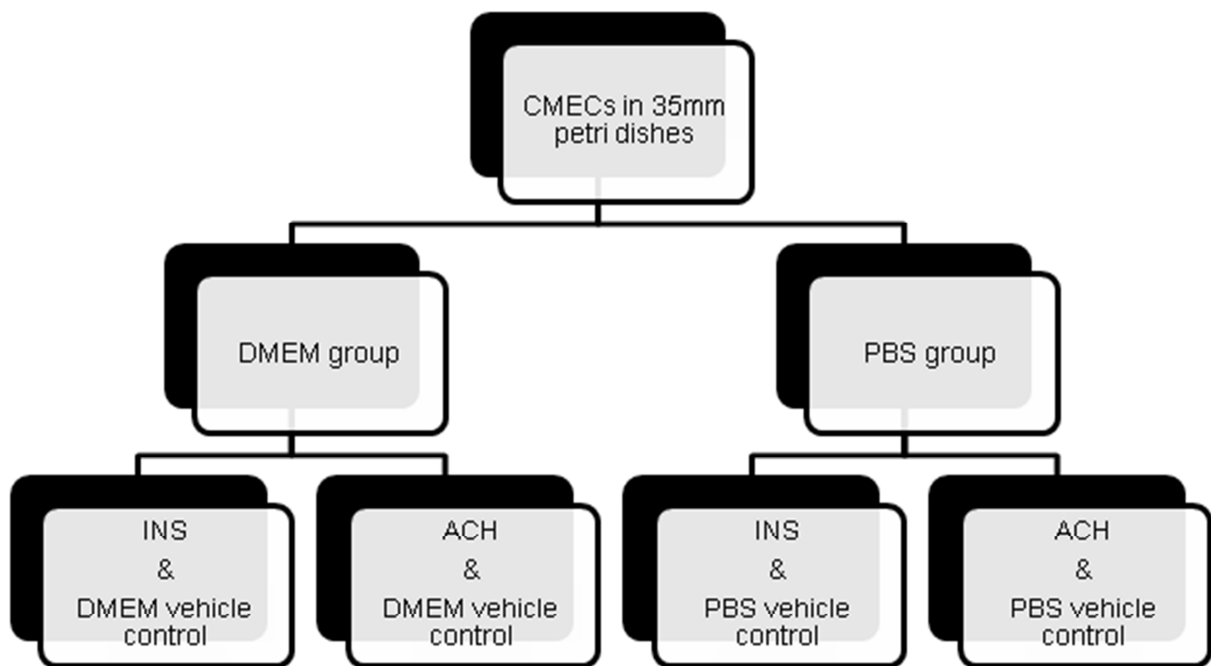
Figure 15: Diagram showing experimental groups for the ISO-NOPF sensor studies (CMECs in 35 mm petri dishes).
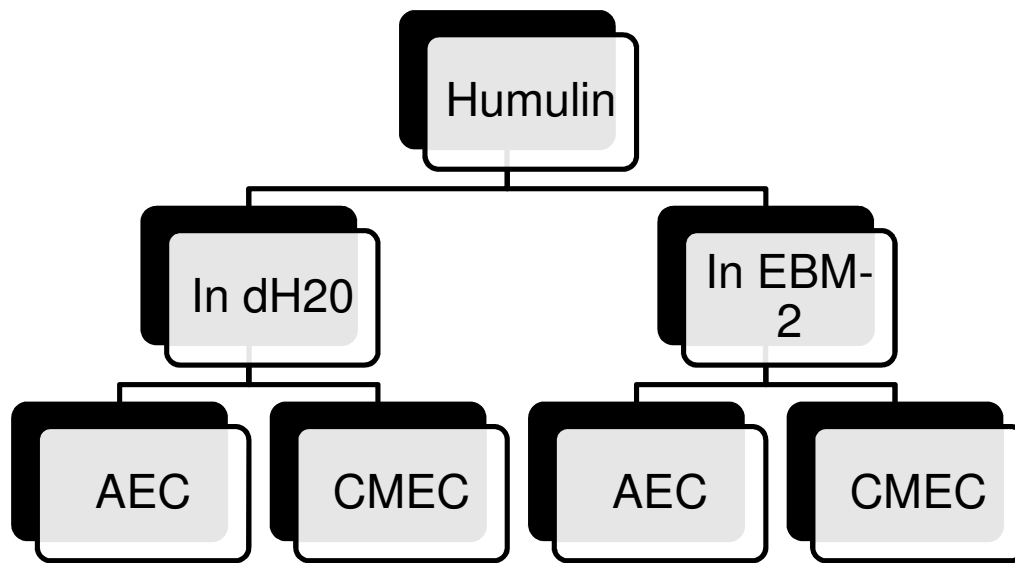
Figure 16: Diagram showing the experimental groups for Humulin studies.

2.1.1.2.2) ISO-NOPF carbon fiber tip sensor: CMECs in 24 multi-well plates

In this series of experiments, we cultured CMECs in smaller 24-well plates. In this way, we attempted to: (i) minimize the diffusion area of the drug added, and (ii) minimize the diffusion area of the NO produced to a closer proximity around the sensor. We only performed experiments on CMECs with insulin and acetylcholine administrations in the multiwell experiments and only used EBM as the vehicle for the drugs. In addition, we compared whether there was a difference in the readings when administering the drugs at the surface of the well vs. the bottom of the well. The rationale was to determine whether a mechanical disturbance, such as administering the drug in close proximity to the sensor might have an effect on the reading. Final concentrations achieved for insulin and acetylcholine were 100 nM and 100 µM respectively. The volumes of the vehicle controls were 30 µl.
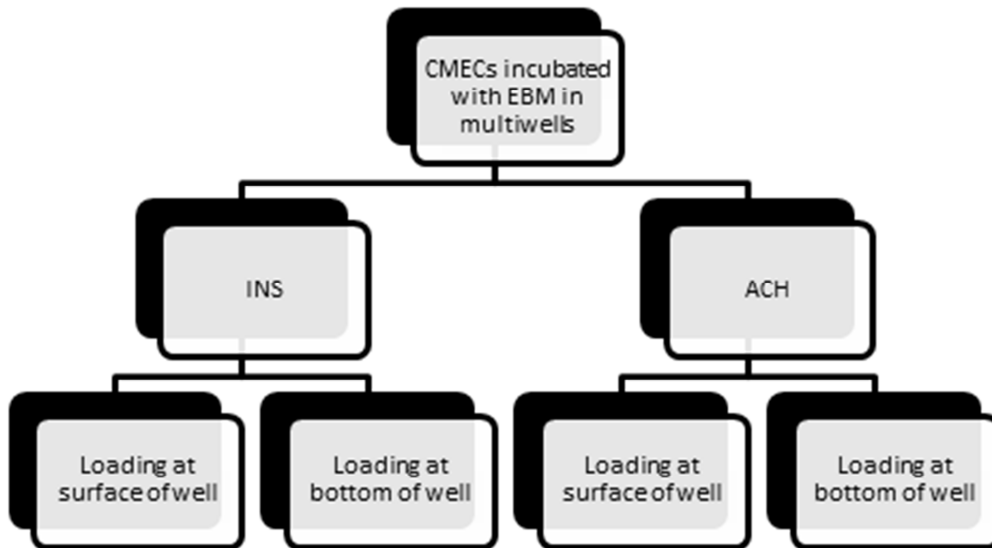
Figure 17: Diagram showing the experimental groups for the ISO-NOPF sensor studies on CMECs in 24 multi-well plates.

2.1.1.2.3) ISO-NOPF carbon fiber tip sensor: Aortic segments

Aortas were harvested from healthy male Wistar rats (as discussed later in 3.4.3) and perivascular fat and connective tissue was removed (adapted from Privett *et al*., 2004). The aortas were cut along the length and opened up to form strips of 15 - 20 mm.

The open aorta was then pinned to the bottom of a 35 mm petridish with a Nipro syringe needle (0.45 mm x 12 mm) and the dish was subsequently filled with EBM growth medium (Fig 18). Aortas were treated with insulin administration using a micropipette (100 nM), and Humulin (0.2 IU). Vehicle controls were administered with KHB for both groups (Fig. 19). Acetylcholine experiments could not be performed due to instability of the sensor.
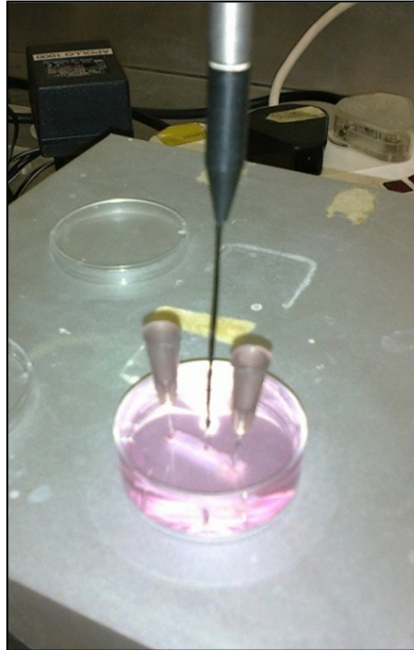
Figure 18: An aortic strip segment pinned down in a 35 mm petri dish.

.
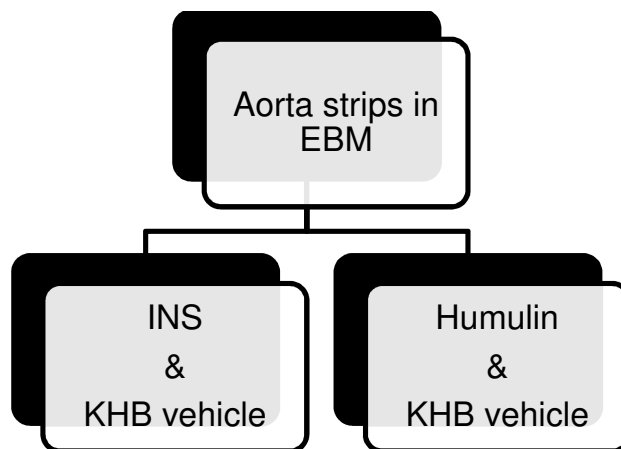
Figure 19: Diagram showing the experimental groups for ISO-NOPF sensor studies on aorta segments.

2.1.1.3) ISO-NOPF L-shaped carbon fiber tip NO sensor studies

An L-shaped carbon fiber tip sensor (Fig. 20) was purchased from WPI for this series of experiments. According to the manufacturers of the sensors, the 90° angle of the tip allowed for a larger area of the sensor tip to be exposed to the cells. Based on this information, the expectation was that more accurate readings could be generated since larger amounts of NO would be detected by the sensor.
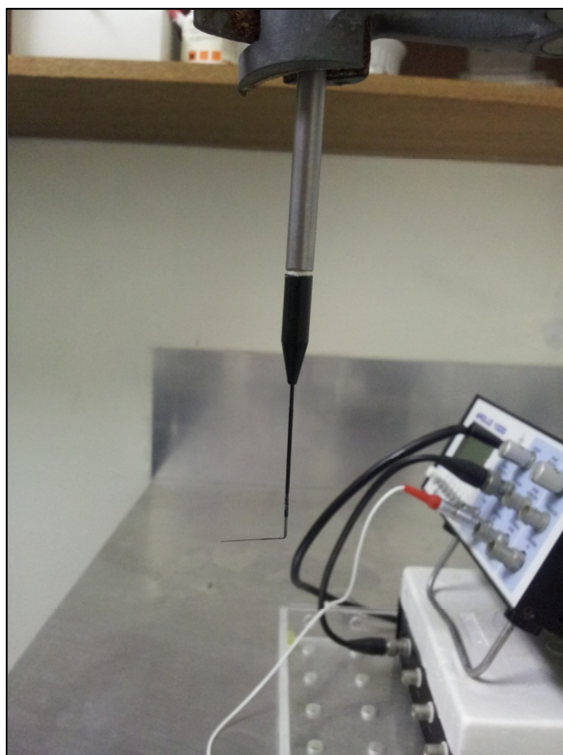
Figure 20: The ISO-NOP L-shaped sensor.

Calibration of the L-shaped sensor was identical to that of the ISO-NOPF carbon fiber tip sensor. The L-shaped sensor was polarized in $CuCl_2$ until a stable baseline reading

41

was reached. Five aliquots of the SNAP/EDTA solution were then added in order to set up a standard curve, as described earlier for the ISO-NOPF carbon fiber tip sensor.

2.1.1.3.1) ISO-NOPF L-shaped carbon fiber tip NO sensor: CMECs in 24 multi-well plates

For initial experiments with the L-shaped sensor we cultured CMEC's in 24-well plates. Culture medium was removed prior to the experiments and wells were filled with 5 ml of fresh EBM growth medium. We then administered insulin (100 nM), acetylcholine (100 µM) and 10 µl EBM with a micropipette both at the surface of the wells as well as at the bottom near the sensor tip. This was done in order to determine whether the sensor readings were influenced by possible mechanical disturbances while administering the drugs close to the sensor, and to determine whether diffusion of the drug from the surface of the wells was sufficient to induce NO release from the cells.
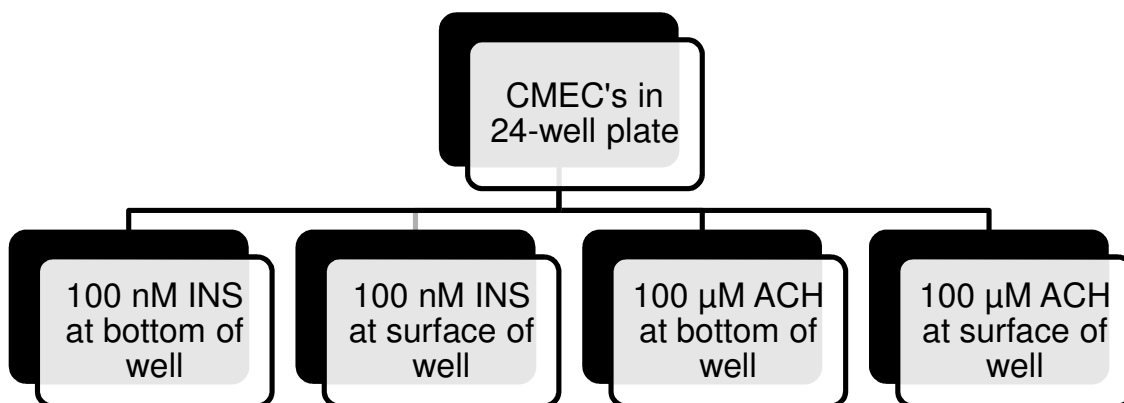
Figure 21: Diagram showing experimental groups for L-shaped ISO-NOPF sensor in multi-well plate.

2.1.1.3.2) ISO-NOPF L-shaped carbon fiber tip NO sensor: Aorta segments

The L-shape sensor was also investigated in segments of aorta. Experiments were carried out by inverting the aortas (i.e. exposing the endothelium to the outside) and placing the sensor next to the aorta. For these experiments acetylcholine concentrations of 10 µM and 100 µM, and insulin concentrations of 100 nM and 1 µM respectively, were administered with micropipettes. Drugs were dissolved in EBM.
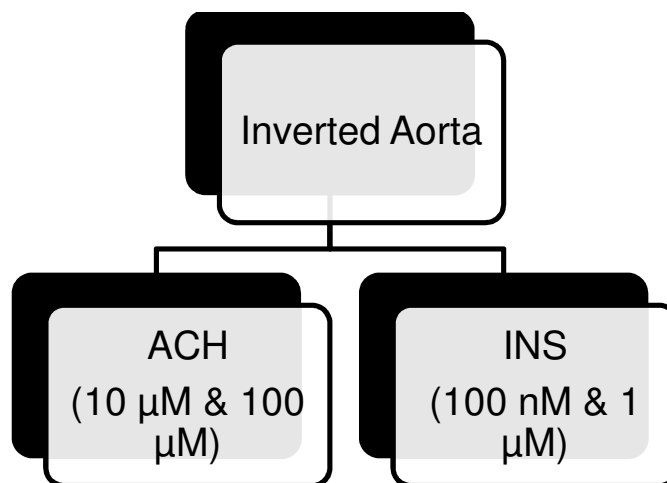
Figure 22: Experimental design for L-shaped sensor on inverted aortic tissue.

Shear stress caused by blood flow against the endothelial layer in vasculature can lead to eNOS-mediated increased NO production. Several candidate shear stress sensors have been proposed for endothelial cells, including adhesion proteins, shear stress responsive K^+ channels and stretch activated channels (Resnick *et al.*, 2003). In the next set of experiments, we wanted to investigate the effect of shear stress on NO release in aortic tissue and AEC's. The purpose of these experiments was two-fold: (i)

To investigate whether increased NO levels could be detected when exposing our cells due to shear stress; and (ii) To assess whether the sensor readings previously obtained with some of the drug administration experiments were in fact the result of the drug effects, and not due to mechanical stimulation brought about by shear stress associated with administering the drugs with a pipette.

Aortas were removed and cleaned of excess fat and connective tissue. This was followed by cutting open the aorta in its length in order to form a strip and thus exposing the endothelial layer. The strip was then pinned down with a Nipro syringe needle (0.45 mm x 12 mm) on the bottom of a 35 mm petri dish. EBM growth medium (100 µl and 200 µl) was injected with a micropipette on the aortic strip in an attempt to simulate shear stress and thereby stimulating NO release. As a control, the endothelial layer of the strips was removed ("denuded") by gently rubbing the aortic strip with a cotton swab. The EBM additions were then repeated on the denuded aortic strips. Furthermore, shear stress experiments were carried out on AEC's in culture. EBM growth medium (100 µl and 200 µl) was injected with a micropipette on the cells. As a control, the experiments were repeated in petri dishes containing only EBM and no cells.
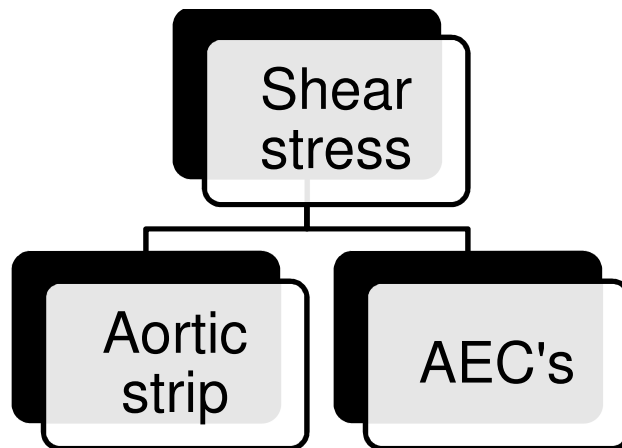
Figure 23: Experimental design for shear stress experiments with the L-shaped sensor.

2.1.2) NO_2^-/NO_3^- measurements

For NO_2^- and NO_3^- measurements the ArrowSTRAIGHT™ NO detection system was purchased from Lazar Research Laboratories, Inc. (Fig. 4) The system consists of separate NO_2^- and NO_3^- injection ports that lead to their respective flow chambers containing the sensors. The sensors function on amperometric principles as discussed earlier. Connected to each of the sensors is a data analyzer. The analyzers are in turn connected to a computer containing LabTrax data capturing software.

2.1.2.1) Calibration and standardization

To calibrate the NO_2^-/NO_3^--measurement system, 0.1 M stock solutions of NO_2^- and NO_3^- respectively were prepared. The NO_2^- stock solution was prepared by dissolving 6.9 g of $NaNO_2$ (Sigma Aldrich; St. Louis, Missouri, USA) and 10 ml of 1 M NaOH in 1 liter of distilled H_2O (d H_2O). The NO_3^- stock solution was prepared by adding 8.5 g of $NaNO_3$ (Sigma Aldrich; St. Louis, Missouri, USA) and 10 ml of 1 M NaOH to 1 L of dH_2O. As part of the calibration procedure, a buffer solution also had to be prepared

consisting of 142 g of Na_2SO_4 (Sigma Aldrich; St. Louis, Missouri, USA) and 10 ml glycerin (Merck; Darmstadt, Germany) dissolved in 1 L of dH_2O. The buffer solution for NO_2^- calibration was adjusted to a pH of 1.5, and that for the NO_3^- calibration adjusted to 2.5. Aliquots of 10 µM and 100 µM were prepared by mixing 180 µl of the NO_2^- and NO_3^- stock solutions with 20 µl of the respective buffer solutions in order to keep the pH of the solution in the working range of the sensor and subsequently injected via the injection ports. After each 200 µl aliquot was injected, the software recorded and stored the millivolt readings acquired for the 10 µM and 100 µM concentrations respectively.

Standardization was carried out after calibration in order to confirm that the sensor was properly calibrated. Standard solutions (10 µM and 100 µM) were prepared as described earlier and injected into the system. The software should then read a concentration value similar or close to the calibration values. If this is carried out successfully, experimental protocols can be carried out.

2.1.3) The Griess method

Both CMEC's and AEC's were used in Griess method experiments (see fig. 24 for the experimental protocol). Cells were cultured in 24-well plates until confluency was reached. Standards were prepared from a stock solution of 200 uM $NaNO_2$ (0.0007 g / 50 ml PBS) as follows: 0 nM, 400 nM, 2 µM, 4 µM, 7 µM and 10 µM (Fig. 25). For positive control purposes, we treated cells with 100 µM diethylamine NONOate diethylammonium salt (DEA/NO; Sigma Aldrich, St Louis, Mo, USA) (Fig. 25). We also investigated the effects of fenofibrate administration (Sigma Aldrich, St. Louis, Missouri, USA) (50 µM; previously shown to increase NO production in our laboratory) for 1 h and 24 h on NO production. Bradykinin (10 µM) and insulin (100 nM), two other known

inducers of NO production, were also investigated. Dimethyl sulfoxide (DMSO) was used as a vehicle control for fenofibrate. In order to determine whether NOS was involved in NO-production, we administered the eNOS inhibitor L-NMMA (Merck; Darmstadt, Germany) (100 µM; 1 hour incubation) and the iNOS inhibitor, 1400W (Sigma Aldrich, St Louis, Mo, USA) (80 µM; 2 hour incubation). The FLUOstar Omega platereader (BMG Labtech; Ortenberg, Germany) was used with Omega software for analysis of samples (Fig. 26). Samples were read at a wavelength of 540 nm.
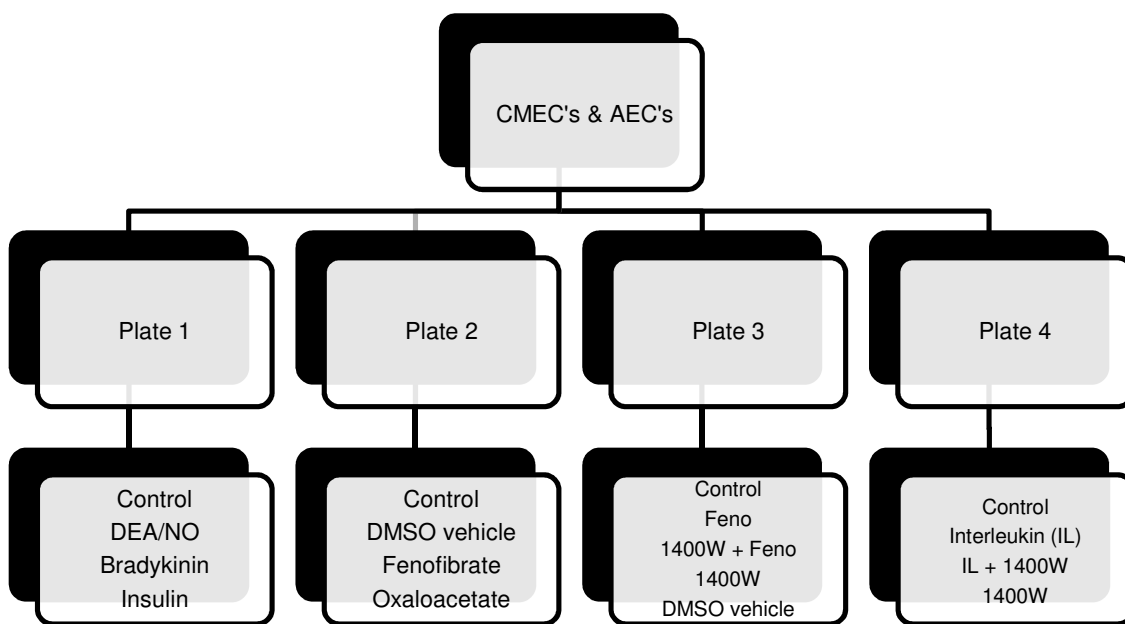
Figure 24: Experimental protocol for the Griess reagent experiments.

Figure 25: A 24-well plate used for the Griess reagent experiments. A gradual increase in colour intensity can be observed in the row containing the standards. DEA/NO positive controls produced an intense colour.

Figure 26: The FLUOstar Omega platereader and computer setup.

2.2.) Measurement of endothelial function in aortic rings

2.2.1) Animals

The use of animals in this study was approved by the Research Ethics Committee for Animal Care and Use, Stellenbosch University (protocol number: SU-ACUM11-00002). Rats were housed in an Association for Assessment and Accreditation of Laboratory Animal Care (AAALAC) facility and had *ad libitum* access to food and water. Pilot investigations were used to set up the apparatus and optimise the various aspects of the protocol. For this purpose, aorta rings obtained from healthy male Wistar rats of 6-8 weeks were used.

2.2.2) Setting up the aorta ring model and pilot investigations

An isolated tissue-organ bath system (AD Instruments, Bella Vista, New South Wales, Australia) was used to measure endothelial function in an *ex vivo* model of aortic ring segments which were harvested from adult rats. This system includes the tissue-organ bath itself, a force transducer (0-25 g) to measure raw contraction and relaxation data, a PowerLab 4/35 data acquisition system, a bridge amp and LabChart Pro 7 data capturing software. A stainless steel stationary hook was fashioned along with a stainless steel hook that was attached to a silk suture and in turn attached to the force transducer (Fig. 27).

Figure 27: The tissue-organ bath with the force transducer above it.
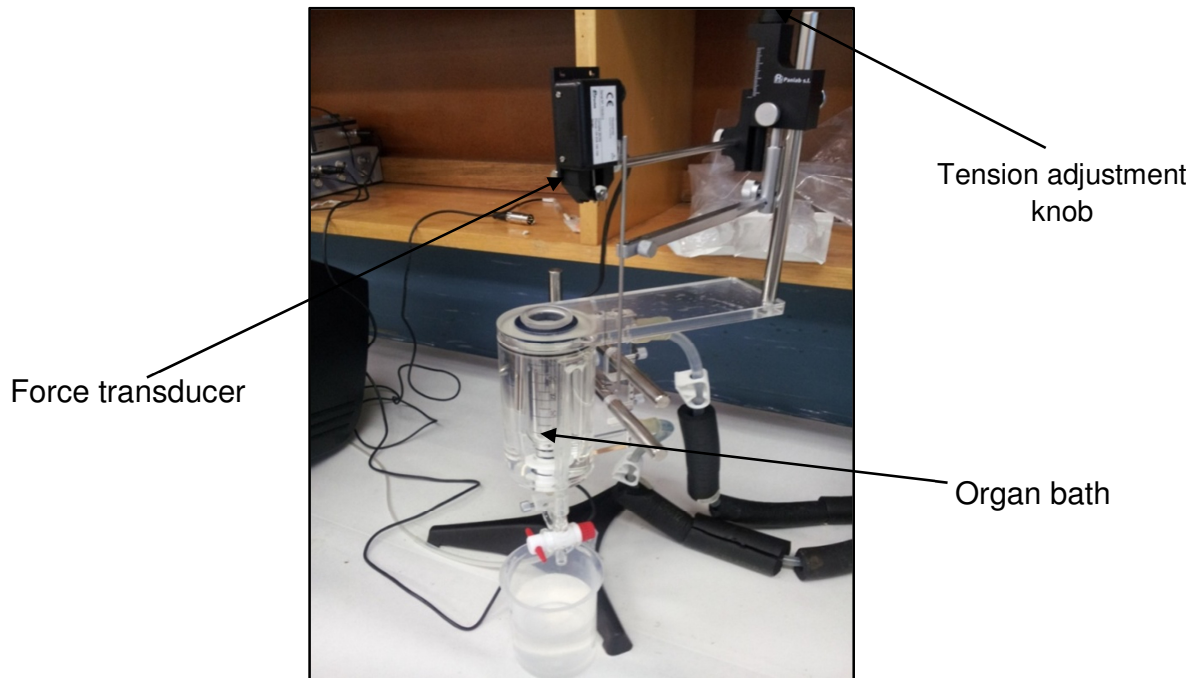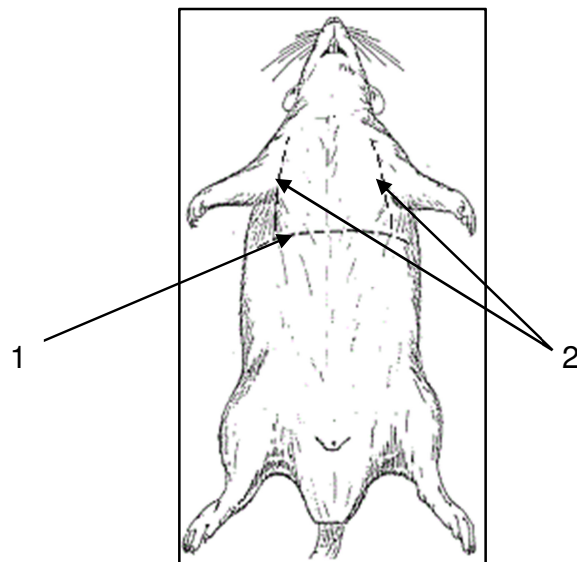

Figure 28: Diagrammatic presentation of incisions made on the rat in order to remove the aorta (Adapted from www.biologycorner.com).
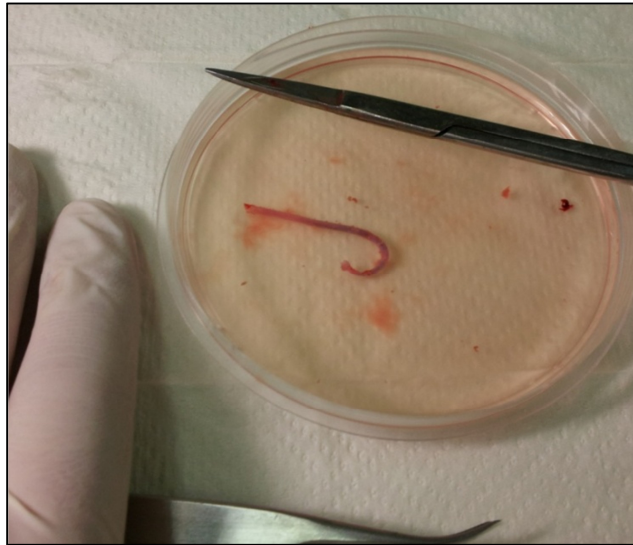
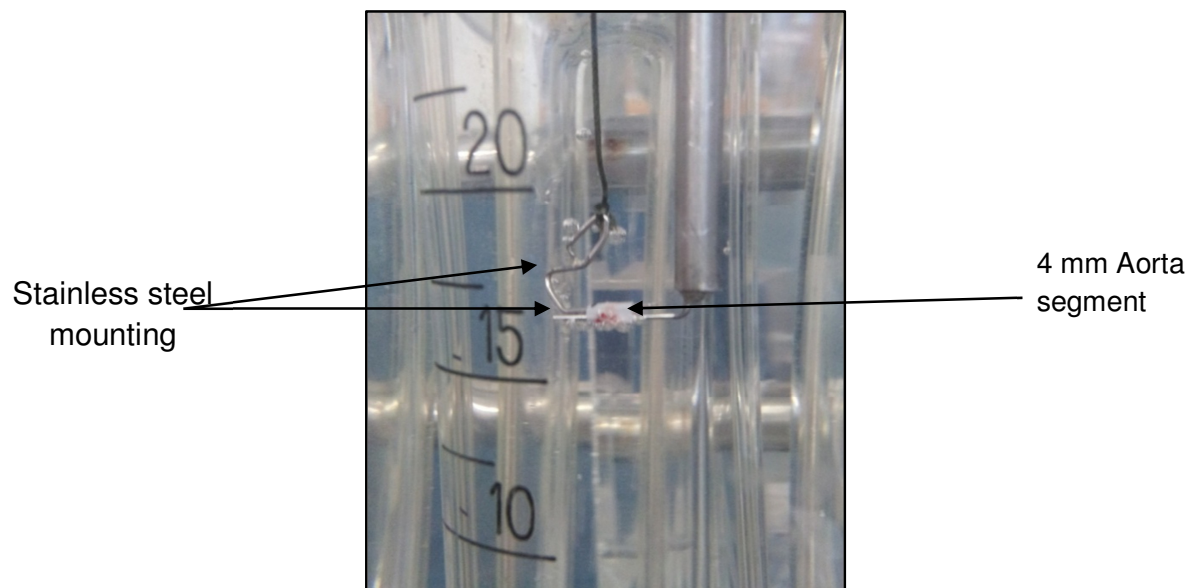**Figure 29: A section of aorta removed from the rat and cleaned.**

Figure 30: An aorta segment that has been positioned onto stainless steel hooks and lowered into the organ bath.

Thoracic aortas were removed from male Wistar rats. Rats were anaesthetized via intra-peritoneal injection of 160 mg/kg pentobarbital. Once the animals ceased responding to foot pinching, an incision was made across the ventral side of the rat just below the thoracic region, starting on the left and ending on the right lateral side (Fig. 28). The diaphragm was then cut open, exposing the thoracic cavity after which the ribcage was cut in a cranial direction on the lateral aspect of the thorax in order to gain better access to the thoracic cavity (Fig. 28). The heart was removed by dissecting the distal end of the aortic arch. The lungs, trachea and oesophagus were also removed, leaving the aorta exposed. Only the thoracic section of the aorta, ranging from above the diaphragm to a point just distal to the aortic arch, was removed and used for the experiments. After removal, the excised aorta was placed in cold Krebs-Henselheit buffer (KHB).

Perivascular fat and connective tissue was quickly removed (Fig. 29) and the aorta was cut into ring segments of 4 mm. One of the aortic rings was then positioned onto the stainless steel hooks and lowered into the organ bath (Fig. 30) containing KHB at 37℃ and gassed with 95% O_2 and 5% CO_2. The resting tension of the aortic ring was then manually set to 1.5 g in order to mimic the resting tension *in vivo* and was kept constant during a 30 min stabilization period. Other pilot investigations that were carried out to help in optimizing the apparatus and protocols included the administration of 12.5 μM SNAP (NO-donor), L-NMMA (100 μM for 10 min) (eNOS inhibitor) and TNFα (10 ng/ml for 30 min; previously shown to reduce NO-production in our cell-based experiments). The purpose of the SNAP administration studies was to achieve endothelium independent relaxation, thereby ensuring intact smooth muscle function. The

administration of L-NMMA served as a negative control as it inhibits eNOS with subsequent reduced NO-release from the endothelium and thus reduced vasodilatation. Similarly, TNFα administration was also applied to simulate endothelial dysfunction by decreasing NO-release from the endothelium. A diagrammatic representation of the experimental design of the pilot studies can be seen in Fig. 31.
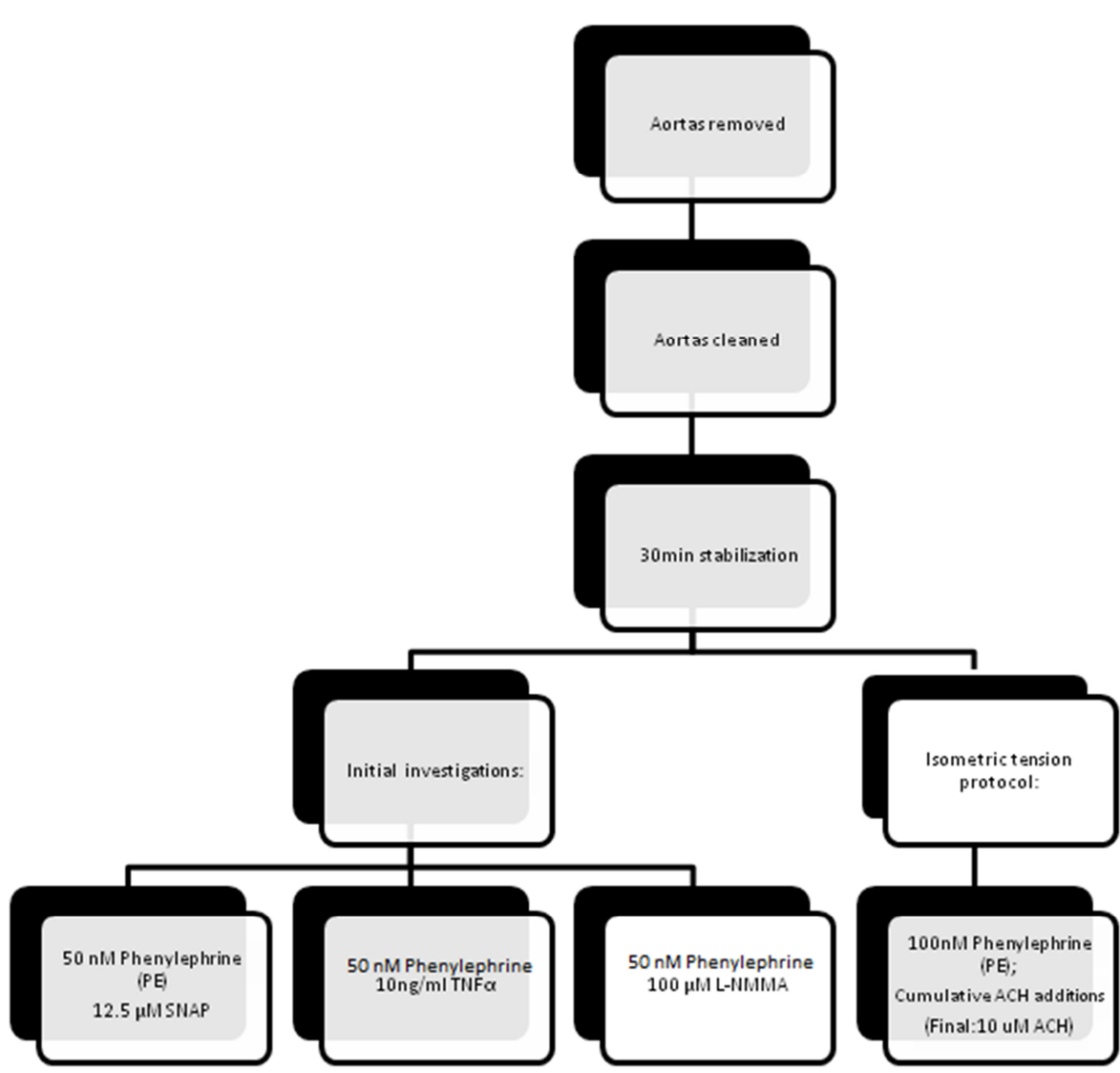

Figure 31: Diagrammatic representation of the experimental design of pilot investigations conducted on aortic ring segments harvested from healthy rats.

2.2.3) The isometric tension measurement protocol (Fig. 32)

The aortic ring contraction-relaxation protocol was adapted from a previously published protocol (Privett, Kunert and Lombard, 2004). After the 30 min stabilization of the aortic ring at a baseline tension of 1.5 g, a first contraction/relaxation protocol was carried out. This entailed contraction of the ring segment by addition of 100 nM phenylephrine (PE), which is a selective α_1-adrenergic receptor agonist. After the aortic ring contraction reached a plateau, a single dose of 10 uM acetylcholine (ACH) was administered to induce endothelial dependent relaxation. If the relaxation of the segment was less than 60% of maximum PE-induced precontraction, the aortic ring was discarded.

After successful relaxation (>60%), the KHB was drained out of the organ bath and another stabilization period followed with buffer changes at 10 and 20 minutes while the resting tension was kept at 1.5 g. Following 30 minutes of stabilization, a second contraction/relaxation protocol was carried out. Contraction was induced by addition of 1uM PE. In later experiments focusing on the role of perivascular adipose tissue (PVAT), PE was administered in a cumulative fashion in order to obtain final concentrations of 100 nM, 300 nM, 500 nM, 800 nM and 1 uM respectively after each addition. When the aortic ring contraction tension reached a plateau, cumulative concentrations of ACH were administered in order to obtain final concentrations of 30 nM, 100 nM, 300 nM, 1 uM and 10 uM respectively after each addition. The additions of ACH were not time-dependent, but performed each time maximum relaxation was reached. Relaxation of the aortic ring was measured as gram tension, or expressed as % relaxation of maximum PE-induced precontraction after each addition of ACH.
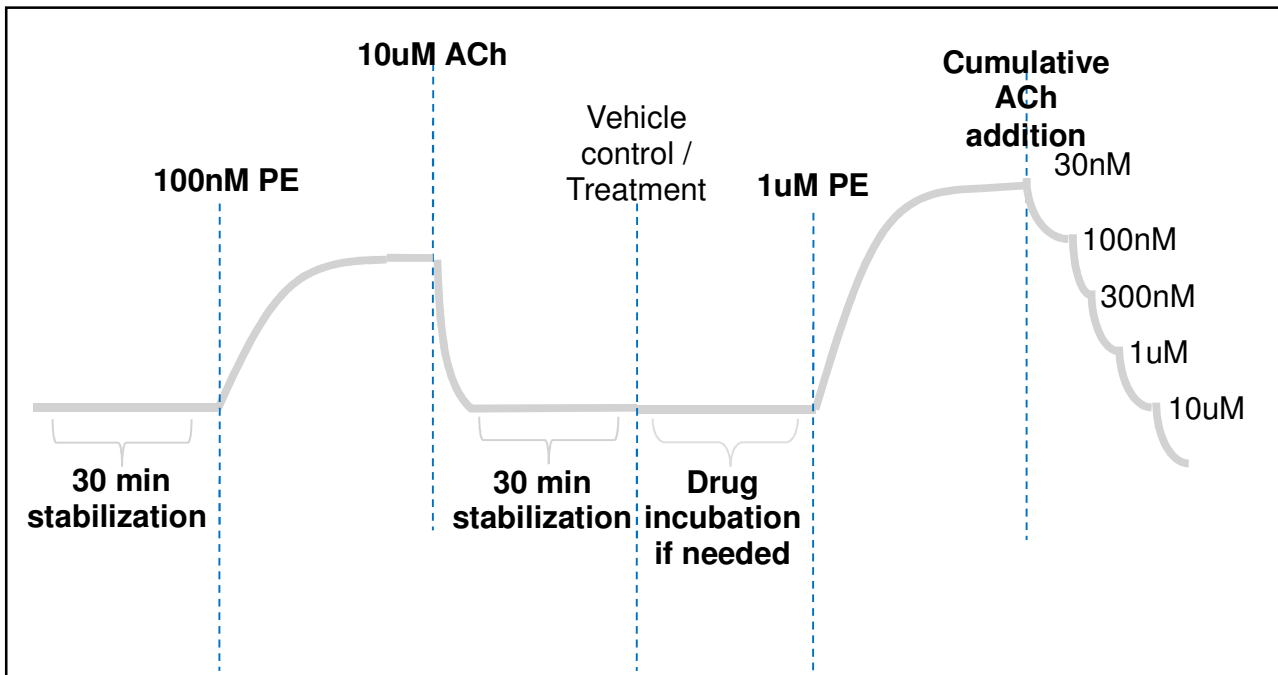
Figure 32: A diagrammatic representation of the isometric tension measurement protocol for the pilot investigations.

2.2.4) Isometric tension studies on aortic ring segments of obese rats

For the diet-induced obese rat studies, animals were divided into 3 groups: a control group of lean animals fed normal rat chow, a high sucrose diet group (HS) and rats fed a high fat diet (HF) containing Holsum cooking fat. The total duration of the feeding programme was 16 weeks, and the rats were 24 weeks old at the time of sacrifice. The compositions of the diets are outlined in Table 1. In order to verify that the HS and HF diets were successful in inducing obesity, biometric measurements of total body mass and intraperitoneal fat mass were recorded for each rat. In the **first part** of the obese rat studies, we followed exactly the same isometric tension measurement protocol as depicted in Fig. 32. In these studies, the perivascular adipose tissue (PVAT) was removed and the endothelium left intact (See Fig. 33 for the experimental design).

	Lean	HS	HF
% Fat	4.8	4.6	11.5
% Protein	17.1	9.4	8.3
% Carbohydrates	34.6	45.8	42
% Sucrose	5.3	23.3	20

Table 1: Composition of the diets

Figure 33: Diagram showing the experimental design of the first part of the obese rat study in which the perivascular adipose tissue (PVAT) was removed and the endothelium was intact.

2.2.5) Western blot analyses of aortic ring segments of obese rats

Thoracic aorta segments harvested from lean, HS and HF rats were frozen in liquid nitrogen and stored at -80˚C. Immunoblotting a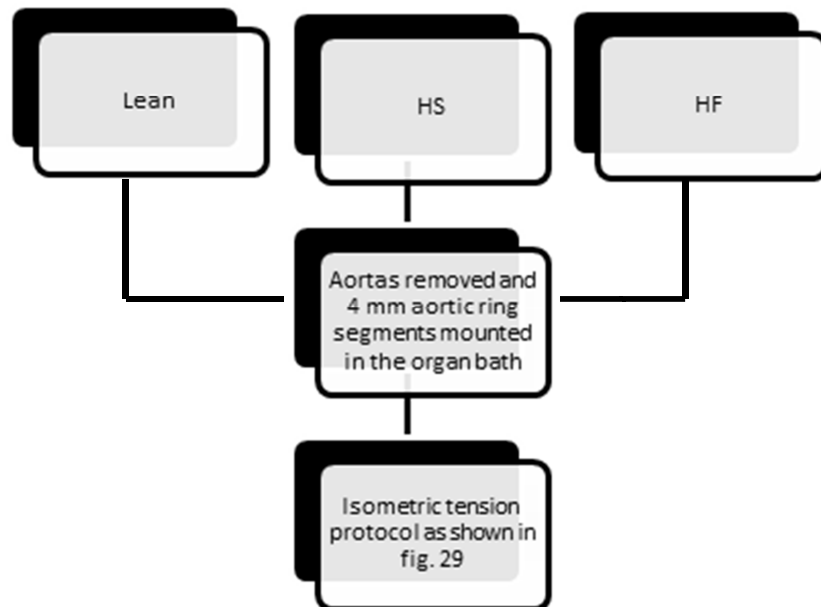nd detection of total- and phospho- PKB and AMPK (Cell Signalling Technology; Boston, MA, USA). Only phospho-p85 (Cell Signalling Technology; Boston, MA, USA) immunoblotting was carried out. Phospho- and total-eNOS and total-iNOS, nitrotyrosine and p22phox were carried out using appropriate antibodies from Santa Cruz Biotechnology Inc. (Dallas, TX, USA). Immunoreactive bands were analyzed using densitometry.

The lysis buffer contained the following: 20 mM Tris-HCl, 1mM EGTA, 1 mM EDTA, 150 mM NaCl, 1 mM β-glycerolphosphate, 1 mM $NaVO_3$ (prepared weekly.), 50 µg/ml PMSF, 10 µg/ml Leupeptin, 10 µg/ml Aprotonin and 1% Triton. PMSF was added last to the buffer. Aortas were pulverised and placed in 250 µl lysis buffer and homogenized using 0.5 mm stainless microbeads and a Bullet Blender (Next Advance, New York, USA). Samples were then centrifuged at 15000 rpm for 10 minutes in order to obtain the cytosolic fraction. Protein determination of each sample was performed according to the Bradford method (Bradford, 1979). The protein concentration of each sample was adjusted to 40 ug / 9 µl with additions of sample and lysis buffer. Samples were then boiled for 5 minutes and stored at – 80˚C.

For Western blot analysis, all samples were subjected to electrophoresis in a 10% polyacrylamide gel (SDS-PAGE) in a BIO-RAD (Hercules, CA, USA) Mini Protean III system, exept when blotting for eNOS and iNOS when a 7.5 % polyacrylamide gel was used. After separation, proteins were transferred to a Immobillon membrane (Millipore; Billerica, MA, USA). Protein loading and proper transfer were routinely assessed by use

of Ponceau staining. Non-specific binding sites on the membranes were blocked by incubating in 5% fat free milk in Tris-buffered saline + 0.1% Tween 20 (TBST) for 1 hour. Membranes were then incubated overnight in the appropriate primary antibody. Membranes were washed (3 x 7 minutes) in TBST and incubated for one hour in a diluted horseradish peroxidase-labelled secondary antibody (Amersham Life Science, Buckinghamshire, UK). Membranes were washed again with TBST (3 x 7 minutes) and covered in ECL detective agents before briefly being exposed to autoradiography film (Amersham Hyperfilm ECL) in order to detect light emission. Films were then analyzed using densitometry software (UN-SCAN-IT, Silk Scientific Inc, USA.)

2.2.6) The role of PVAT on vascular function

In the **second part** of the obese rat studies, we investigated the effect of the presence of PVAT on contraction and relaxation of the aorta ring segments. In these investigations, the aortic rings obtained from HF rats were compared to those from lean rats. Aortas were removed as described earlier but here we created two subgroups in which the PVAT was either left intact or removed respectively. Figure 34 shows the appearance of aortic rings with and without PVAT. Additionally, we also investigated the effect of removing the endothelial layer by gently scraping the inner surface of the aortas with the tip of small forceps (see Fig. 35 for the experimental design). As mentioned earlier, the protocol was adjusted in this section of our study. Phenylephrine was administered in a cumulative fashion during the second contraction/relaxation protocol. Cumulative additions of phenylephrine yielded final concentrations of 100 nM, 300 nM, 500 nM, 800 nM and 1uM respectively (Fig. 36).
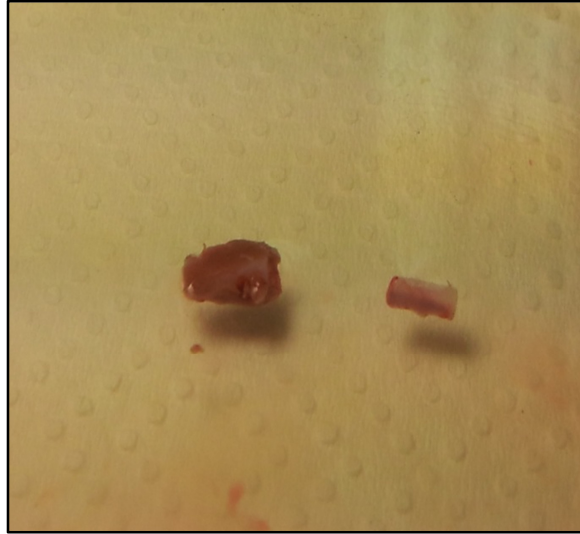
Figure 34: Two aortic ring segments. Left: With PVAT; Right: Without PVAT.
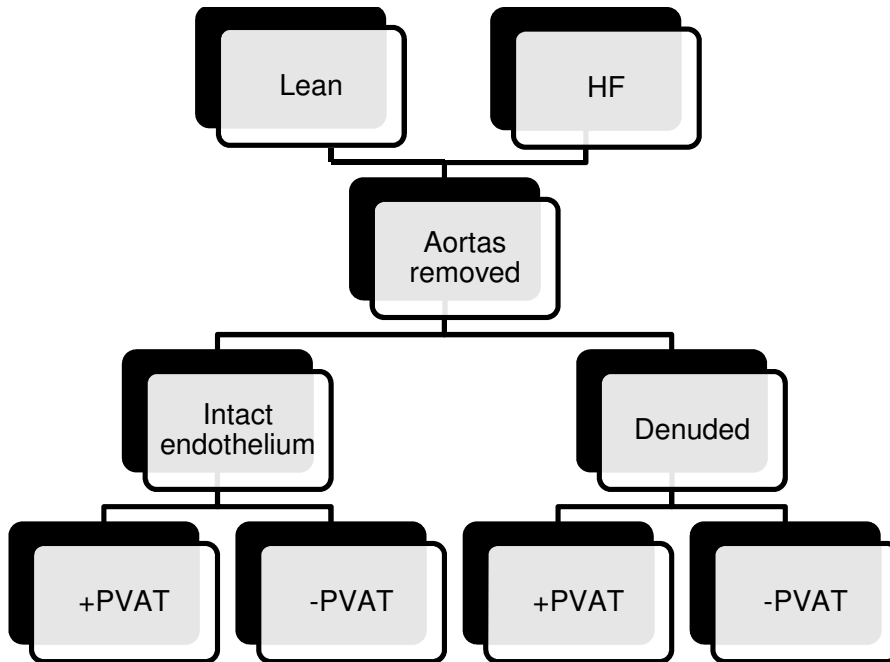
Figure 35: Diagram showing the experimental design of the second part of the obese rat study. In these investigations, we evaluated the effect of PVAT in aortic rings with intact and denuded endothelium.
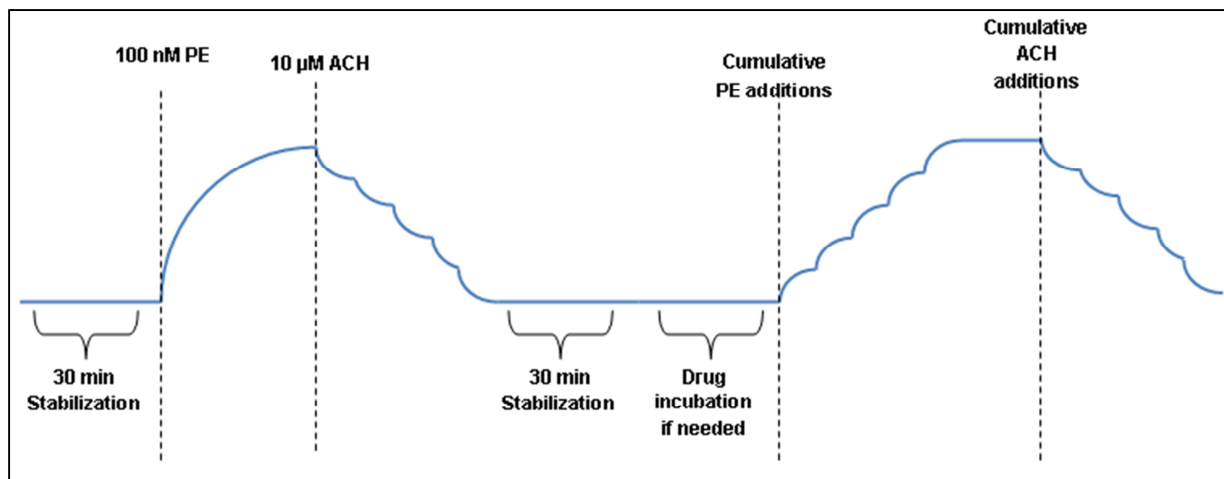
Figure 36: The isometric tension measurement protocol was adjusted for the second part of the obese rat studies, in which we investigated the effects of PVAT and denuded endothelium. The second contraction/relaxation protocol entailed the cumulative administration of PE to yield final concentrations of 100 nM, 300 nM, 500 nM, 800 nM and 1 µM respectively.

2.2.7) Statistical Analysis

Graphpad Prism 5.0 software was used for statistical analysis of data and results are expressed as mean ± standard error of the mean (SEM). A t-test was used when comparing two sets of data, while one-way ANOVA (followed by Bonferonni post-test) was used when comparing more than two sets of data. In the isometric tension (aortic ring) studies we used two-way ANOVA to analyse the data. In all statistical analyses, differences between groups showing a p-value of < 0.05 were considered to be significant.

Chapter 3:

Results

3.1) Amperometric NO measurements

3.1.1) ISO-NOP stainless steel sleeve sensor: CMECs in 35 mm petri dishes

Despite initial success in calibrating the ISO-NOP sensor with $NaNO_2$ (Figs. 37 and 38), the experiments with the ISO-NOP stainless steel sleeve sensor delivered results that could not be statistically analysed due to sensor instability. However, we were able to perform one set of experiments each with acetylcholine and insulin respectively (Figs. 39 and 40) before the readings became extremely unstable. Furthermore, baseline readings progressively started showing drifting, which affected the results.

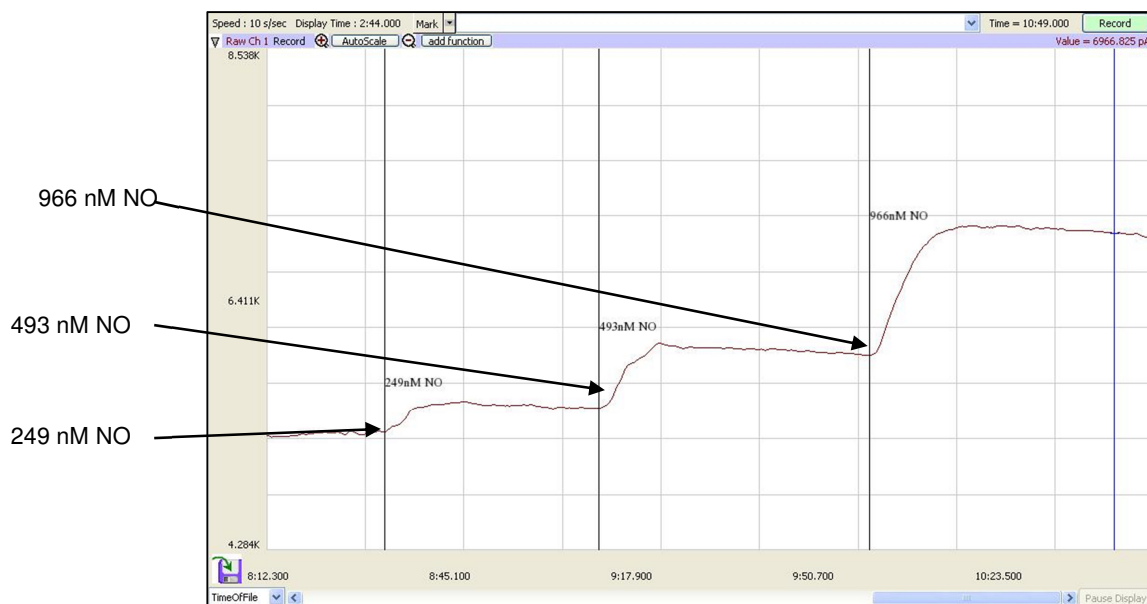**Figure 37: Calibration of the ISO-NOP stainless steel sleeve sensor.**
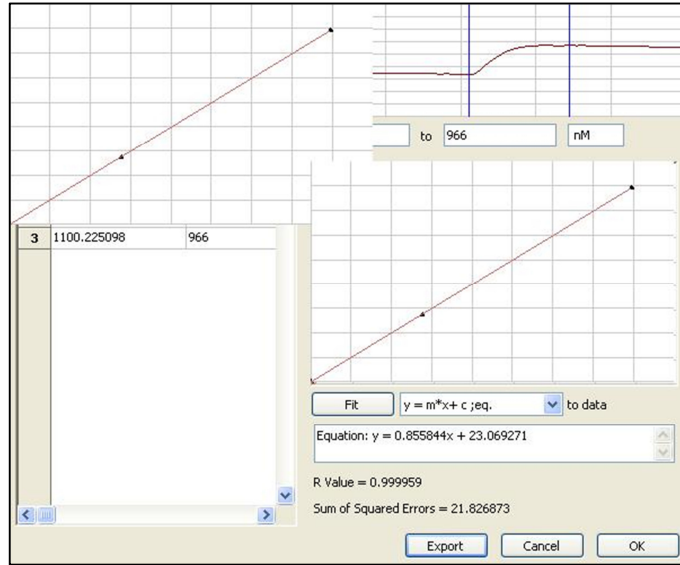
Figure 38: Successful standard curve generated from calibration curve for the ISO-NOP sensor.
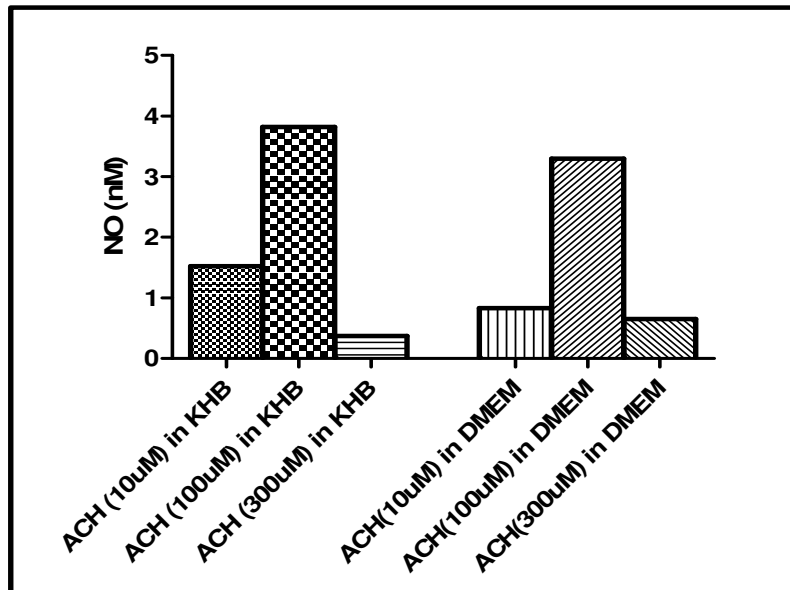
Figure 39: The effect of acetylcholine on NO production from CMEC's. Acetylcholine was either dissolved in KHB or DMEM, but results obtained could not be analyzed as only one experiment could be completed before the sensor became unstable (n = 1).

Figure 40: The effect of different insulin concentrations on NO-release from CMECs as measured with the ISO-NOP stainless steel sleeve sensor. Insulin was either dissolved in Krebs-Henseleit buffer (KBH) or DMEM growth medium. (n = 1).

3.1.2) Carbon fiber tip sensor (ISO-NOPF) studies

3.1.2.1) Cells cultured in 35 mm petri dishes

Calibration of the ISO-NOPF sensor was successful (Figs. 41 and 42). None of the insulin or acetylcholine concentrations administered to the CMECs had any effects on ISO-NOPF carbon fiber tip sensor readings (Figs. 43 – 46). Humulin (dissolved in dH_2O) administration (0.02 IU) however, showed a significant increase in NO (nM) released from CMEC's compared to its vehicle controls (Humulin: 2.150 ± 0.4884 nM vs vehicle control: 0.1205 ± 0.2869 nM; n = 4-6 / group; $p < 0.05$), while Humulin dissolved in EBM showed no difference to EBM vehicle controls (Fig. 47). The effect of humulin dissolved in EBM and dH2O was tested on AEC's. No differences were observed in either of the groups compared to controls (Fig. 48).
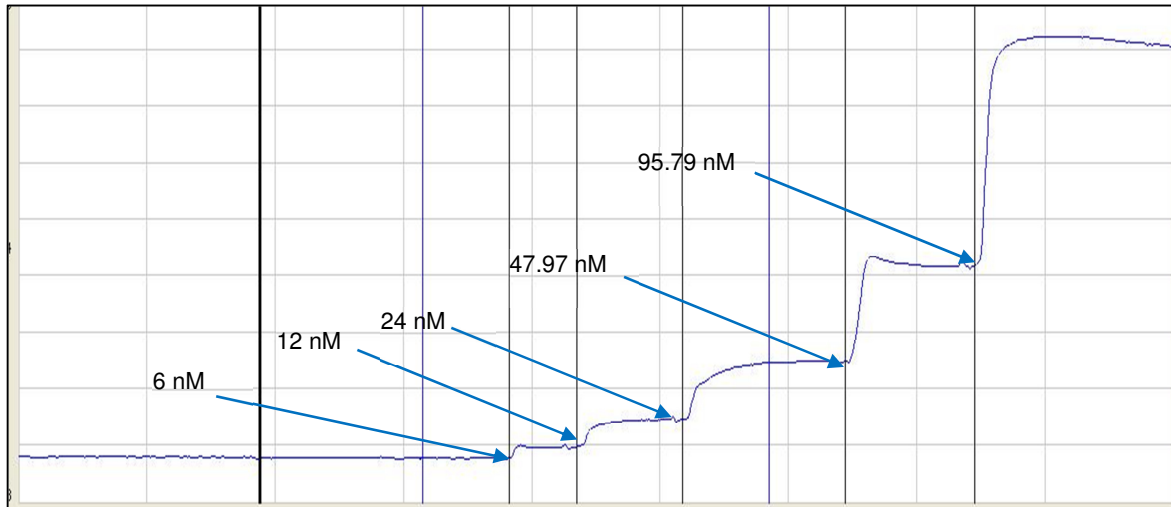
Figure 41: Calibration of the ISO-NOPF carbon fiber tip sensor.
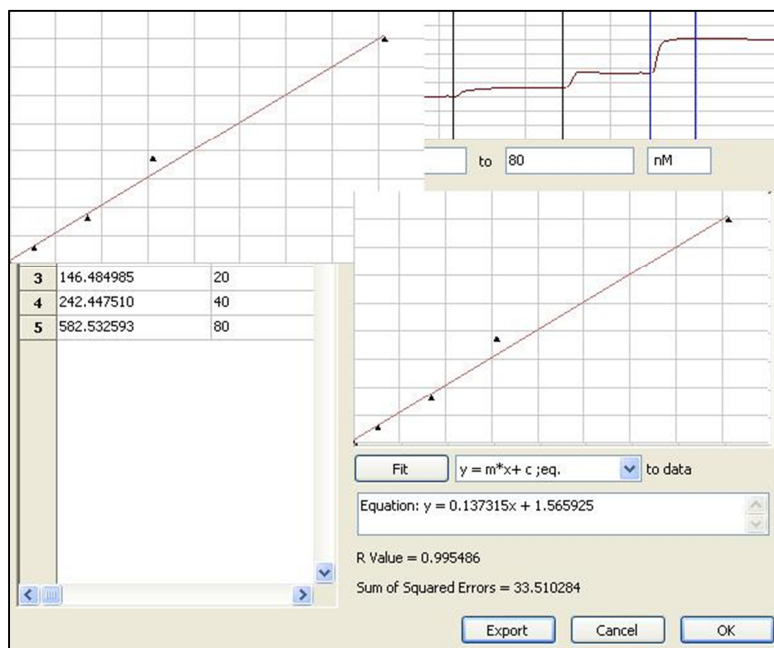
Figure 42: Standard curve generated from calibration curve for the ISO-NOPF carbon fiber tip sensor.

65
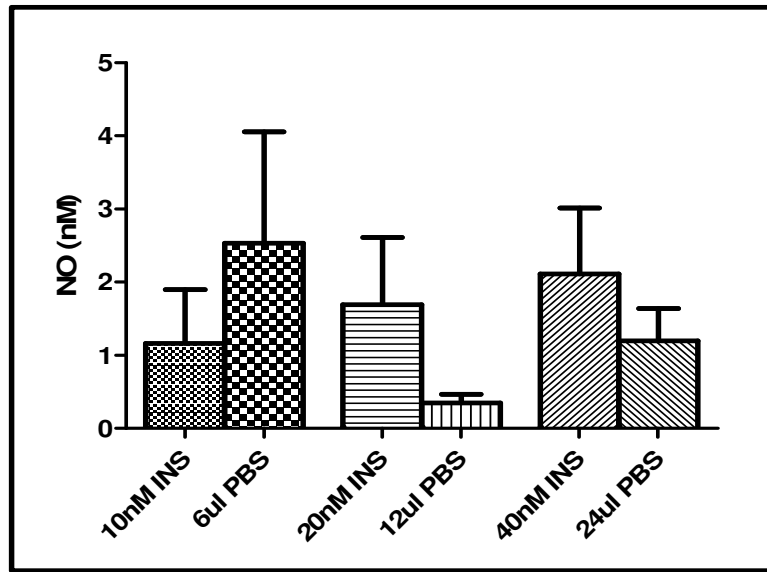
Figure 43: The effect of different insulin concentrations on NO-release from CMECs as measured with the ISO-NOPF carbon fiber tip sensor. Insulin was dissolved in phosphate-buffered saline (PBS) (n = 3).
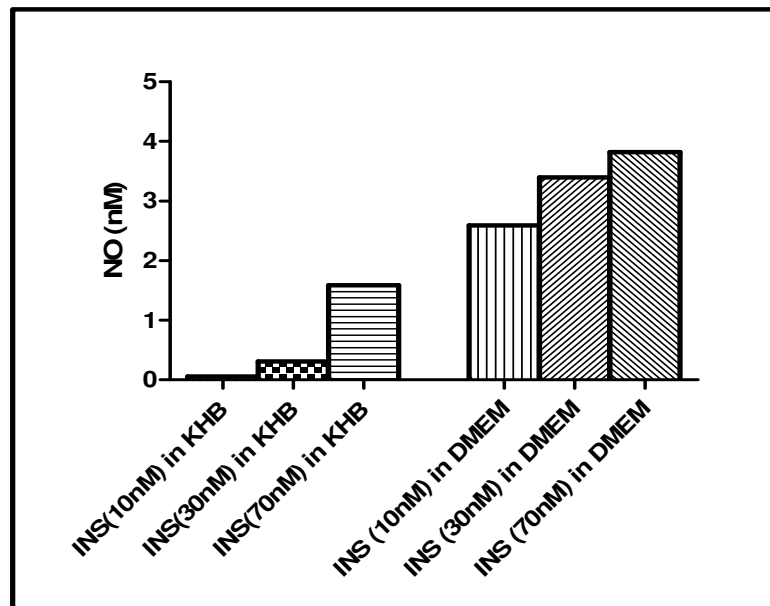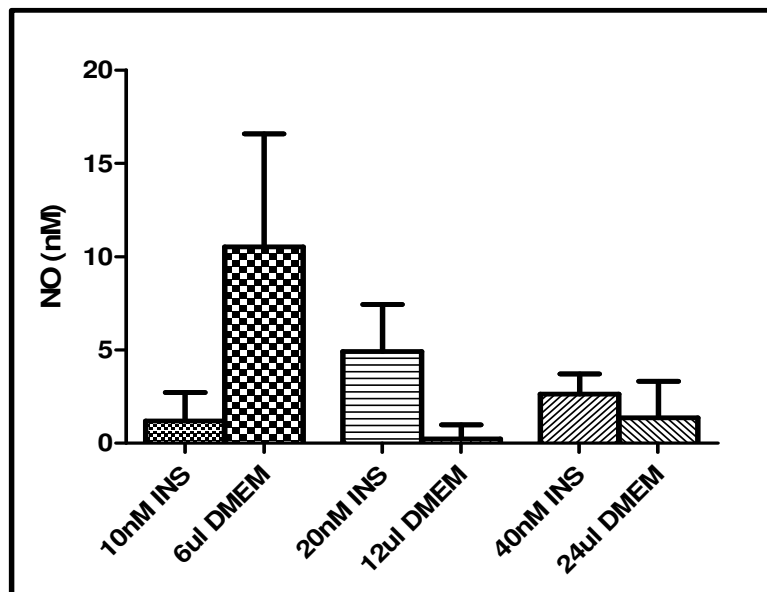

Figure 44: The effect of different insulin concentrations on NO-release from CMECs as measured with the ISO-NOPF carbon fiber tip sensor. Insulin was dissolved in DMEM growth medium (n = 4-8).

66
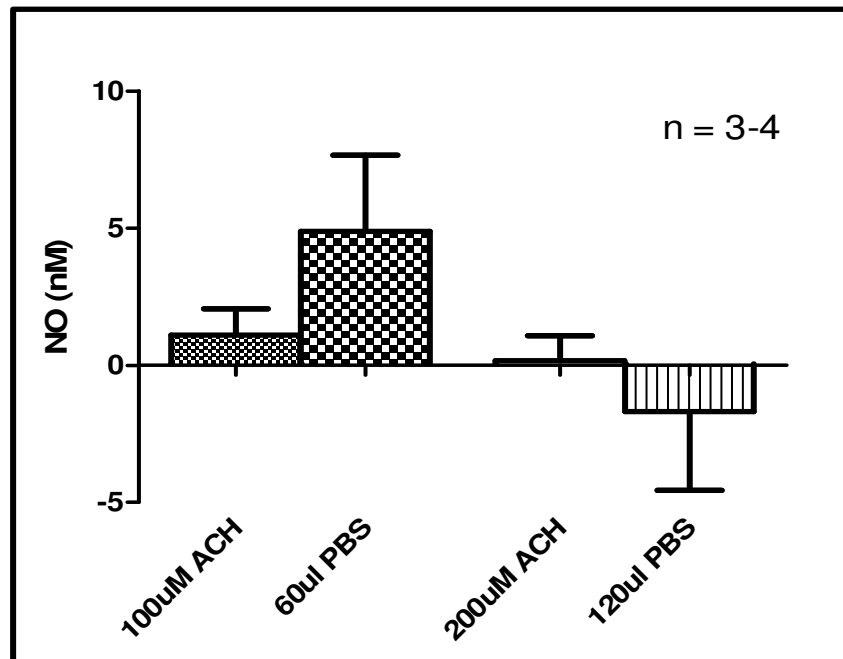
Figure 45: The effect of different acetylcholine (ACH) concentrations on NO-release from CMECs as measured with the ISO-NOPF carbon fiber tip sensor. ACH was dissolved in phosphate-buffered saline (PBS).
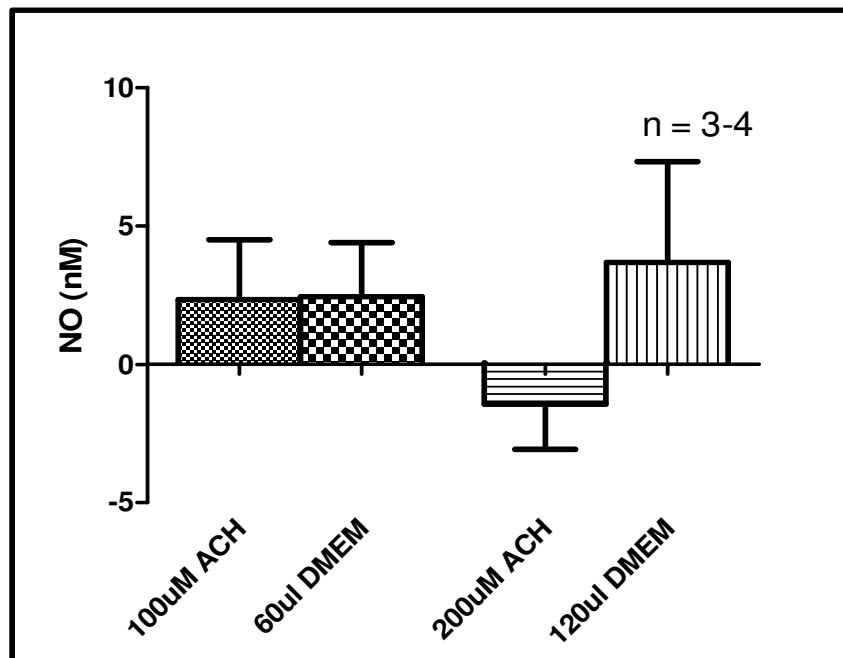
Figure 46: The effect of different acetylcholine (ACH) concentrations on NO-release from CMECs as measured with the ISO-NOPF carbon fiber tip sensor. ACH was dissolved in DMEM growth medium.
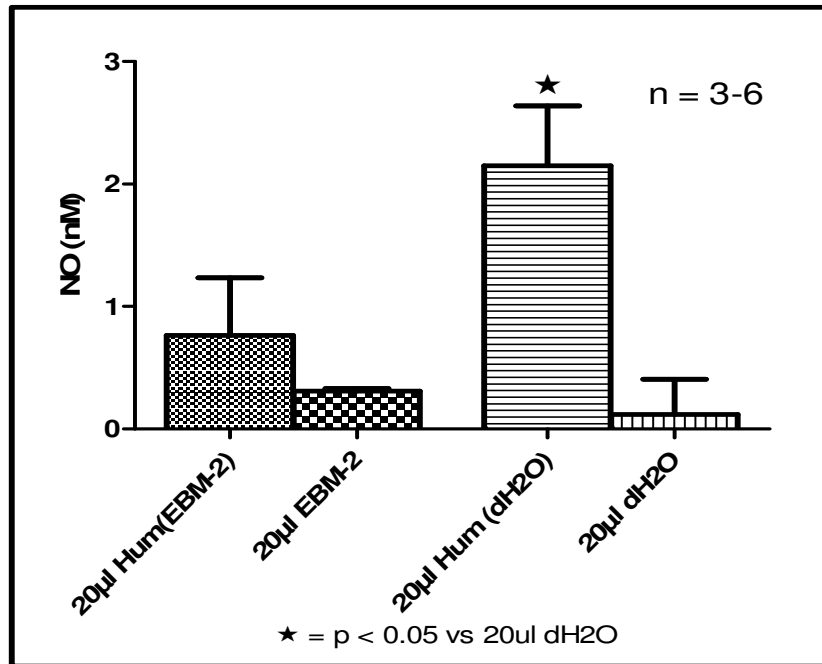
Figure 47: The effect of different Humulin (Hum) solutions on NO-release from CMECs as measured with the ISO-NOPF carbon fiber tip sensor. Hum was dissolved in either EBM-2 growth medium or distilled water.
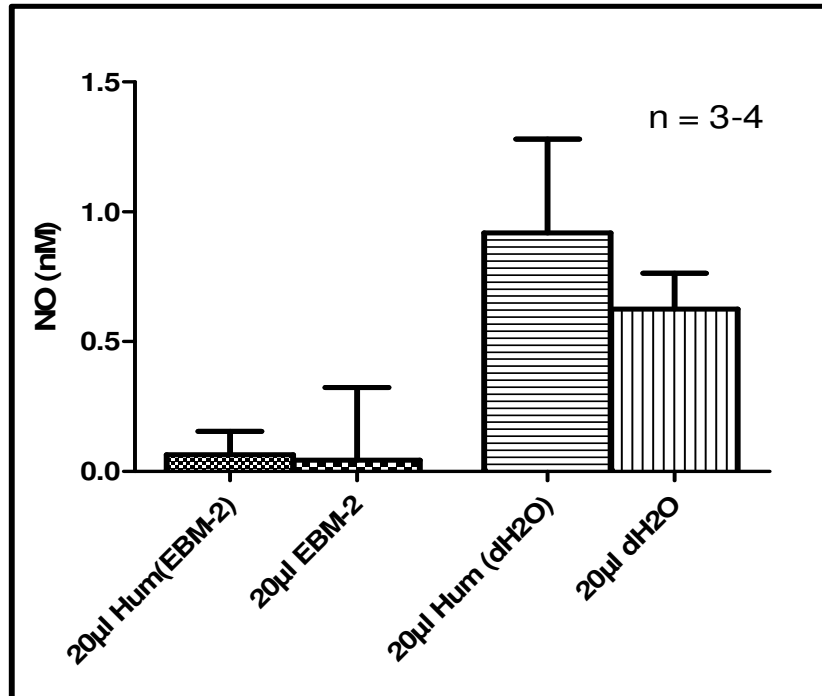
Figure 48: The effect of different Humulin solutions on NO-release from AECs as measured with the ISO-NOPF carbon fiber tip sensor. Humulin was dissolved in either EBM-2 growth medium or distilled water.

3.1.2.2) Cells cultured in 24 multi-well plates

When comparing the administration of insulin and acetylcholine at the surface and bottom of the wells with the ISO-NOPF carbon fiber tip sensor (Fig. 49), we observed a higher response (measured in nM NO) in the 100 nM insulin group when administering at the surface of the well compared to EBM-2 vehicle controls (insulin: 2.975 ± 0.8388 nM vs vehicle control: 0.6258 ± 0.1105 nM; n= 4 / group; $p < 0.05$). Similar results were observed when comparing acetylcholine administered at the top of the wells (ACH: 1.980 ± 0.4442 nM vs vehicle control: 0.6906 ± 0.2027 nM; n=4-5 / group; $p < 0.05$). These results could however not be repeated or expanded upon as the sensor started showing instability when attempting measurements and we progressively experienced difficulties in polarizing and calibrating the sensor.
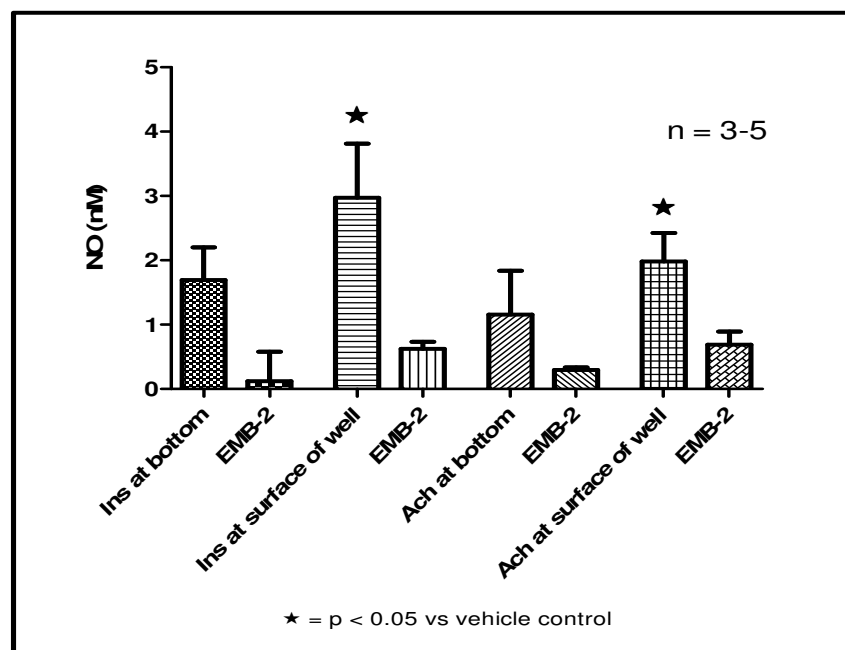
Figure 49: The effect of insulin and acetylcholine (ACH) administered at the surface or bottom of the wells on NO-release from CMECs as measured with the ISO-NOPF carbon fiber tip sensor. Insulin and ACH were dissolved in EBM-2 growth medium.

3.1.2.3) Aortic tissue studies

The ability of the ISO-NOPF carbon fiber tip sensor to detect NO-release was also investigated on 15-20 mm aortic tissue segments (Fig. 50), but due to progressively worsening instability of the sensor during polarization and calibration, only insulin and Humulin experiments could be carried out. Both insulin and Humulin induced increased trends in NO-release from the aortas vs. their respective KHB vehicle controls. Statistical analyses could not be performed, as we only managed to complete two sets of experiments before the sensor readings became unstable.
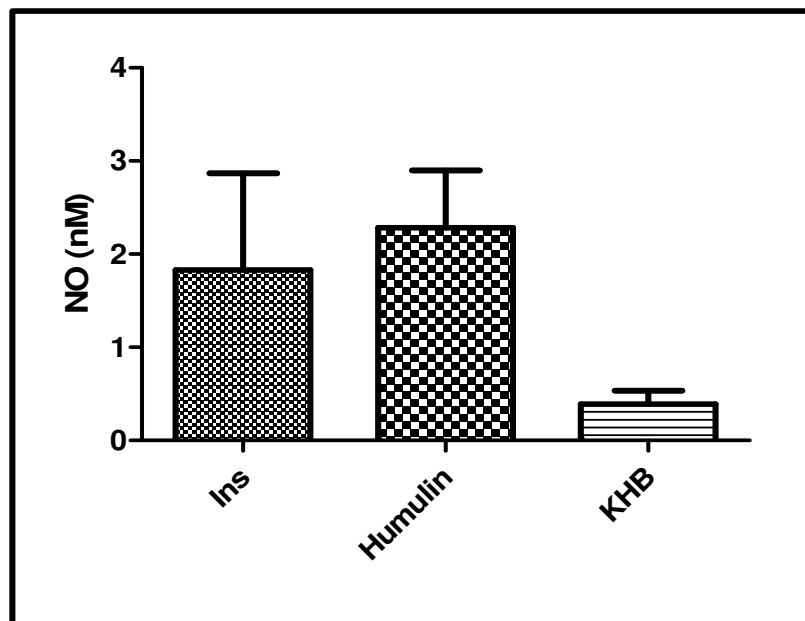
Figure 50: The effect of insulin and Humulin on NO-release from strips of aortas pinned down on the bottom of a 35 mm petri dish as measured with the ISO-NOPF carbon fiber tip sensor. Insulin and Humulin were dissolved in KHB.

3.1.3) ISO-NOPF L-shaped carbon fiber tip sensor studies

3.1.3.1) CMECs in 24 multi-well plates

Calibration and standardisation were successfully completed for this sensor (Figs. 51 and 52). In this series of experiments, we investigated the effects of administering insulin and acetylcholine to CMECs either at the surface of the well or at the bottom of the well, similar to the experiments described earlier (see section 2.1.1.2.2). Although an increased trend was observed in the sensor readings of both insulin and acetylcholine when administered at the surface of the well, no statistical differences were observed (Fig. 53). As a next step, we wanted to investigate whether the increased sensor readings were due to the drugs *per se*, and not due to the mechanical disturbance caused by the injection of the fluid in which the drugs were dissolved. We therefore repeated the experiments in growth medium-filled wells without cells. To our disappointment, drug administration at the surface of the well produced the same increasing trends in the sensor readings (Fig. 54). The results are thus inconclusive regarding the L-shaped sensor in the multiwells and the sensor showed instability when attempting measurements, limiting the number of experiments we could successfully complete.
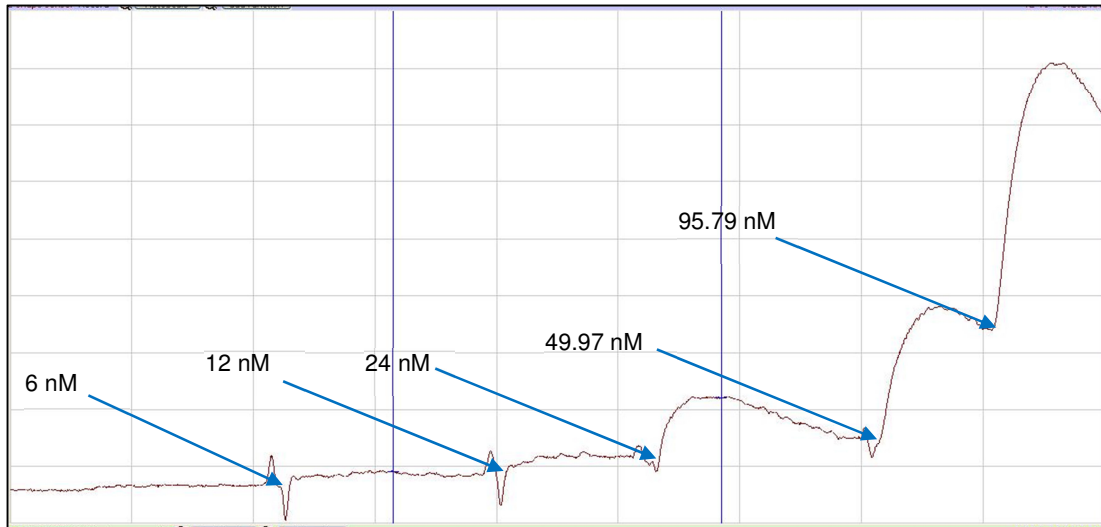
Figure 51: Calibration of the ISO-NOPF L-shaped sensor.
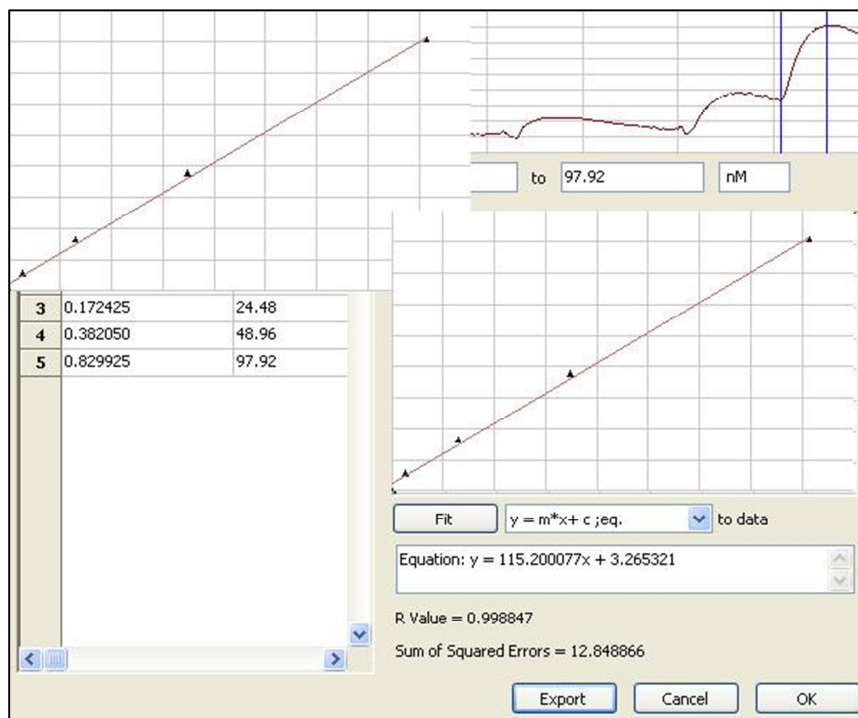
Figure 52: Standard curve of the ISO-NOPF L-shaped sensor.
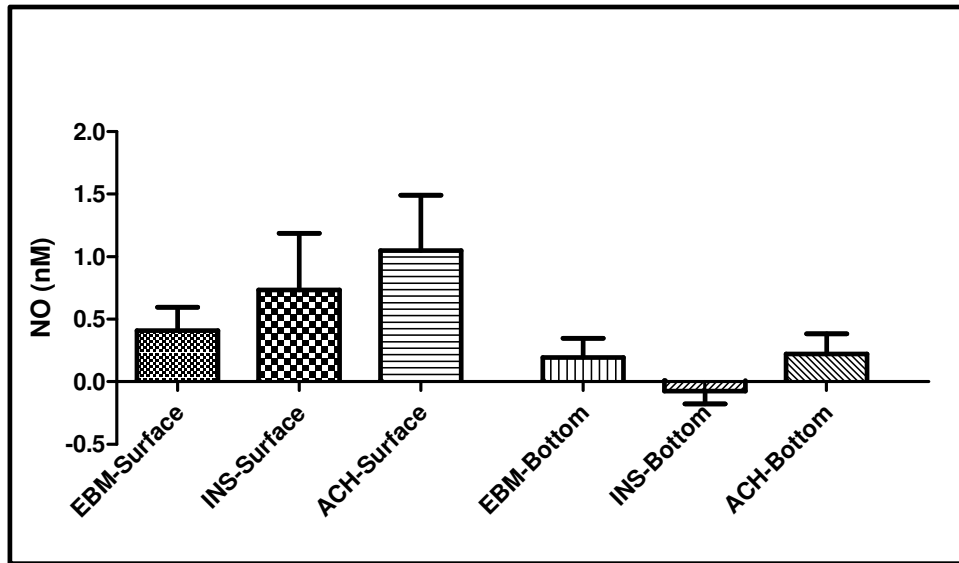
Figure 53: The effect of insulin and acetylcholine (ACH) administered at the surface or bottom of the wells on NO-release from CMECs as measured with the ISO-NOPF L-shaped carbon fiber tip sensor. Insulin and ACH were dissolved in EBM-2 growth medium (n = 7 - 28).
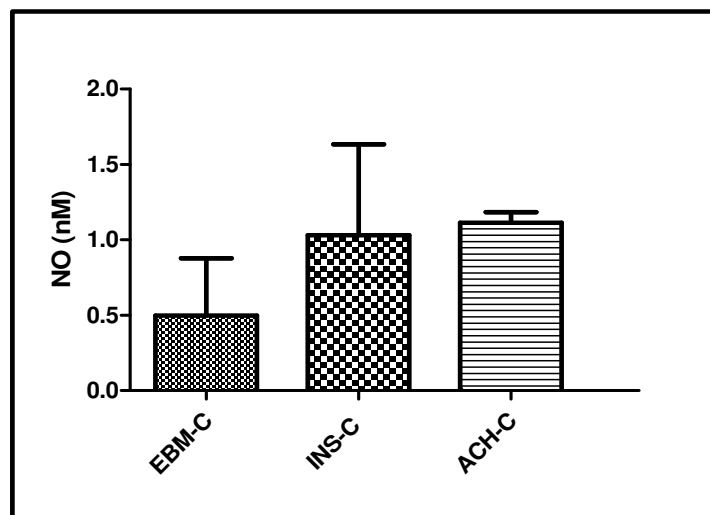

Figure 54: The effects of drug administration at the surface of a growth medium-containing well in the absence of cells (EBM no cell control = EBM-C; Insulin no cell control = INS-C; Acetylcholine no cell control = ACH-C) (n = 3).

3.1.3.2) Aortic tissue experiments

The effects of acetylcholine and insulin were tested on inverted rat aortas. Sensor readings (nM NO) were significantly increased in the 1 µM insulin group vs 100 nM insulin and vs EBM-2 vehicle controls (Insulin 1 µM: 7.618 ± 2.800 nM vs Insulin 100 nM: 0.3603 ± 0.3652 nM vs EBM-2 vehicle control: 1.244 ± 0.6014 nM; n=6-13; P < 0.05 vs insulin 100 nM and EBM-2 vehicle control) (Figure 55).

Shear stress experiments on aortas that were cut open in length to form strips (Fig. 56) showed an increase in the L-shaped carbon fiber tip sensor readings in aortas with intact endothelium compared to control aortic strips without endothelium ("denuded"). In these studies, we injected 100 µl and 200 µl of EBM with a micropipette onto a region just adjacent to the aortic strips in order to create shear stress. The results (nM NO) were as follows. 100 µl injection: intact endothelium strips: 4.996 ± 1.265 nM vs denuded strips: 0.3575 ± 0.3476 nM; p < 0.05; n = 4-9 / group, and 200 µl injection: intact endothelium strips: 6.781 ± 0.8742 nM vs denuded strips: 3.090 ± 1.482 nM; p < 0.05; n = 4-9/ group.

The effect of shear stress was also investigated in cultured AECs (Fig. 57). There were no differences in the L-shaped sensor readings in petri dishes containing AECs compared to dishes with no cells. However, the AEC's that received 200 µl EBM produced significantly more NO compared to the AEC's that received 100 µl EBM. (200 µl group: 6.766 ± 0.7906 nM; p < 0.001; n = 12; 100 µl group: 2.788 ± 0.3214 nM; p < 0.001; n = 12).
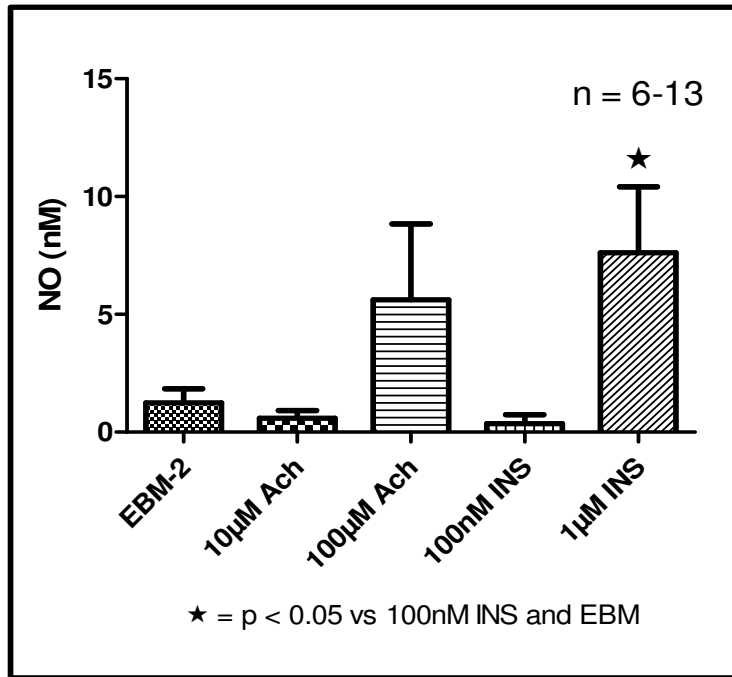
Figure 55: The effects of acetylcholine and insulin on L-shaped ISO-NOPF sensor readings in inverted aortic segments. The drugs were dissolved in EBM-2 growth medium.
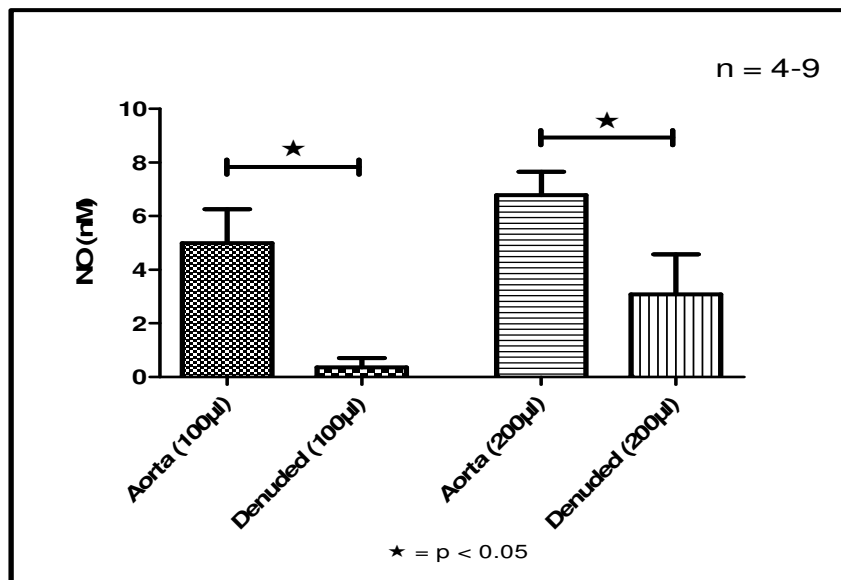
Figure 56: The effects of shear stress on L-shaped ISO-NOPF sensor readings in aortic segments with intact endothelium vs denuded aortic segments. EBM-2 growth medium was injected to simulate shear stress.
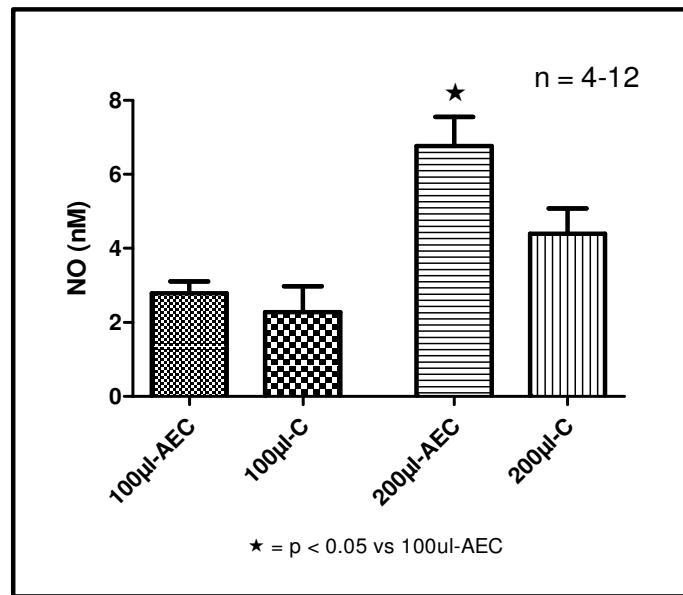
Figure 57: The effects of shear stress on L-shaped ISO-NOPF sensor readings on AEC's vs. No-cell control. EBM-2 growth medium was injected to simulate shear stress (100 µl-C = 100 µl no cell control; 200 µl-C = 200 µl no cell control).

3.2) NO_2^- / NO_3^- measurements

Difficulty was experienced with calibration and standardization, when using the ArrowSTRAIGHT™ NO_2^-/NO_3^- sensor. The NO_2^- sensor was able to successfully detect both standards, but when adding the second standard (10 µM) the difference in mV reading between the two concentrations were not as it should be according to the user manual (prescribed difference: 49 mV to 59 mV). As a result, when adding the NO_2^- standards (10 µM and 100 µM) after calibration, only the 100 µM NO_2^- standard produced acceptable readings (Fig: 58: A) and a standard curve could thus not be generated successfully. Similarly, the NO_3^- sensor did not produce satisfactory calibration results. The NO_3^- sensor was able to detect both standards, but again the difference in mV reading was not as the user manual stipulated. As a result a calibration

curve could not be generated and when the standards were added again after the calibration attempt, only the 10 µM standard produced acceptable results (Fig. 58: B). The lack of calibration data meant that no experiments could be attempted and as a result the protocols using this sensor were abandoned.
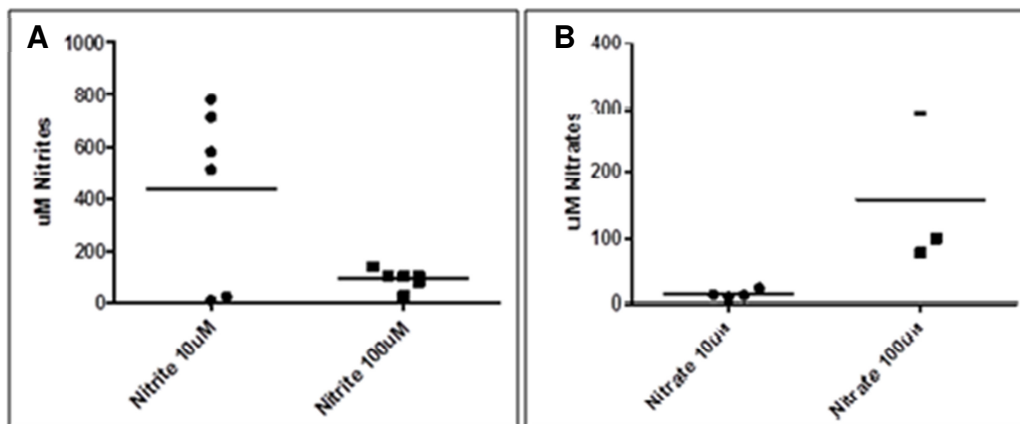
Figure 58: Calibration data plots of nitrite (left) and nitrate (right) sensor. Calibration was only successful with the 100 µM nitrite and 10 µM nitrate standards. Despite several attempts to calibrate and standardise, we were unsuccessful and experiments could not be carried out.

3.3) Nitrite measurements with the Griess reagent

In order to generate a standard curve, six of the 24 wells of the plate contained no cultured cells. In these wells a stock solution of $NaNO_2$ (200 µM) was used to create standards of increasing concentration. The standard concentrations were as follows: 0 nM, 400 nM, 2 µM, 4 µM, 7 µM, 10 µM. After the multi-well plate had been analyzed by the plate reader, the absorbance values (optical density; OD) obtained from the standards were used to generate a standard curve (Fig. 59) from which the data of the experimental samples were derived (nM nitrites).

As expected, 1 h treatment of CMECs with the NO-donor, DEA/NO (100 µM), significantly increased nitrite concentrations (DEA/NO: 14.97 ± 1.229 µM vs. control: 2.468 ± 0.2071 µM; $p < 0.05$; n = 18-31) vs. control (Fig. 60). However, both 10 µM bradykinin (1.277 ± 0.1243 µM; n = 6) and 100 nM insulin (3.375 ± 0.5735 µM; n = 8) failed to increase nitrite production compared to controls. When the cells were treated with fenofibrate (previously shown to increase NO-production in our laboratory) at 50 µM for 1 h, nitrite levels increased significantly compared to controls (fenofibrate: 2.247 ± 0.09280 µM; vs. control: 1.405 ± 0.1750 µM; $p < 0.05$; n = 3) (Fig. 61). Pretreatment with the iNOS inhibitor, 1400W (80 µM), failed to reduce the fenofibrate-induced increase in nitrite levels. When the CMECs were treated for 1 hour with 40 µM Oleanolic (OA) acid, another compound previously shown to increase NO-production in our laboratory, the nitrite levels increased significantly (OA: 5.546 ± 0.6653 µM vs. control: 2.468 ± 0.2071 µM; $p < 0.05$; n = 10-31) (Fig. 62). When the CMECs were treated with the cytokine, interleukin-1ß (IL; 5 ng/ml) for 24 h, nitrite levels increased significantly (IL: 20.92 ± 1.502 µM vs. control 4.641 ± 0.3428 µM; $p < 0.05$; n = 3-8). Pretreatment with the iNOS inhibitor, 1400W (80 µM) resulted in a significant reduction in nitrite levels compared to IL-treated groups (IL+1400W: 12.17 ± 1.531 µM; $p < 0.05$ vs IL; n = 3) (Fig. 63).

$$y = 2E-05x + 0.015$$
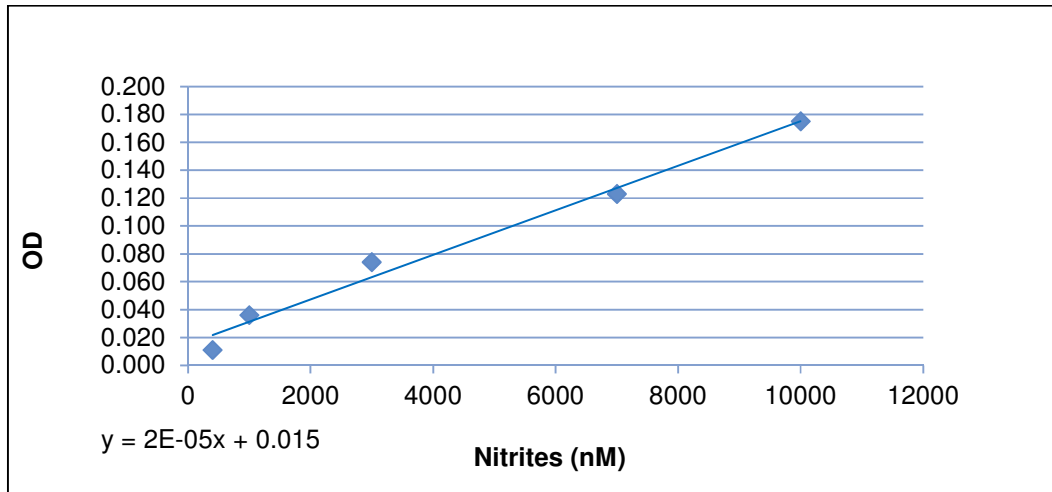
Figure 59: A nitrite standard curve generated with the Griess Reagent from cumulative NaNO$_2$ additions.
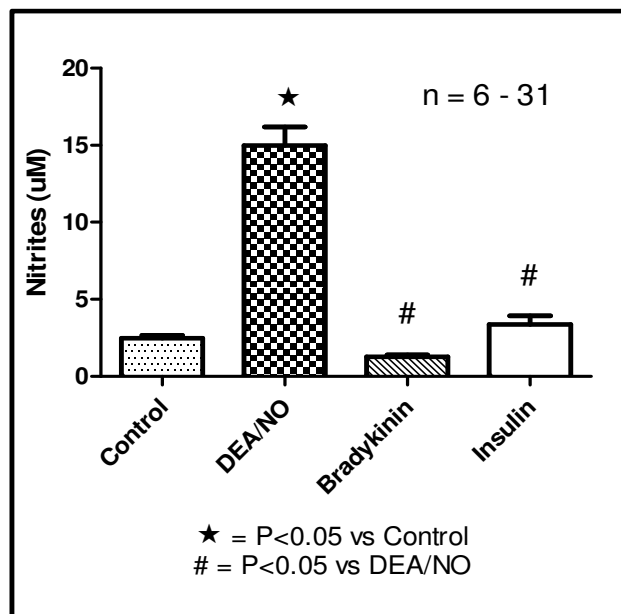
Figure 60: The effects of one hour treatments with DEA/NO, bradykinin and insulin on nitrite release by CMECs as measured by the Griess Reagent.
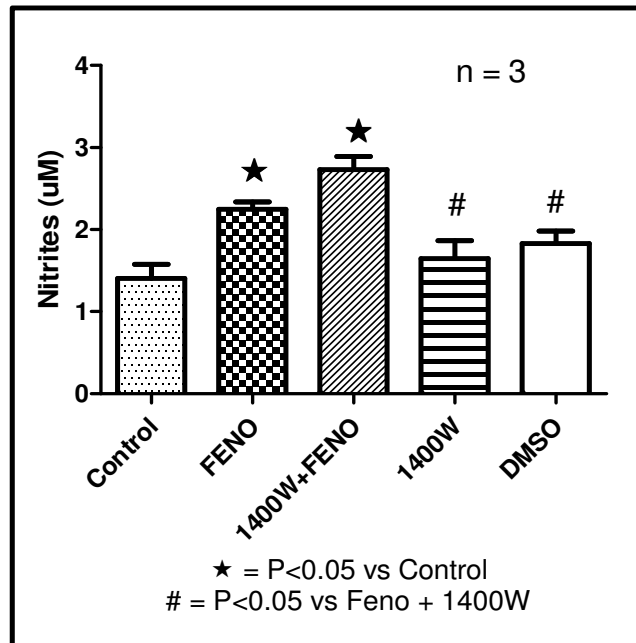
Figure 61: The effects of one hour treatment with fenofibrate (50 μM), the iNOS inhibitor 1400W (80 μM) and appropriate vehicle control (0.001% DMSO) on nitrite release by CMECs measured by the Griess Reagent.
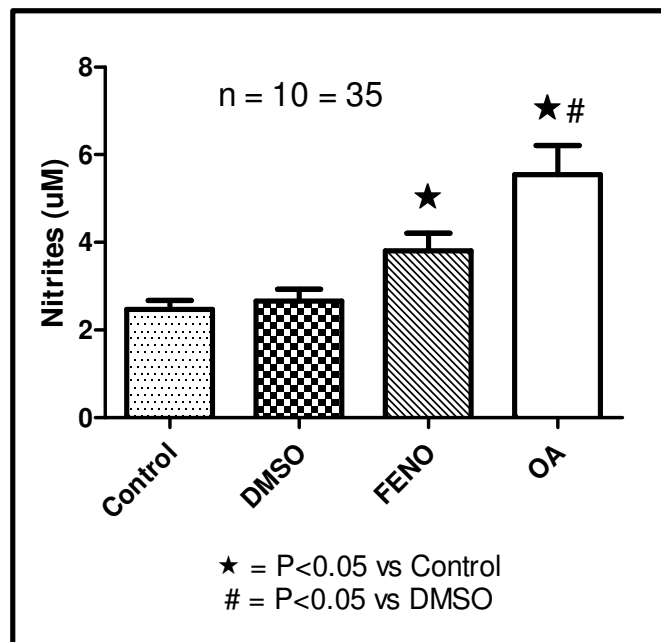
Figure 62: The effects of one hour treatment with fenofibrate (50 μM) and oleanolic acid (OA; 40 μM) on nitrite release by CMECs measured by the Griess Reagent.
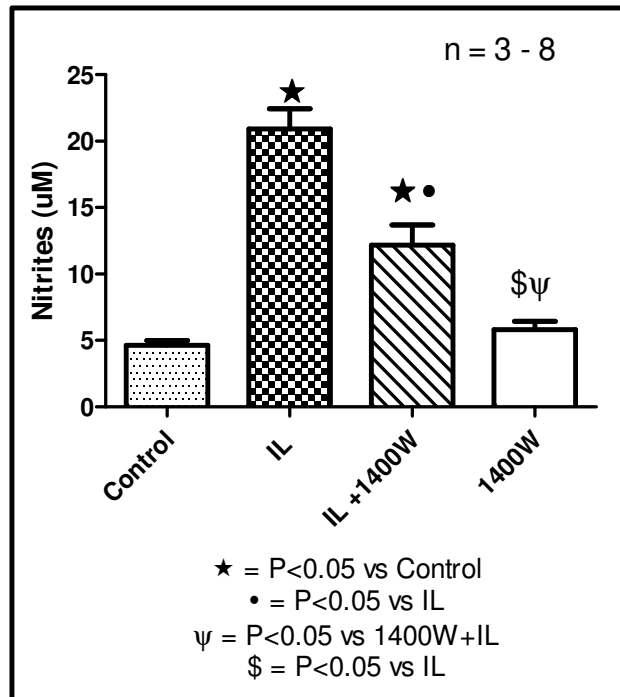
Figure 63: The effects of 24 h treatment with IL-1ß and IL-1ß + 1400W on nitrite release by CMECs measured by the Griess Reagent.

3.4) Measurement of endothelial function in aortic rings: isometric tension studies

3.4.1) Pilot studies: setting up the aortic ring model

Pilot studies were carried out to set up and optimize the isometric tension measurement protocol of aortic rings. Figure 64 shows the aortic ring relaxation data obtained with a very basic protocol whereby aortic rings were precontracted with 100 nM phenylephrine (PE), and then subsequently treated with a series of cumulative acetylcholine concentrations. Furthermore, we investigated the ability of the vascular smooth muscle of aortic rings to undergo endothelium-independent relaxation by direct administration of the NO-donor, SNAP (Fig. 65).

81

The model was further characterised by the administration of the eNOS-inhibitor, L-NMMA (100 µM) 10 minutes prior to the ACH treatment. Data showed that the % relaxation induced by the cumulative ACH concentrations was significantly inhibited by L-NMMA, indicating that the aortic ring relaxation was dependent on NO-release from the endothelium (Fig. 66). Finally, as part of the pilot investigations, we treated the aortic rings with TNF-α (10 ng / ml) 30 minutes prior to ACH treatment, as TNF-α was previously shown in our laboratory to reduce NO-production in cultured endothelial cells. The data showed that TNF-α pretreatment significantly inhibited ACH-induced relaxation (Fig. 67).
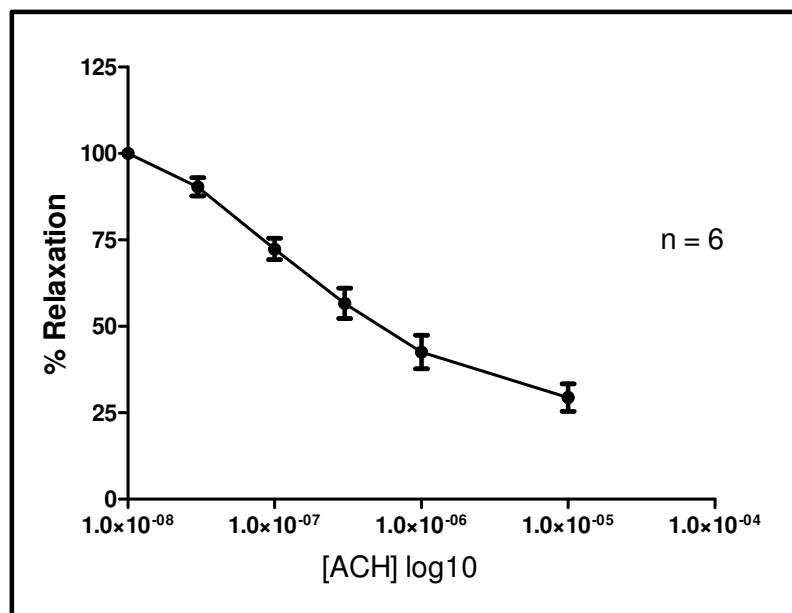
Figure 64: Graph illustrating the relaxing effects of cumulative ACH concentrations on PE-induced precontracted aortic rings. Aortic ring relaxation data are expressed as % isometric tension of tension at maximum precontraction.
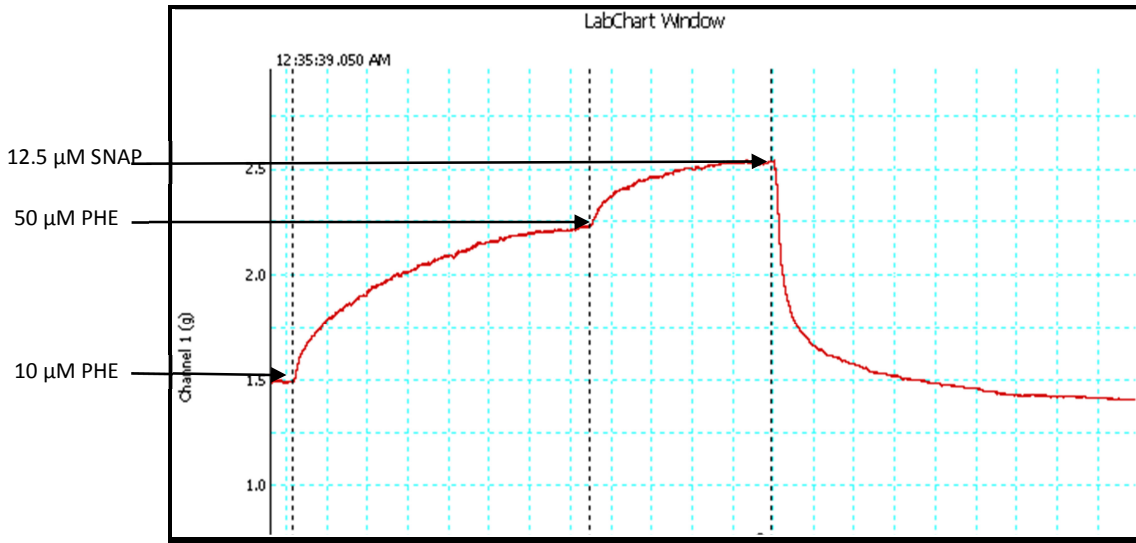
Figure 65: The vasorelaxing effect of SNAP treatment on precontracted aortic rings (50 µM PHE final concentration).
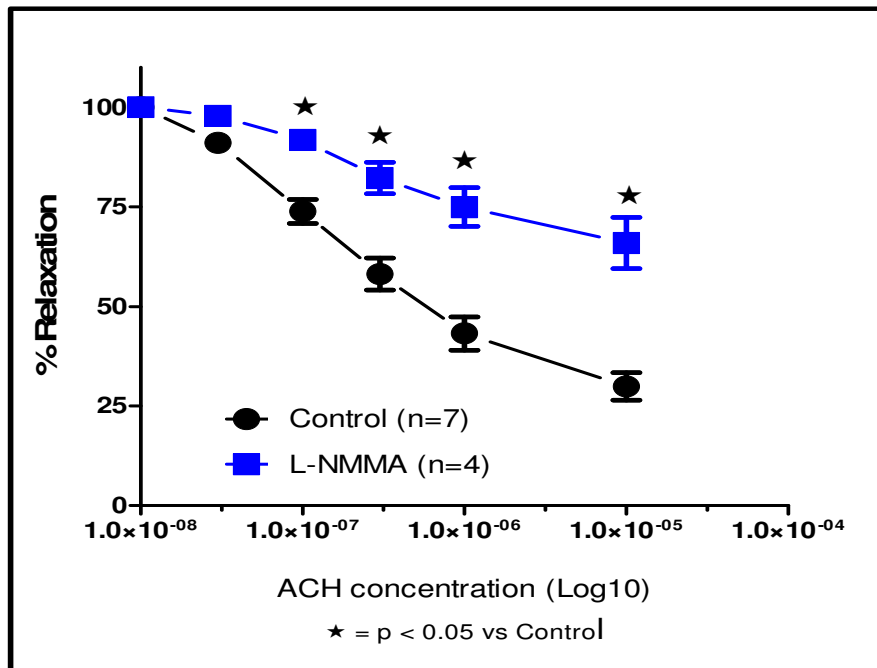
Figure 66: The effect of L-NMMA pretreatment on acetylcholine-induced relaxation of aortic rings.

83
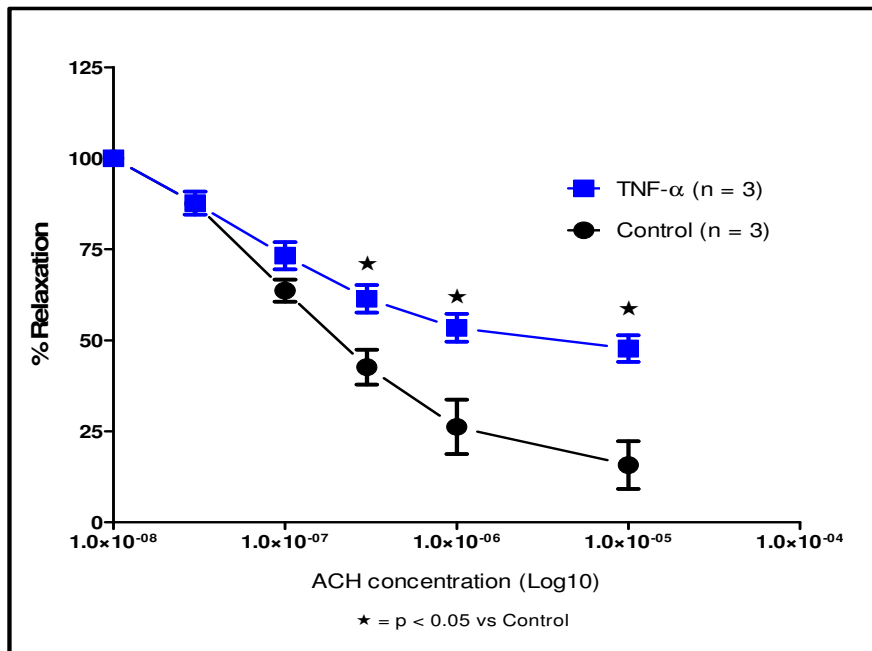
Figure 67: The effect of TNFα pretreatment on acetylcholine-induced relaxation of aortic rings.

3.4.2) Isometric tension studies on aortic rings obtained from obese rats

3.4.2.1) Biometric data

Figure 68 shows the total body mass of the rats used in the diet study. Rats on the high sucrose (HS) diet and high fat (HF) diet both showed a significant increase in total body mass compared to lean (L), age-matched control rats (L: 370.3 ± 7.036 g vs. HS: 441.4±15.6 g; $p < 0.05$ and vs HF: 493.4±21.28 g; $p < 0.001$; n = 7-11).
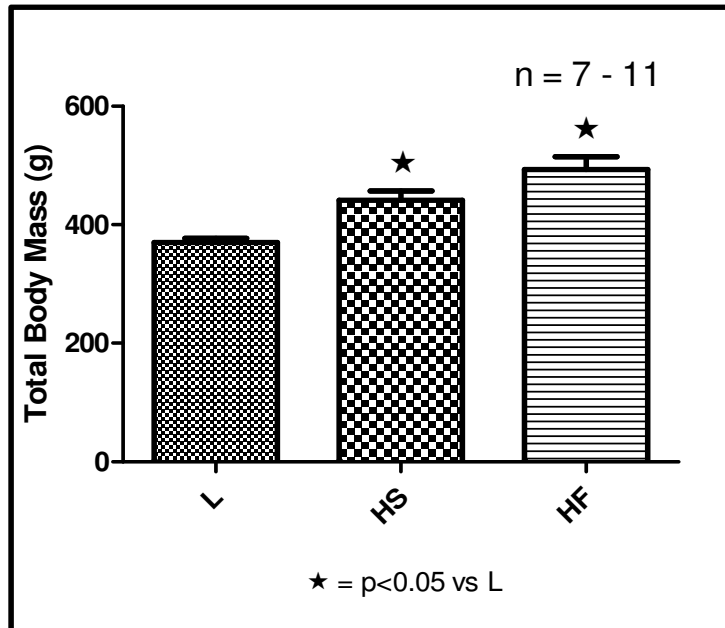
Figure 68: The mean total body mass measured in the respective diet groups.

Figure 69 shows the total intra-peritoneal fat mass of the rats from the different diet groups. Rats on the HF diet showed a higher intra-peritoneal fat mass compared to lean controls as well as compared to rats on the HS diet (HF: 29.08 ± 1.677 g vs HS: 21.59 ± 1.978 g vs lean controls: 12.40 ± 0.5382 g; n = 8/group; $p < 0.05$). Furthermore, rats on the HS diet showed higher intra-peritoneal fat mass compared to lean controls.
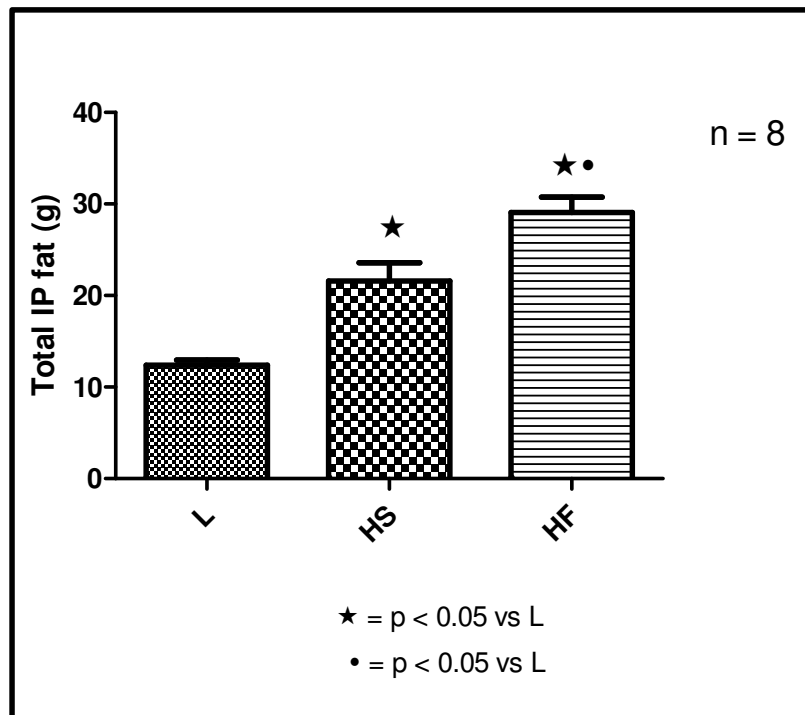
Figure 69: The mean total intraperitoneal fat mass measured in the respective diet groups.

3.4.2.2) Isometric tension studies on aortic rings without PVAT, precontracted with a single PE administration

Figure 70 shows the aortic ring relaxation data of the **first part** of the obese rat study, in which the perivascular adipose tissue (PVAT) of the aortic rings was removed, and where we followed a precontraction protocol of a single 1 µM PE administration followed by cumulative ACH relaxation. In this series of experiments, no differences were noted between HS and L relaxation; however, a significantly greater % relaxation was observed in aortic rings from HF rats compared to L at the 1 µM ACH cumulative concentration.
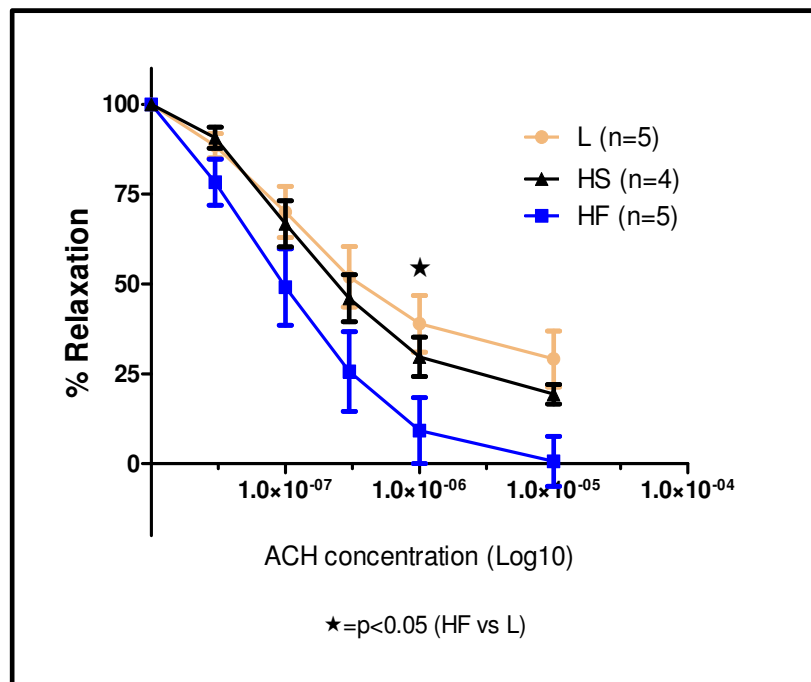
Figure 70: The effects of High Sucrose (HS) and High Fat (HF) diets on the % aortic ring relaxation induced by cumulative ACH concentrations.

3.4.2.3) Western blot analyses performed on aortas of lean, HS and HF rats

Western blot analysis was carried out on aortic tissue (without PVAT) to determine the activation status of proteins involved in NO production (eNOS and iNOS) as well as upstream activators of these proteins (PKB and AMPK). Furthermore we investigated the activation of proteins involved in superoxide production (p22phox) and compounds that are indicative of nitrosative stress (nitrotyrosine). Aortic tissue from HS and HF rats was compared to the lean group. All data are shown as % of lean controls (controls adjusted to 100%).

Activation of eNOS (phospho eNOS / total eNOS ratio) was significantly downregulated (Fig. 71) in both the HS and HF groups compared to lean rats (L: 100%; vs. HS: 38.78 ±

9.204% vs. HF: 31.59 ± 2.055%; p < 0.001; n = 3). No difference was observed in the phospho PKB/Akt / total PKB/Akt ratio between the groups (Fig. 72), however the phospho AMPK / total AMPK ratio was significantly decreased (Fig. 73) in the HS group compared to lean and HF (Lean: 100% vs. HS: 51.33 ± 3.480% vs. HF: 86.67 ± 8.838; p < 0.05 HS vs. lean and HF; n = 3). Total iNOS expression (Fig. 74) was significantly decreased in HS and HF compared to lean, as well as in HS vs. HF (L: 100% vs HS: 33.54 ± 2.927% vs. HF: 67.22 ± 11.59%; p < 0.01; n = 3). Only the HF group showed a significantly decreased expression of total p22phox compared to the lean group (L: 100% vs. HF: 53.38 ± 0.7833%; p < 0.05; n = 3) (Fig. 75). Similarly, the expression of nitrotyrosine was significantly decreased in the HF group compared to lean (L: 100% vs. HF: 41.67 ± 11.35%; p < 0.05; n = 3) (Fig. 76).
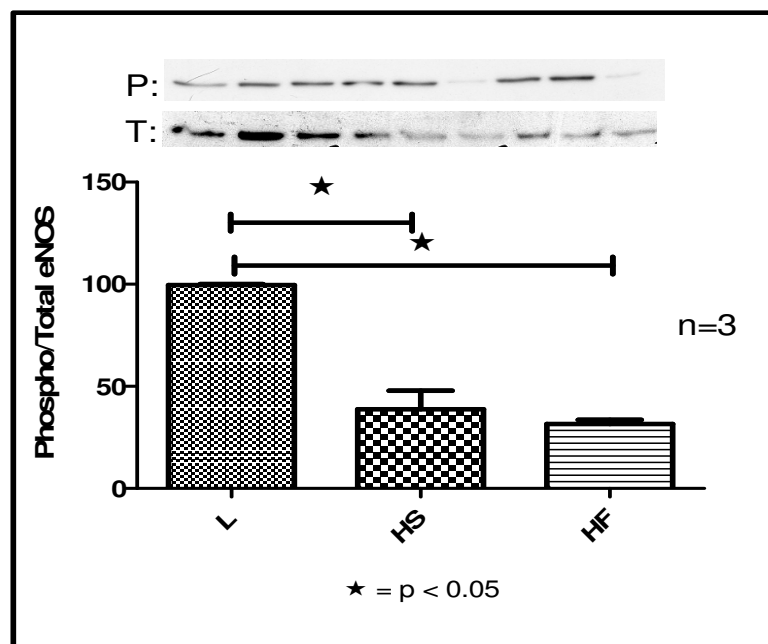
Figure 71: The effects of HS and HF diets on the phosphorylated / total eNOS levels.
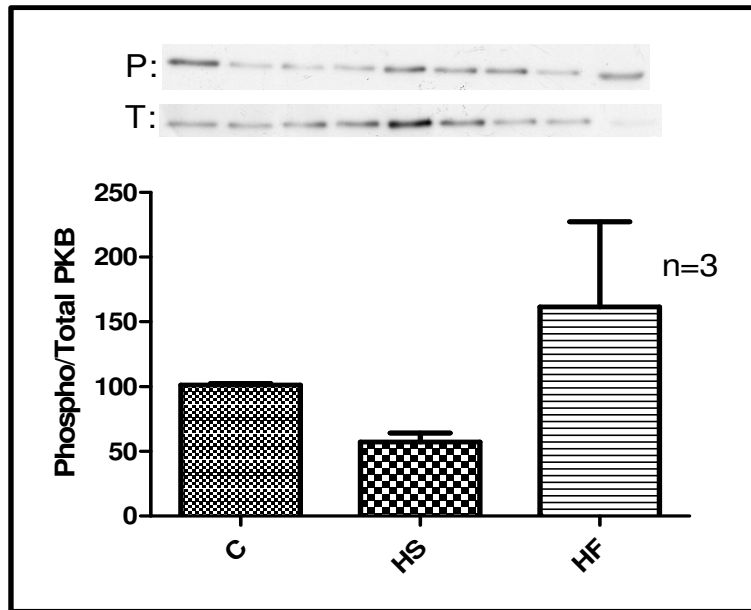
Figure 72: The effects of HS and HF diets on the phosphorylated / total PKB/Akt levels.
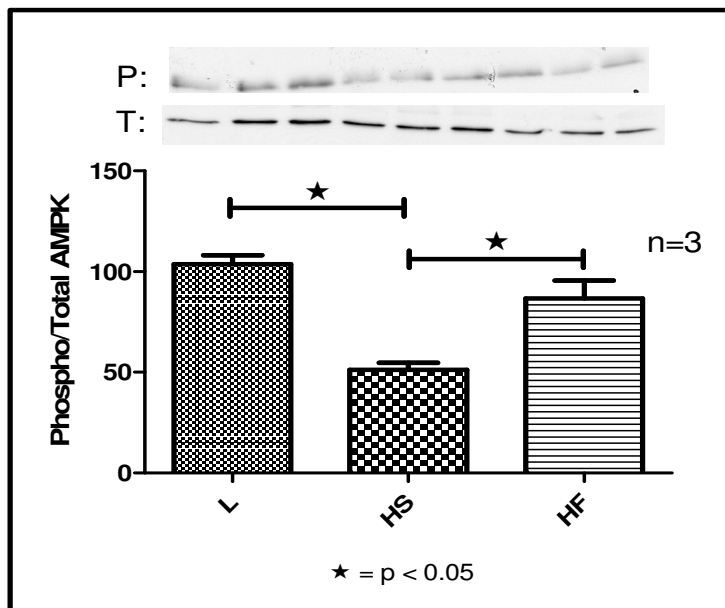
Figure 73: The effects of HS and HF diets on the phosphorylated / total AMPK levels.
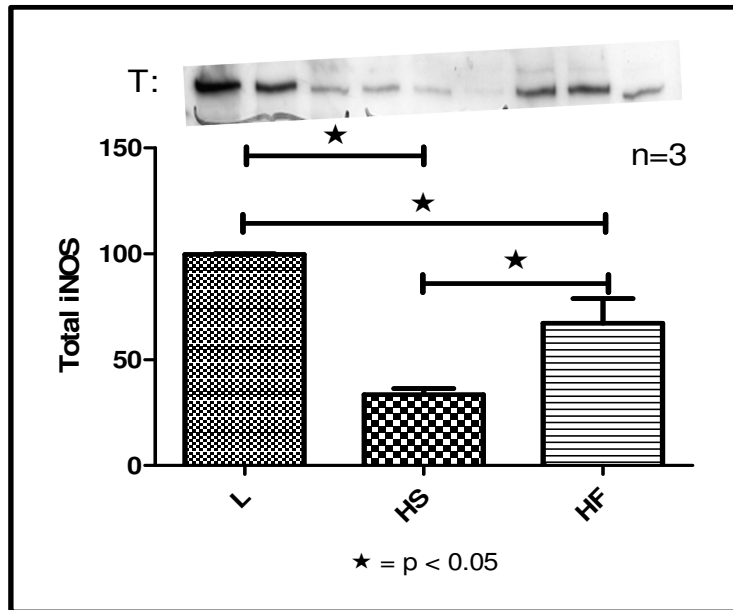
Figure 74: The effects of HS and HF diets on the total iNOS expression.
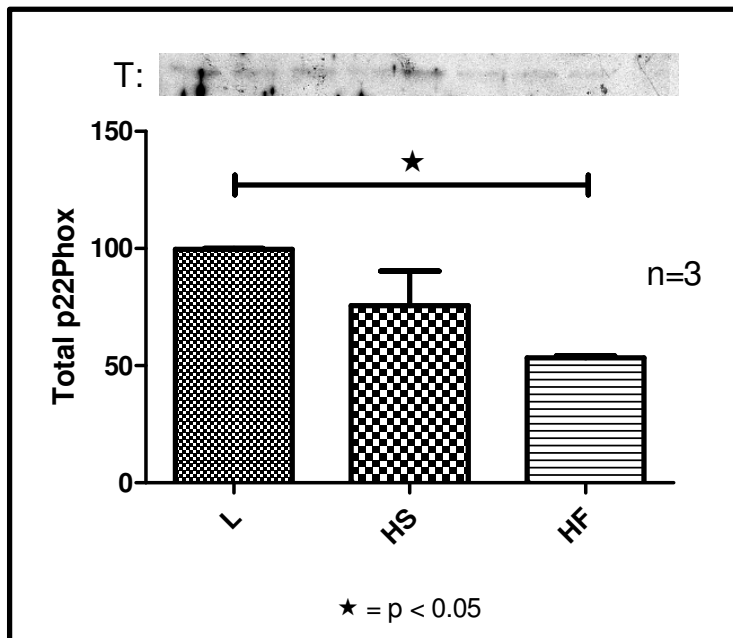
Figure 75: The effects of HS and HF diets on the total p22phox expression.
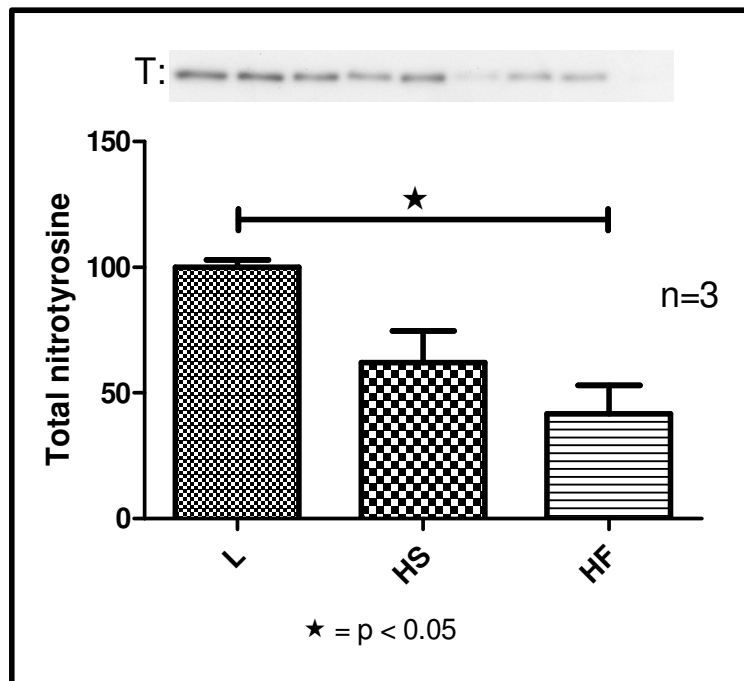
Figure 76: The effects of HS and HF diets on the total nitrotyrosine expression.

3.4.2.4) Isometric tension studies: the role of PVAT

In the **second part** of the obese rat study, we investigated whether the presence or absence of perivascular adipose tissue (PVAT) exerted any effects on aortic ring contraction and relaxation. In this part of the study, we only focussed on aortic rings obtained from lean control rats and rats fed with the HF diet. Furthermore, we modified the PE-induced precontraction protocol from a single 1 µM PE administration to a cumulative PE administration protocol, which allowed us to more carefully evaluate the contractile response of the aortic rings.

3.4.2.4.1) Cumulative PE-induced contraction data: With and Without PVAT

First, we wanted to investigate whether there were any differences in cumulative PE-contraction between lean control and HF groups. Fig. 77 depicts the data obtained from lean control vs HF aortic rings with PVAT, and Fig. 78 shows data from lean control vs HF aortic rings without PVAT. No differences were observed in the % contraction in any of these scenarios. In the next set of experiments, we evaluated the intra-group effects of PVAT on contraction in lean control and HF groups respectively. The data for lean control and HF rings are shown in Figs. 79 and 80 respectively. The presence or absence of PVAT played no role in the contraction profile of the lean control rat aortic rings (Fig. 79); however, in the HF aortic rings, the presence of PVAT exerted an anti-contractile effect at lower cumulative PE concentrations (100 nM and 300 nM) (Fig. 80).
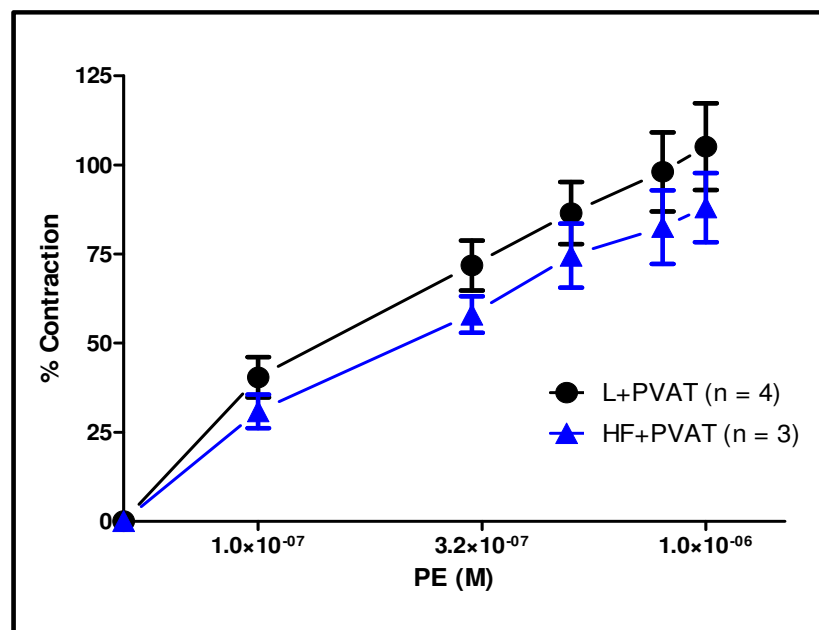
Figure 77: The effects of HF diet (vs. lean control) on PE-induced aortic ring contraction in the presence of PVAT.

92
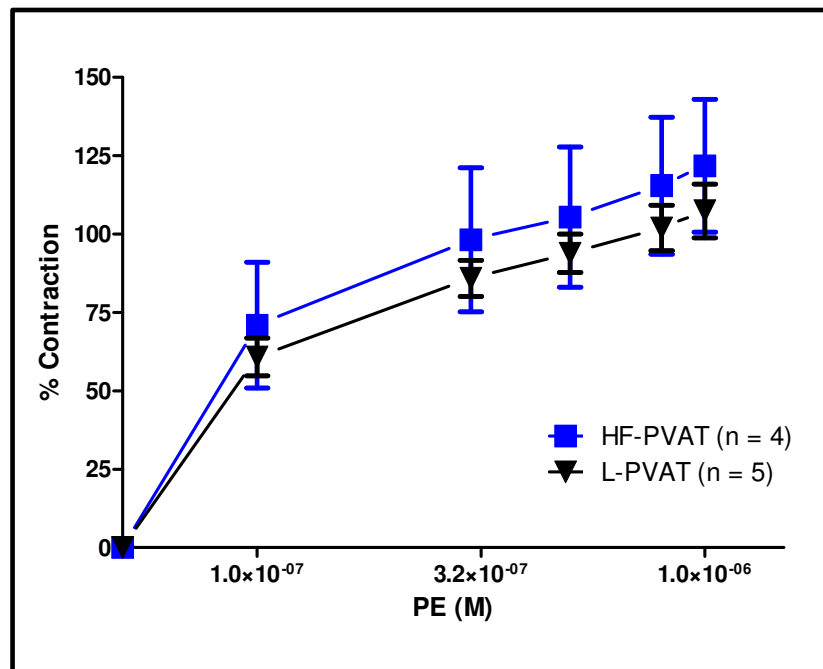
Figure 78: The effects of HF diet (vs. lean control) on PE-induced aortic ring contraction in the absence of PVAT.
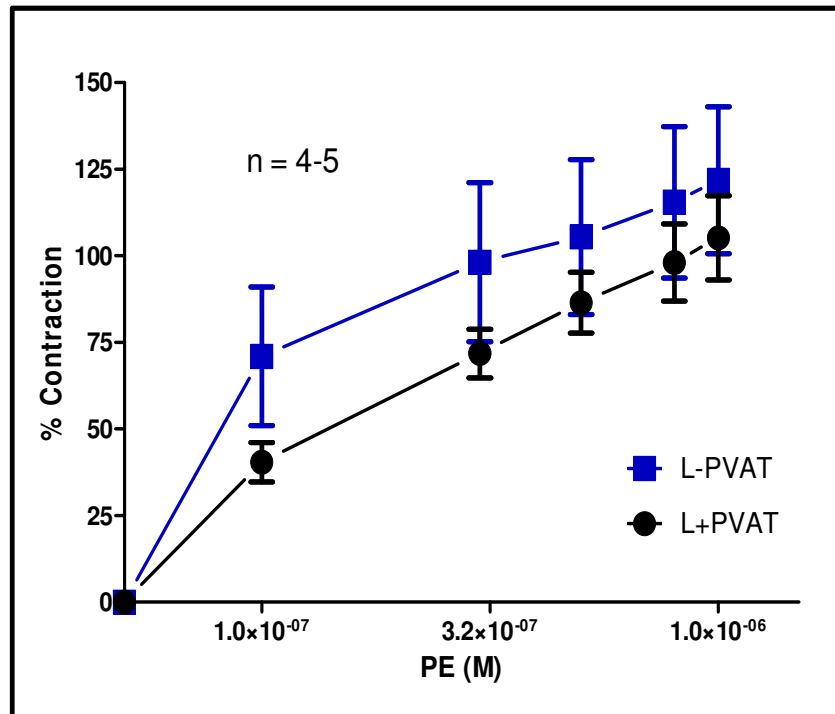
Figure 79: The effects of PVAT on cumulative PE-induced contraction in lean, control rat aortic rings.

93
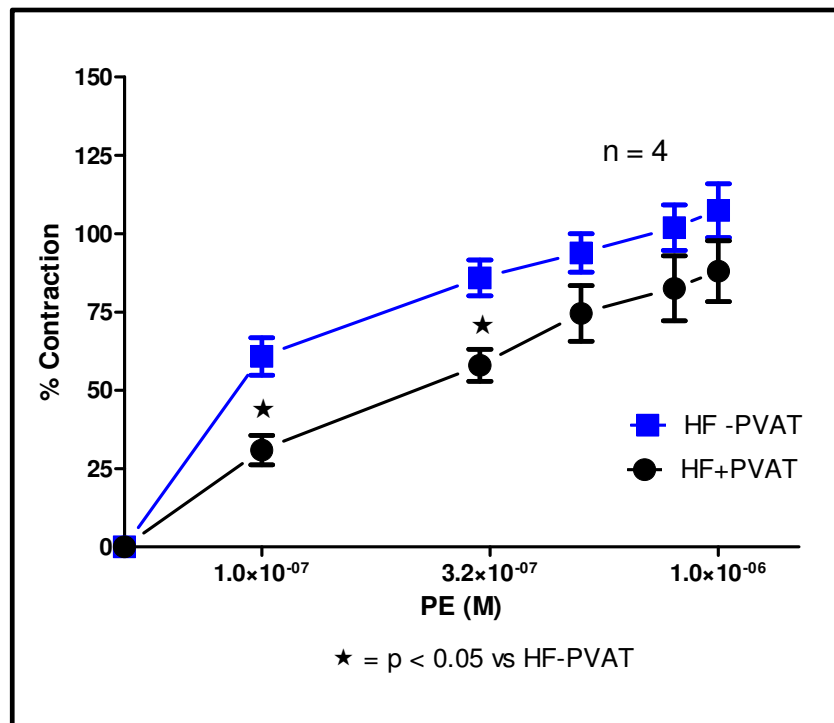
Figure 80: The effects of PVAT on cumulative PE-induced contraction in HF rat aortic rings.

3.4.2.4.2) Cumulative acetylcholine-induced relaxation data: With and Without PVAT

In this series of experiments, we investigated whether there were differences in acetylcholine-induced aortic ring relaxation between lean control and HF groups. Figure 81 depicts the data obtained from lean control vs HF aortic rings without PVAT, and the results show that the % relaxation in aortic rings from HF rats was significantly greater than those from lean rats, particularly at 1 μM and 10 μM ACH. Figure 82 shows data from lean control vs HF aortic rings with PVAT. It is clear from the results that the trends observed in the experiments without PVAT continued when PVAT was present, although the differences lost their significance. Furthermore, we also investigated the intra-group effects of PVAT on relaxation in lean control and HF groups respectively.

The data for lean control and HF rings are shown in Figs. 83 and 84 respectively. The presence of PVAT had an outspoken anti-relaxation effect in the lean control aortic rings, with significantly reduced % relaxation observed at ACH cumulative concentrations of 300 nM, 1 µM and 10 µM (Fig. 83). In the HF groups, PVAT-containing aortic rings showed significantly decreased relaxation at ACH concentration of 10 µM (Fig. 84).
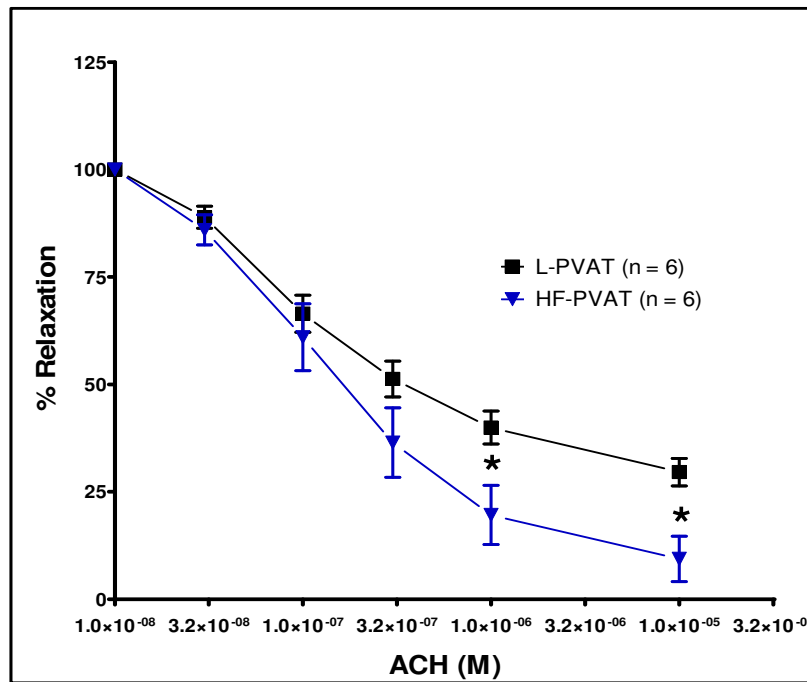
Figure 81: A comparison of ACH-induced relaxation between Lean and HF groups in the absence of PVAT.
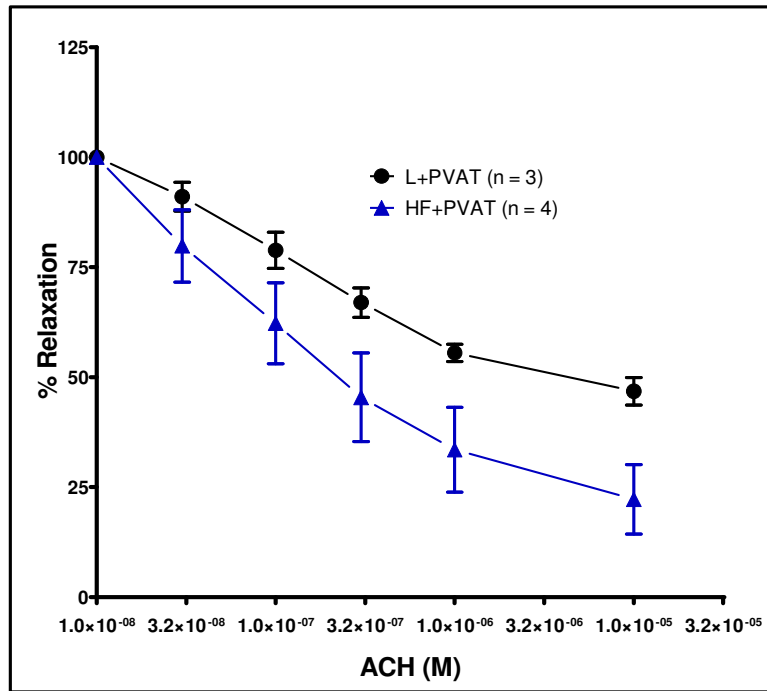
Figure 82: A comparison of ACH induced relaxation between Lean and HF groups in the presence of PVAT.
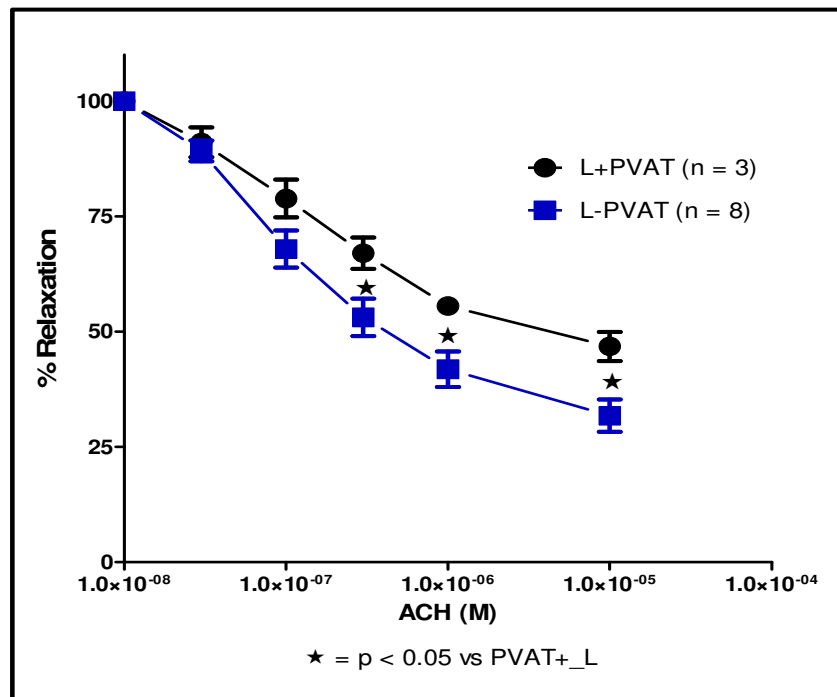
Figure 83: The effects of PVAT on cumulative ACH-induced relaxation in Lean, control rat aortic rings.
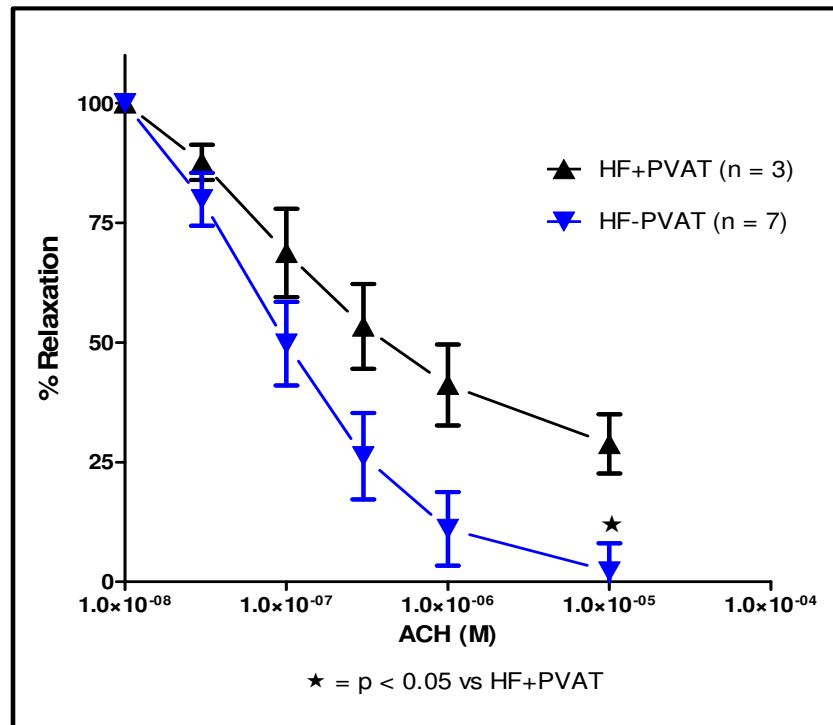
Figure 84: The effects of PVAT on cumulative ACH-induced relaxation in HF rat aortic rings.

3.4.2.4.3) The role of endothelial denudation in aortic rings

In this series of experiments, we investigated whether the removal of the vascular endothelium ("denudation") would affect cumulative contraction and relaxation in aortic rings in the presence or absence of PVAT. First of all, we wanted to confirm that our denudation technique was successful. We compared the cumulative relaxation of all the groups (Lean controls with PVAT, Lean controls without PVAT, HF with PVAT and HF without PVAT), and the data showed that there was no ACH-induced (i.e. endothelium-dependent) relaxation present, thereby confirming that the rings were successfully denuded of their endothelium (Fig 85).

Next, we compared the effects of endothelial denudation on cumulative PE-induced contraction in aortic rings from lean control rats vs HF rats. As shown in figures 86 and 87, there were no differences observed in the cumulative contraction of Lean vs HF aortic rings when the endothelium was removed (regardless of the presence or absence of PVAT). Further investigations showed no differences between the contraction of denuded aortic rings vs aortic rings with intact endothelium from lean rats in the absence of PVAT (Figure 88). However, when PVAT was left intact, the denuded aortic rings showed a significant pro-contractile response (Figure 89). Similar results were observed in aortic rings from HF rats (Figures 90 + 91).
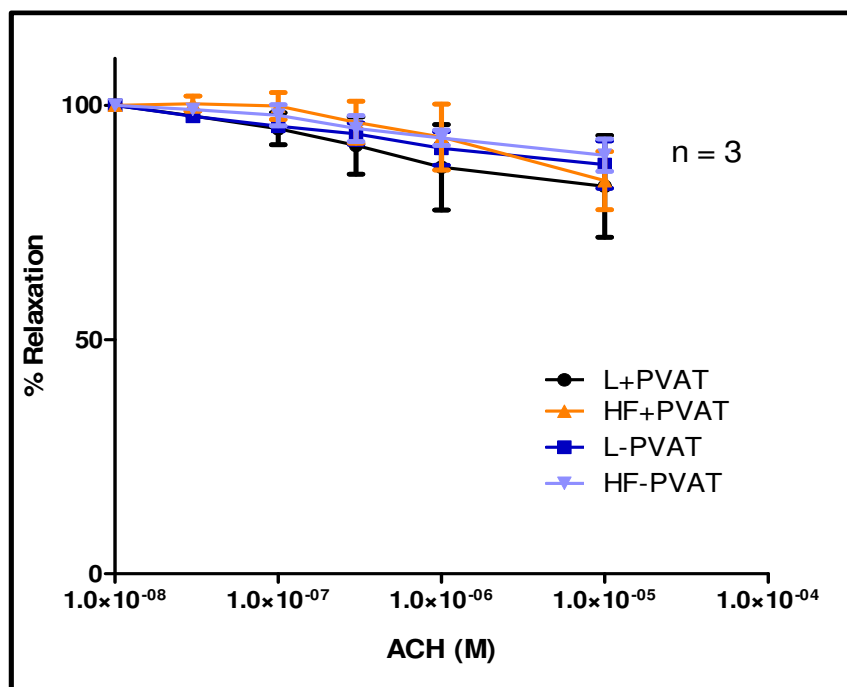
Figure 85: The effect of endothelial denudation on the % relaxation in aortic rings from lean control and HF rats.
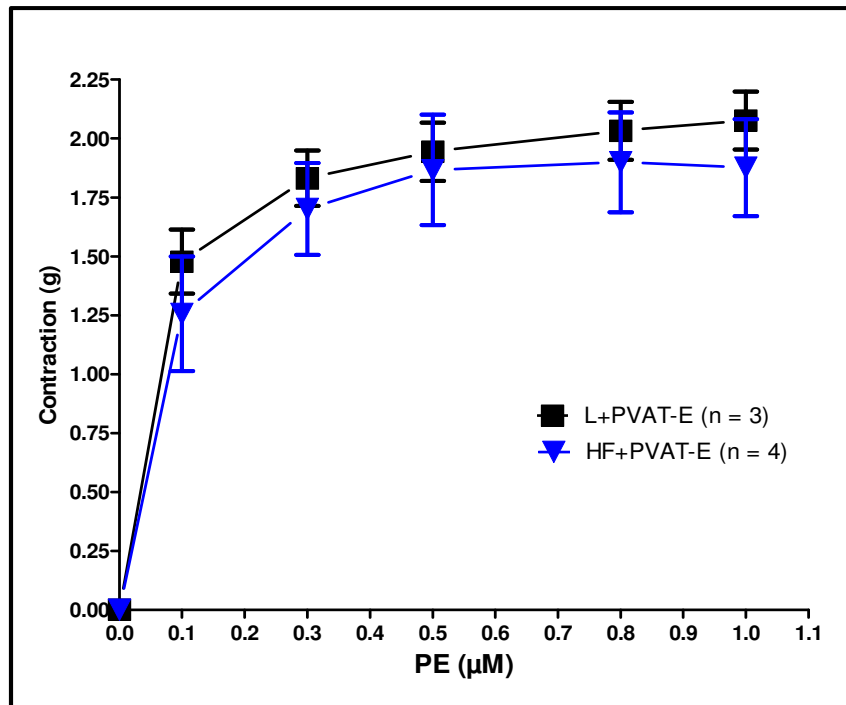
Figure 86: Comparison of denuded aortic rings from Lean and HF groups with PVAT.
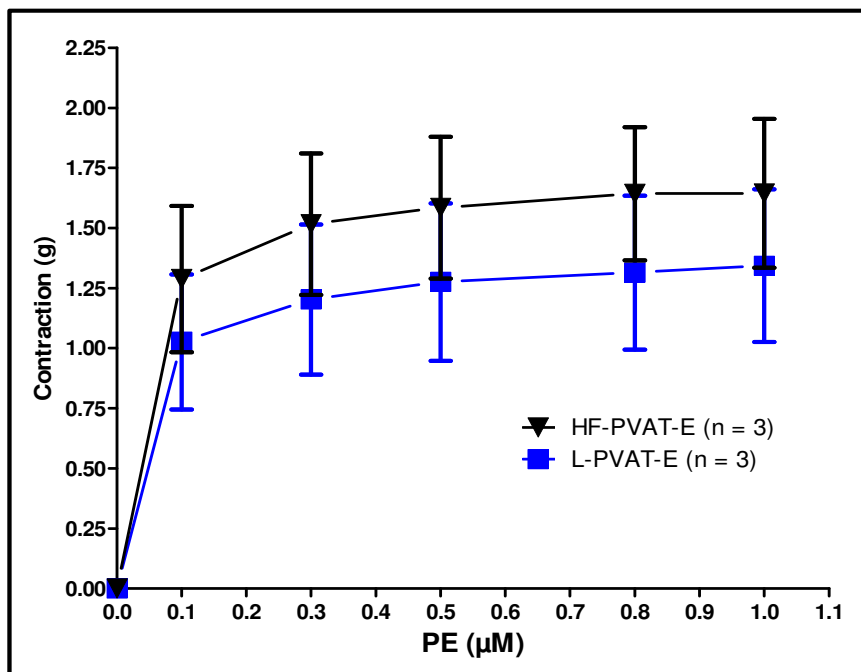
Figure 87: Comparison of denuded rings from Lean and HF groups without PVAT.
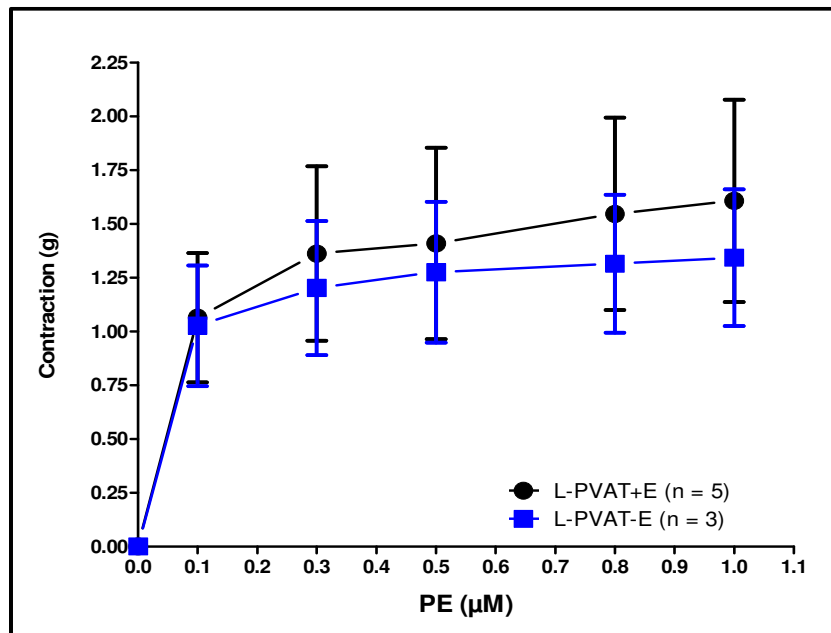
Figure 88: The effect of endothelial denudation on cumulative PE-induced contraction in aortic rings from lean control rats in the absence of PVAT.
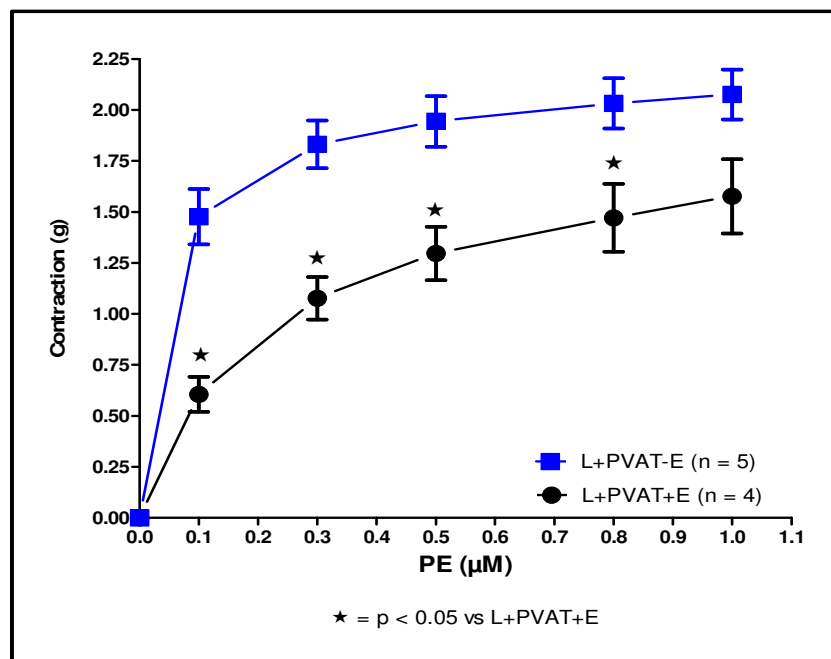
Figure 89: The effect of endothelial denudation on cumulative PE-induced contraction in aortic rings from lean control rats in the presence of PVAT.

100
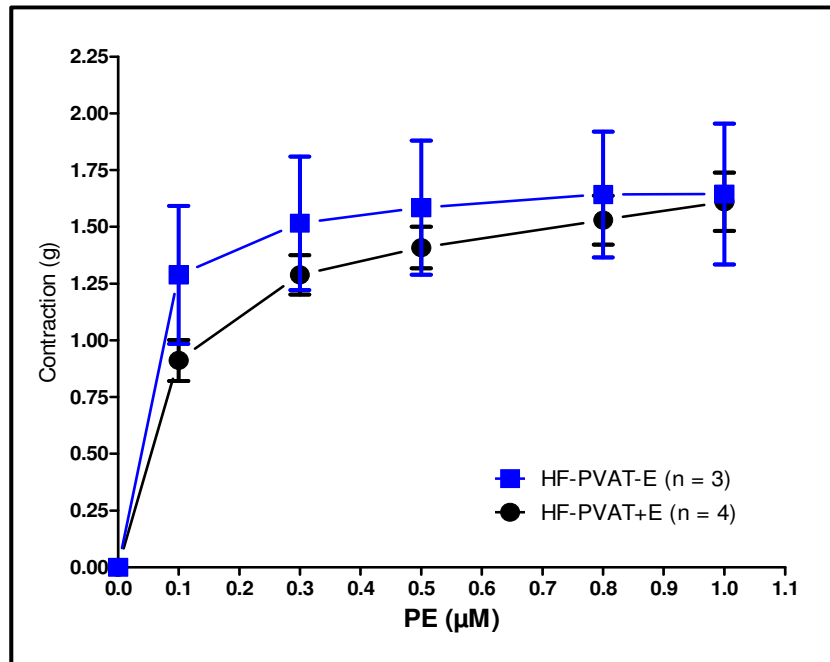
Figure 90: The effect of endothelial denudation on cumulative PE-induced contraction in aortic rings from HF rats in the absence of PVAT.
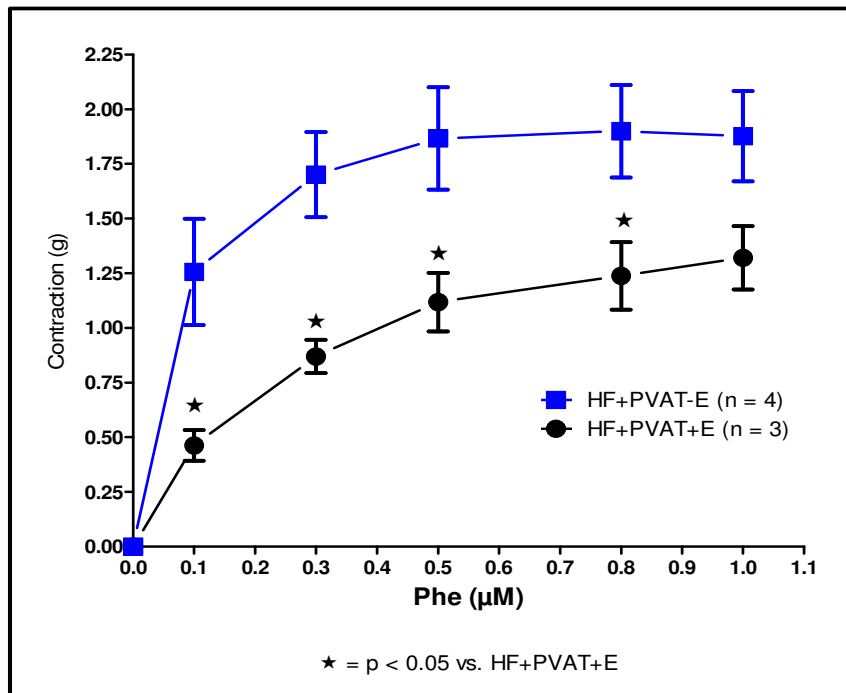
Figure 91: The effect of endothelial denudation on cumulative PE-induced contraction in aortic rings from HF rats in the presence of PVAT.

Chapter 4:

Discussion and Conclusion

4.1) Nitric oxide sensors

4.1.1) ISO-NOP stainless steel sleeve sensor

We were uncertain whether or not the ISO-NOP sensor was still functional at the start of the project seeing as it was already older than a year at that time. Polarization and calibration were initially carried out with success (Figs. 37 and 38), although the sensor had to be kept in the polarization solution overnight and it was thus a time consuming process. The results obtained with the initial acetylcholine and insulin experiments were promising (Fig. 39 and 40), but due to increasing instability of the sensor during experiments and problems with polarization and calibration, we were unable to complete more experiments and the sensor was deemed to be out of order.

The preparation of the stainless steel sleeve sensor is also a drawback as the sleeve had to be filled with an electrolyte solution after which the sensor must be carefully inserted into the sleeve without damaging the sensor or the NO selective membrane at the end of the sleeve. Adding to this, the distance of the sensor tip to the membrane and possible formation of air bubbles in the electrolyte solution can influence the diffusion of NO toward the sensor tip. This in turn can cause unstable or no readings at all during experiments. More difficulties were experienced with the sensor in the form of

temperature changes, movement of the researcher's hand around the sensor and possible interferences with radio frequencies e.g. cell phone signals.

There was thus a large number of variables that could potentially influence the sensitivity of the sensor, even when the sensor was still deemed to be operational, and as a result we decided not to carry on with experiments using the ISO-NOP sensor.

4.1.2) ISO-NOPF carbon fiber tip sensor

In view of the above, we purchased the ISO-NOPF from the same company in order to investigate whether the manufacturer's claims of "higher sensitivity, selectivity and reaction time" could be realised in our hands and possibly produce more easily obtainable and accurate results. Again, we were successful in calibrating and standardising the sensor (Figs. 41 and 42). For the ISO-NOPF investigations, we introduced vehicle controls (depending on the medium in which the drugs were dissolved) for the first time as part of the experimental protocols. The first set of insulin and acetylcholine experiments with the ISO-NOPF sensor yielded no significant effects on NO-release from CMECs (Figs. 43 – 46). However, when the biosynthetic human insulin formulation, Humulin, was introduced as a potential inducer of NO release from CMECs, the findings were more promising, particularly when Humulin was dissolved in distilled H_2O (Fig. 47). The Humulin experiments were repeated in AECs, and similar trends were observed (Fig. 48). Although these results were promising, we remained concerned about the functionality of the sensor and whether it was applied correctly. Furthermore, although satisfied with the findings observed with Humulin administration, we could not find information on the exact composition of the commercial Humulin

solution, and there was thus a possibility that our findings might have been due to an unknown compound reacting with the sensor itself.

In the next set of ISO-NOPF sensor experiments, we were interested in investigating whether different results would be achieved when culturing the cells in smaller wells (24-multiwell plates) as opposed to the rather large 35mm petri dishes. In this way, we believed that a potential limitation of the total diffusion area of NO may increase the amount of NO in the area surrounding the sensor tip. At the same time, however, we were concerned that the administration of the drugs in close proximity to the sensor might cause false positive readings and we therefore also compared drug administration at the surface of the wells with administration at the bottom of the well closer to the sensor. Interestingly, we found that the administration of insulin and acetylcholine at the surface of the well showed significant increases in NO production compared to their respective vehicle controls, although the observed increases were not larger than administration at the bottom of the wells (Fig. 49).

We next conducted experiments with the ISO-NOPF sensor on aortic tissue strips pinned down to the bottom of a petri dish. Neither insulin nor humulin administration showed a significant increase in NO production (Fig. 50) and acetylcholine experiments could not be carried out. At this point, we started experiencing increasing difficulties with polarization and calibration and we became concerned about the lifetime of the sensor, which at this stage was only a few weeks in use. We also experienced problems with the sensitivity of the sensor during experiments, which started generating erratic readings. The sensor reacted to hand movements as well as to ambient room temperature changes. The readings would for example show a spike whenever a hand

was moved near to it when attempting to administer the drugs and this made experiments frustratingly difficult. Polarization difficulties also further complicated experiments as the baseline reading would not stabilize, but instead show a constant inclining baseline reading. This made it difficult to determine whether increases in readings were due to the drug administrations or merely due to an increasing baseline. We therefore decided to discontinue using the ISO-NOPF sensor.

4.1.3) ISO-NOPF L-shaped sensor

After consulting with the manufacturers (World Precision Instruments) about the difficulties we were experiencing with the sensors, they recommended that we purchase the latest addition to their sensors, namely the L-shaped ISO-NOPF sensor as this would supposedly be more suitable for our purposes. The L-shape of the sensor means that a larger area of the sensor tip is in close proximity to the cells and should thus lead to more accurate readings.

After successfully calibrating and standardising the sensor (Figs. 51 and 52), we repeated the surface vs bottom administration of drugs as with the previous sensor (CMECs cultured in 24-multiwell plates). Similar trends were observed (albeit not statistically significant), with higher readings achieved when the drugs were administered at the surface (Fig. 53). We were disappointed, however, when we observed that the sensor readings showed a drift when administering insulin and acetylcholine at the surfaces of wells in which there were no cells. This suggested that the higher readings observed in previous experiments may not have been due to NO-release by cells (Fig. 54).

Results obtained with the initial L-shaped sensor-aortic tissue experiments were promising. Insulin administration (1 µM) generated a drift compared to vehicle control and compared to 100 nM insulin (Fig. 55). When we introduced shear stress as a possible inducer of NO release by the aortic strips, we observed a significant drift when injecting 100 ul and 200 µl EBM-2 on aortic strips with intact endothelium compared to denuded aorta controls (Fig. 56). These results were very promising, and suggested that shear stress may be a viable future option to induce NO production. We were equally pleased to observe increased sensor readings when shear stress (achieved by injecting 200 µl of EBM-2 growth medium on the cells) was applied to AECs in culture compared to cell-free wells (Fig. 57). At this point, and to our great disappointment, we started experiencing similar difficulties with the L-shaped sensor as with the previous sensors. Albeit to a lesser extent, temperature changes and movement around the sensor influenced readings, and baseline readings became unstable.

In summary, the concept of the sensors seems to offer a user-friendly, quick, sensitive and reliable method to measure direct NO production in real-time. However, in our hands, operating the sensors proved to be challenging and frustrating at times. The sensors' sensitivity to external factors (that are difficult to control for) such as changing ambient temperature and hand movements caused considerable problems. In our view, more research and development by the manufacturers are needed to improve the reliability and lifespan of these sensors. Our experience with working with the WPI sensors was further hampered by the fact that there are no representatives of the company in South Africa. Communication with their technicians had to take place via e-mail to Florida in the USA. This was of course time consuming due to time zone

differences and occasionally caused our research to come to a complete standstill. Due to the fact that time was moving on, and that the sensor investigations eventually consumed almost a full year of my MSc studies, my supervisor and I decided that we would discontinue the sensor studies, and move on to the next NO-detection techniques.

4.2) NO_2^-/NO_3^- sensor

The ArrowSTRAIGHT™ NO_2^-/NO_3^- sensor was an appealing option for our laboratory. The direct measurement of NO_2^- and NO_3^- separately and then adding the values to calculate the amount of NO produced is a method that has not previously been utilised in our laboratory. However, to our great disappointment, we progressed no further than the calibration and standardization phase of setting up this technique (Fig. 58). Apart from the time consuming task of preparing fresh buffer and standards for each sensor on a regular basis, we specifically experienced difficulty with the NO_2^- sensor. The sensor had to be manually assembled and disassembled at the start and end of experiments. This entailed insertion of the glass encased sensor into an electrolyte filled plastic sleeve body without puncturing or damaging the NO_2^- selective membrane at the end of the sleeve. The glass body of the sensor is however longer than the plastic sleeve and judging the depth of the glass body in the plastic sleeve is thus very difficult. This greatly increases the chances of the membrane being damaged as the glass body of the membrane can easily pierce the membrane. Furthermore, if the sensor body is not close enough to the membrane, the diffusion distance is too great, resulting in impaired detection of NO_2^-. The above mentioned aspects contributed to the difficulties experienced in calibrating and standardizing of the NO_2^- sensor. The NO_3^- sensor in turn

was a lot more user-friendly as there was no assembly and disassembly required, but difficulties were also experienced during calibration and standardization. The flow chambers that the sensors are placed in during experiments also caused some difficulties. Air pockets would form inside the chambers from time to time and cause difficulty with reading samples. Our efforts were complicated further when attempting to contact the manufacturers in the USA. The response time to our e-mail enquiries was poor, and we often waited days to weeks before our e-mails were answered. In addition, the replies were often not helpful at all, and we were merely referred back to the manual, which we had already done. As a result of the above mentioned difficulties and poor support from the manufacturer, we decided not to perform experiments as any results produced would be useless without any proper calibration and standardization values.

In conclusion the concept of the NO_2^-/NO_3^- sensor is a promising method for NO detection in the laboratory, however practical application of the protocols is made difficult by physical design faults of the sensor, poor technical support and the time consuming nature of the experiments. Changes need to be made in order to simplify the protocol. Lastly, the researcher's involvement in assembly of the sensor, injection of samples and deciding when to take a reading can influence the results and thus ads a matter of subjectivity to the experiment.

4.3) Griess method

Indirect measurement of NO-production by the Griess method is one of the most popular NO-detection assays used by researchers in this field. In this study, we aimed to investigate whether or not the Griess method was a viable option in our laboratory in

addition to our gold standard of flow cytometric measurement of DAF/2-DA fluorescence. It was evident from early on that this technique was considerably more reliable and reproducible than both the amperometric sensors and the ArrowSTRAIGHT™ system. The success was further enhanced by the relative ease of executing the assay, the cost-effectiveness of the reagent and of course the availability of a state-of-the-art platereader in our laboratory. After successfully completing the calibration and standardisation for NO_2^- measurements (Fig. 59), we designed a set of experiments using several compounds as positive controls: (i) The NO-donor, DEA/NO, (ii) the eNOS activator, bradykinin, (iii) the eNOS activator, insulin, (iv) fenofibrate, (v) oleanolic acid (OA), and (vi) the iNOS inducer, IL-ß1. DEA/NO (Fig. 60), fenofibrate (Figs. 61 and 62), OA (Fig. 62) and IL-1ß (Fig. 63) all generated significantly increased NO_2^- production compared to their respective controls; however, neither bradykinin nor insulin (Fig. 60) succeeded in increasing NO_2^- levels released by CMECs. We are not sure why bradykinin and insulin failed to elicit a NO-response in the CMECs; however, it has to be added that similar trends have previously been shown with our existing DAF-2/DA–flow cytometry technique, which may point to a CMEC-specific phenomenon. In summary, we were satisfied that the Griess method constituted a sensitive and fast alternative to methods already employed in our laboratory. In future, a priority for our laboratory will be to focus on incorporating the conversion of nitrates to nitrites in our studies. This would allow us to measure all the metabolites from the NO produced under a given circumstance and thus be able to get a more accurate representation of NO production.

4.4) Measurement of endothelial function in aortic ring segments: The isometric tension protocol

After some initial challenges with the new isometric tension organ bath system from ADInstruments, we were able to establish the protocol in a relatively short period of time. An important aspect that can only be achieved by practice included mastering the skill of careful dissection of the aorta and of course aortic ring preparation without harming the integrity of the vascular wall. We also had to replace the mounting hooks supplied by the manufacturers with smaller, custom-made stainless steel hooks. The hooks supplied with the system showed early signs of rust which could influence the functionality of the organ bath setup. After adjusting our protocol to one published by Privett, Kunert and Lombard (2004), we achieved successful phenylephrine induced contraction and acetylcholine induced relaxation of healthy male Wistar rat aortas (Fig. 64). In a further attempt to characterise the model, we were able to successfully induce endothelial independent relaxation through the addition of the NO-donor, SNAP, thus proving that the smooth muscle layer in the aorta segment was intact, fully functional and therefore not harmed by the aortic ring preparation (Fig. 65). In order to test whether our organ bath setup and protocols were ready for experimental interventions, we investigated whether inhibition of eNOS (pretreatment with 100 µM L-NMMA) would attenuate acetylcholine-induced relaxation. We also pretreated the aortic rings with TNF-α (10 ng / ml). TNF-α had previously been shown in our laboratory to decrease NO-production in cultured endothelial cell preparations. Both interventions were successful in reducing the % relaxation generated by acetylcholine, thereby confirming

that relaxation was not only endothelium-dependent but also NO-dependent (Figs. 66 and 67).

In the final part of my MSc study, we decided to utilise the isometric tension system and investigate the vascular function of aortas isolated from diet-induced obese rats. Our laboratory has developed different models of diet-induced obesity and insulin resistance and many studies have since been performed mainly to determine the effects of obesity on cardiac and metabolic function. In the current MSc study, we aimed to further characterise these models of rat obesity to include the effects on aortic and endothelial function.

In the **first part** of the obesity study, we performed isometric tension studies on aortas obtained from rats subjected to 16 weeks of either a high sucrose (HS) diet or a high fat (HF) diet, compared to rats receiving normal rat chow for 16 weeks (Lean) (See Table 1). The effectiveness of the HS and HF diets were validated by biometric analyses: the total body weight and intraperitoneal fat mass was weighed and results showed that these parameters were higher in both the HS and HF group compared to the lean control group (Fig. 68 and 69). In these initial studies, our isometric tension protocol included a single-dose phenylephrine induced contraction, followed by cumulative acetylcholine relaxation (Fig. 32). Furthermore, the rings did not contain PVAT. The results showed an overall greater % relaxation observed in the HF aortic rings, and the % relaxation was significantly greater at the 1 µM cumulative acetylcholine concentration compared to the lean control group (Fig. 70). We were surprised by these findings, as the expectation, based on previous studies in the literature, was that the HF aortic rings would perform worse due to obesity-induced endothelial dysfunction (Aubin

111

et al., 2008). One explanation could be that the improved relaxation response was an adaptive consequence of the sudden removal of the aortas from a harmful high fat *in vivo* environment to a fat-free organ bath solution. Similar improved functional responses have been observed in isolated perfused hearts from obese rats, which was abolished when the perfusion buffer was changed to a high fatty acid containing buffer (personal communication: Prof Amanda Lochner). Future investigations where the aortic rings are immersed in a high fatty acid containing solution in the organ bath could shed more light on this matter.

In order to further investigate cellular mechanisms underlying the vascular function of the HS and HF animals, we performed western blot analysis of proteins involved with NO production and oxidative stress in aortic tissue. We were not surprised to find that eNOS activation was downregulated in both the obese groups compared to the lean group (Fig. 71). Although the eNOS findings pointed to a state of endothelial dysfunction, they contradicted our aortic ring relaxation results observed particularly in the HF aortic rings as described earlier. Next, we investigated the effects of obesity on two major upstream activators of eNOS, namely PKB/Akt and AMPK. We observed no changes in the activation of PKB/Akt (Fig. 72); however the HS group showed decreased activation of AMPK compared to the lean group (Fig. 73). The decreased activation observed in eNOS and AMPK is similar to findings from Ma *et al*. (2010), who also showed a decrease in eNOS and AMPK activation with a subsequent increase in mTOR activation. The iNOS data were also interesting (Fig. 74). The expression of this high NO-output NO isoform was profoundly downregulated in particularly the HS group, but also in the HF group compared to aortas from lean rats. The combined

downregulation of iNOS and eNOS in the aortas of the obese rats provides overwhelming evidence that the NO-generating systems were significantly disabled by obesity. Unexpectedly, the expression of p22phox (a known marker of NADPH-oxidase activation and superoxide production) was significantly downregulated in the HF groups, thereby suggesting that superoxide-derived oxidative stress was unlikely to be present, if attenuated (Fig. 75). This is in contrast to previous reports in the literature that increased activity of NADPH, and thus increased levels of p22phox are observed in obese individuals (Sonta *et al.*, 2004).The combined effects of reduced superoxide production and reduced NO-production via eNOS and iNOS could explain the decreased expression of nitrotyrosine in the HF aortas, a known marker of nitrosative stress (Fig. 76). Again, our nitrotyrosine findings are in contrast to previous studies that found increased nitrotyrosine levels in the vascular tissue of obese animals (Kagota *et al.*, 2005). The western blot data in this study are indeed interesting, ranging from the expected (e.g. decreased eNOS activation, decreased AMPK activation, and decreased iNOS expression) to the unexpected (e.g. decreased p22phox and nitrotyrosine expression). In view of the fact that our aortic tissue samples excluded PVAT, which is now accepted to be a major role-player in overall vascular function, our future studies should aim to include PVAT in the samples prepared for analyses.

In view of the above findings, we decided to include a second set of experiments in the obese studies where PVAT was included. In this series, we only used aortas from HF rats, and we also modified the phenylephrine-induced contraction protocol from a single dose administration to a cumulative model (Fig. 36). There were no differences in the % cumulative contraction between lean and HF aortic rings, regardless of whether PVAT

was present of absent (Figs. 77 and 78). However, when we investigated the contractile effects of PVAT in aortic rings from HF rats, we observed a significant **anti-contractile** effect exerted by PVAT, which was abolished when PVAT was removed (Fig. 80). Our observations are supported by similar findings by Lohn *et al* (2002). According to the authors, the explanation for the anti-contractile effects of PVAT possibly lies in the secretion of a PVAT derived relaxation factor that was shown to exert its function via ATP-dependent K^+-channels, as inhibition of these channels abolished the anti-contractile effects.

We next investigated the effect of PVAT on % relaxation. HF aortic rings showed an increased % relaxation compared to lean aortic rings in the absence of PVAT (Fig. 81), which supports our earlier findings in the first part of the obese rat studies (Fig. 70). Similar results were observed in the presence of PVAT although no significance was found between the groups (Fig. 82). The HF rings thus showed an increased relaxation regardless of the presence of PVAT. When performing intra-group comparisons on the effect of PVAT on relaxation, we observed increased % relaxation in the absence of PVAT in both the lean (Fig. 83) and the HF group (Fig. 84).

Therefore, it appeared as if the presence of PVAT in the rings exerted an **anti-relaxation** effect, which seems to be a counterintuitive finding given that PVAT also exerted anti-contractile effects in the rings. In order to explain the anti-relaxation effects, one has to consider the secretion profile of PVAT. H_2O_2 could be one possible role-player as many opposing vasoactive effects have been reported for it depending on experimental conditions as well as vascular beds. Santiago *et al*. (2013) recently showed the pro-contractile effects of H_2O_2 in rat coronary arteries through an

endothelium dependent mechanism, possibly by inducing smooth muscle Ca^{2+} entry through L-type and non-L-type channels as well as a number of intracellular mechanisms including production of NADPH-oxidase derived superoxide. Before further investigation on our part however, we can only speculate on the results that we observed.

In the final series of experiments, we investigated whether denudation of the aortic rings would affect the contractile effects in the presence or absence of PVAT, in other words we aimed to establish whether there was cross-talk between PVAT and the endothelium. In the denuded ring segments where PVAT was present, we observed a pro-contractile effect in both the lean and the HF diet groups (Figs. 89 and 91). From these data, it appeared as if the presence of the endothelium was necessary to attenuate the pro-contractile effects exerted by PVAT, regardless of whether the aortic rings were obtained from lean or HF animals. It is possible that the PVAT secretes a factor that induces the release of an endothelium-dependent anti-contractile molecule, which is absent in the denuded aortic rings.

The field of study on the effects of PVAT on vascular function is still in its early stages and a lot of work still needs to be done in order to gain greater clarity on the subject. The secretion profile of PVAT is large and assigning specific factors to effects observed *ex vivo* is difficult and still requires more investigation. The differences observed in the effects of PVAT on vascular function between different species, different diets and different vascular beds, further complicates the subject.

Our study however succeeded in setting up and standardizing a vascular isometric tension protocol. This will enable us to carry out investigations using different vaso-relaxing and –contracting agents and possibly test the effects of different vascular beds. This protocol could thus serve as an important tool to be used in conjunction with other established methods e.g. Proteomics, western blot analysis and the Griess method in order to gain greater clarity on endothelial NO production and the functional effects thereof.

4.5 Conclusion

Direct and real-time measurements of NO production from cultured cells and vascular tissue are crucially important in the field of vascular and endothelial research, as this molecule is regarded by many as the most prominent and potent endothelium-derived vasodilator. In our laboratory, we have developed and characterised a fluorescence-based assay that utilises the detection of DAF-2/DA fluorescence by the flow cytometer. In the current study, we aimed to investigate alternative methods of NO measurement including amperometric-based techniques, NO_2^-/NO_3^- measurements and the Griess method. In our hands, the problems experienced with the amperometric NO sensors, as well as with the NO_2^-/NO_3^- system meant that these methods were not deemed feasible for our purposes at the time as we were unable to set up protocols that produced reproducible and reliable results. We thus concluded that the sensors are not yet an affordable, user friendly or time saving method for NO-sensing in our laboratory.

However, the Griess method used together with the plate reader delivered promising results. We were able to successfully measure NO_2^- from cells in culture when treated with different drugs. Furthermore, we were able to produce results that showed the

116

effect of inhibitors on NO production. The data obtained from the Griess investigations also compared favourably to those from the DAF-2/DA–flow cytometry technique. Future work on the Griess method might include converting NO_3^- metabolites to NO_2^- in order to produce a more accurate representation of NO production.

Our isometric tension protocol allowed us to measure the functional effects of vascular endothelium in aortic ring segments. We experienced initial difficulties with the protocol but after making physical and protocol changes to our setup, we were able to successfully employ the protocol in a diet induced obesity study using Wistar rats. In future work we might consider using blood vessel sections from different vascular beds and also adjusting the buffer used to include fatty acids in order to produce results that are more similar to the *in vivo* environment of the vasculature.

In conclusion, with this MSc study, I managed to set up, standardize and characterise two new techniques not previously used in our laboratory that can add value to our studies and aid us in future vascular and endothelial research.

References

Archer, S. 1993, "Measurement of Nitric Oxide in Biological Models ", *FASEB Journal,* vol. 7, pp. 349.

Aubin, M., Lajoie, C., Clément, R., Gosselin, H., Calderone, A. & Perrault, L.P. 2008, "Female Rats Fed a High-Fat Diet Were Associated with Vascular Dysfunction and Cardiac Fibrosis in the Absence of Overt Obesity and Hyperlipidemia: Therapeutic Potential of Resveratrol", *The Journal of Pharmacology and Experimental Therapeutics,* vol. 352, pp. 961.

Avogaro, A. & de Kreutzenberg, S.V. 2005, "Mechanisms of endothelial dysfunction in obesity", *Clinica Chimica Acta,* vol. 360, pp. 9.

Barter, P., Gotto, A.M., LaRosa, J.C., Maroni, J., Szarek, M., Grundy, S.M., Kastelein, J.J.P., Bittner, V. & Fruchart, J.C. 2007, "HDL Cholesterol, Very Low Levels of LDL Cholesterol, and Cardiovascular Events", *The New England Journal of Medicine,* vol. 357, pp. 1301.

Bedioui, F. & Villeneuve, N. 2003, "Electrochemical Nitric Oxide Sensors for Biological Samples - Principle, Selected Examples and Applications", *Electroanalysis,* vol. 15, pp. 5.

Bigornia, S.J., Mott, M.M., Hess, D.T., Apovian, C.M., McDonnell, M.E., Duess, M., Kluge, M.A., Fiscale, A.J., Vita, J.A. & Gokce, N. 2010, "Long-term Successful

Weight Loss Improves Vascular Endothelial Function in Severely Obese Individuals", *Obesity,* vol. 18, pp. 754.

Bigornia, S.J., Mott, M.M., Hess, D.Y., Apovian, C.M., McDonnell, M.E., Duess, M., Kluge, M.A., Fiscale, A.J., Vita, J.A. & Gokce, N. 2010, "Long-term Successful Weight Loss Improves Vascular Endothelial Function in Severely Obese Individuals", *Nature,* vol. 18, pp. 754.

Boo, Y.C., Tressel, S.L. & Jo, H. 2007, "An improved method to measure nitrate/nitrite with an NO-selective electrochemical sensor", *Nitric Oxide,* vol. 16, pp. 306.

Brandes, R.P. 2007, "The fatter the better? Perivascular adipose tissue attenuates vascular contraction through different mechanisms", *British Journal of Pharmacology,* vol. 151, pp. 303.

Bruyndonckx, L., Hoymans, V.Y., Van Craenenbroeck, A.H., Vissers, D.K., Vrints, C.J., Ramet, J. & Conraads, V.M. 2013, "Assessment of Endothelial Dysfunction in Childhood Obesity and Clinical Use", *Oxidative Medicine and Cellular Longevity,* .

Bult, H., Boeckxstaens, G.E., Pelckmans, P.A., Jordaens, F.H., Van Maercke, Y.M. & Herman, A.G. 1990, "Nitric Oxide as an Inhibitory Non-Adrenergic Non-Cholinergic Neurotransmitter", *Nature,* vol. 345, pp. 346.

Campos, P., Saguy, A., Ernsberger, P., Oliver, E. & Gaesser, G. 2006, "The epidemiology of overweight and obesity: public health crisis or moral panic?", *International Journal of Epidemiology,* vol. 35, pp. 55.

Cockell, C.S. & Rothschild, L.J. 1999, "The Effects of UV Radiation A and 6 on Diurnal Variation in Photosynthesis in Three Taxonomically and Ecologically Diverse Microbial Mats", *Photochemistry and Photobiology,* vol. 69, pp. 203.

Cordaillat, M., Fort, A., Virsolvy, A., Elghozi, J., Richard, S. & Jover, B. 2007, "Nitric oxide pathway counteracts enhanced contraction to membrane depolarization in aortic rings of rats on high-sodium diet", *Am J Physiol Regul Integr Comp Physiol,* vol. 292, pp. 1557.

Cosby, K., Partovi, K.S., Crawford, J.H., Patel, R.P., Reiter, C.D., Martyr, S., Yang, B.K., Waclawiw, M.A., Zalos, G., Xu, X., Huang, K.T., Shields, H., Kim-Shapiro, D.B., Schechter, A.N., Cannon, R.O. & Gladwin, M.T. 2003, "Nitrite Reduction to Nitric Oxide by Deoxyhemoglobin Vasodilates the Human Circulation", *Nature Medicine,* vol. 9, pp. 1498.

Crabtree, M.J., Tatham, A.L., Al-Wakeel, Y., Warrick, N., Hale, A.B., Cai, S., Channon, K.M. & Alp, N.J. 2008, "Quantitative Regulation of Intracellular Endothelial Nitric-oxide Synthase (eNOS) Coupling by Both Tetrahydrobiopterin-eNOS Stoichiometry and Biopterin Redox Status: Insights from Cells with TET-Regulated GTP Cyclohydrolase I Expression", *Journal of Biological Chemistry,* vol. 284, pp. 1136.

Deanfield, J.E., Halcox, J.P. & Rabelink, T.J. 2007, "Endothelial Function and Dysfunction : Testing and Clinical Relevance", *Circulation,* vol. 115, pp. 1285.

Dhanakoti, S.N., Gao, Y., Nguyen, M.Q. & Raj, J.U. 2000, "Involvement of cGMP-dependent protein kinase in the relaxation of ovine pulmonary arteries to cGMP and cAMP", *J Appl Physiol,* vol. 88, pp. 1637.

Falaschetti, E., Hingorani, A.D., Jones, A., Charakida, M., Finer, N., Whincup, P., Lawlor, D.A., Smith, G.D., Sattar, N. & Deanfield, J.E. 2010, "Adiposity and cardiovascular risk factors in a large contemporary population of pre-pubertal children", *European Heart Journal,* vol. 31, pp. 3063.

Förstermann, U. & Münzel, T. 2006, "Endothelial Nitric Oxide Synthase in Vascular Disease : From Marvel to Menace", vol. 113, pp. 1708.

Furchgott, R.F. & Zawadzki, J.V. 1980, "The Obligatory Role of Endothelial Cells in the Relaxation of Arterial Smooth Muscle by Acetylcholine", *Nature,* vol. 288, pp. 373.

Gao1, Y.J., Lu, C., Su, L.Y., Sharma, A.M. & Lee, R.M.K.W. 2007, "Modulation of Vascular Function by Perivascular Adipose Tissue: The Role of Endothelium and Hydrogen Peroxide", *British Journal of Pharmacology,* vol. 151, pp. 323.

Giustarini, D., Rossi, R., Milzani, A. & Dalle-Donne, I. 2008, "Nitrite and Nitrate Measurement by Griess Reagent in Human Plasma: Evaluation of Interferences and Standardization", *Methods in Enzymology,* vol. 440, pp. 362.

Greenstein, A.S., Khavandi, K., Withers, S.B., Sonoyama, K., Clancy, O., Jeziorska, M., Laing, I., Yates, A.P., Pemberton, P.W., Malik, R.A. & Heagerty, A.M. 2009, "Local

Inflammation and Hypoxia Abolish the Protective Anticontractile Properties of Perivascular Fat in Obese Patients", *Circulation,* vol. 119, pp. 1661.

Griess, J.P. 1879, "No Title Available", *Ber.,* vol. 12, pp. 426.

Grundy, S.M., Cleeman, J.I., Daniels, S.R., Donato, K.A., Eckel, R.H., Franklin, B.A., Gordon, D.J., Krauss, R.M., Savage, P.J., Smith, S.C., Spertus, J.A. & Costa, F. 2005, "Diagnosis and Management of the Metabolic Syndrome An American Heart Association/National Heart, Lung, and Blood Institute Scientific Statement", *Circulation,* vol. 112, pp. 2735.

Ignarro, L.J., Buga, G.M., Wood, K.S., Byrns, R.E. & Chaudhuri, G. 1987, "Endothelium-derived relaxing factor produced and released from artery and vein is nitric oxide", *Proceedings of the National Academy of Sciences,* vol. 84, pp. 9265.

Jackson, W.F., König, A., Dambacher, T. & Busse, R. 1993, "Prostacyclin-induced vasodilation in rabbit heart is mediated by ATP-sensitive potassium channels", *The American Journal of Physiology,* vol. 264, pp. 238.

Kagota, S., Yamaguchi, Y., Tanaka, N., Kubota, Y., Kobayashi, K., Nejime, N., Nakamura, K., Kunitomo, M. & Shinozuka, K. 2006, "Disturbances in nitric oxide/cyclic guanosine monophosphate system in SHR/NDmcr-cp rats, a model of metabolic syndrome", *Life Sciences,* vol. 78, pp. 1187.

Kanai, A.J., Pearce, L.L., Clemens, P.R., Birder, L.A., VanBibber, M.M., Choi, S., de Groat, W.C. & Peterson, J. 2001, "Identification of a Neuronal Nitric Oxide Synthase

in Isolated Cardiac Mitochondria Using Electrochemical Detection", *Proceedings of the National Academy of Sciences of the United States of America,* vol. 98, pp. 14126.

Kim, J., Montagnani, M., Koh, K.K. & Quon, M.J. 2006, "Reciprocal Relationships Between Insulin Resistance and Endothelial Dysfunction: Molecular and Pathophysiological Mechanisms", *Circulation,* vol. 113, pp. 1888.

Kojima, H., Nakatsubo, N., Kikuchi, K., Kawahara, S., Kirino, Y., Nagoshi, H., Hirata, Y. & Nagano, T. 1998, "Detection and Imaging of Nitric Oxide with Novel Fluorescent Indicators: Diaminofluoresceins", *Analytical Chemistry,* vol. 70, pp. 2446.

Komori, K. & Vanhoutte, P.M. 1990, "Endothelium-derived hyperpolarizing factor", *Blood Vessels,* vol. 27, pp. 238.

Lars, H.L., Lars, R.D., Kjár, T., Stenstrém, T., Lynggaard-Jensen, A. & Revsbech, N.P. 2000, "Fast Responding Biosensor for On-Line Determination of Nitrate/Nitrite in Activated Sludge", *Water Research,* vol. 34, pp. 2463.

Leone, A.M., Furst, V.W., Foxwell, N.A., Cellek, S. & Moncada, S. 1996, "Visualisation of Nitric Oxide Generated by Activated Murine Macrophages", *Biochemical and Biophysical Research Communications,* vol. 221, pp. 37.

Lewis, C.E., McTigue, K.M., Burke, L.E., Poirier, P., Eckel, R.H., Howard, B.V., Allison, D.B., Kumanyika, S. & Pi-Sunyer, F.X. 2009, "Mortality, Health Outcomes, and

Body Mass Index in the Overweight Range: A Science Advisory From the American Heart Association", *Circulation,* vol. 119, pp. 3263.

López-Figueroa, M.O., Caaman, C., Morano, M.I., Rønn, L.C., Akil, H. & Watson, S.J. 2000, "Direct Evidence of Nitric Oxide Presence within Mitochondria", *Biochemical and Biophysical Research Communications,* vol. 272, pp. 129.

Lohn, M., Dubrovska, G., Lauterbach, B., Luft, F.C., Gollasch, M. & Sharma, A.M. 2002, "Periadventitial fat releases a vascular relaxing factor", *The FASEB Journal,* vol. 16, pp. 1057.

Ma, L., Ma, S., He, H., Yang, D., Chen, X., Luo, Z., Liu, D. & Zhu, Z. 2010, "Perivascular fat-mediated vascular dysfunction and remodeling through the AMPK/mTOR pathway in high-fat diet-induced obese rats", *Hypertension Research,* vol. 33, pp. 446.

Masaki, E. & Kondo, I. 1999, "Methylene Blue, a Soluble Guanylyl Cyclase Inhibitor, Reduces the Sevoflurane Minimum Alveolar Anesthetic Concentration and Decreases the Brain Cyclic Guanosine Monophosphate Content in Rats", *Anesthesia and Analgesia,* vol. 89, pp. 484.

Mineo, C., Deguchi, H., Griffin, J.H. & Shaul, P.W. 2006, "Endothelial and Antithrombotic Actions of HDL", *Circulation research,* vol. 98, pp. 1352.

Miranda, K.M., Espey, M.G. & Wink, D.A. 2001, "A Rapid, Simple Spectrophotometric Method for Simultaneous Detection of Nitrate and Nitrite", *Nitric Oxide: Biology and Chemistry,* vol. 5, pp. 62.

Münzel, T., Daiber, A., Ullrich, V. & Mülsch, A. 2005, "Vascular Consequences of Endothelial Nitric Oxide Synthase Uncoupling for the Activity and Expression of the Soluble Guanylyl Cyclase and the cGMP-Dependent Protein Kinase", *Arterioscler Thromb Vasc Biol,* vol. 25, pp. 1551.

Owu, D.U., Orie, N.N., Nwokocha, C.R., Clapp, L.H. & Osim, E.E. 2013, "Comparative Effect of Type 1 and Type 2 Diabetes Mellitus on Vascular Responses of Rat Thoracic Aorta to Potassium Ion Channel Openers", *British Journal of Medicine & Medical Research,* vol. 3, pp. 748.

Pan, S. 2009, "Molecular Mechanisms Responsible for the Atheroprotective Effects of Laminar Shear Stress", *Antioxidants & Redox Signalling,* vol. 11, pp. 1669.

Peterson, D.A., Peterson, D.C., Archer, S. & Weir, E.K. 1992, "The Non Specificity of Specific Nitric Oxide Synthase Inhibitors", *Biochemical and Biophysical Research Communications,* vol. 187, pp. 797.

Porterfield, D.M., Laskin, J.D., Jung, S., Malchow, R.P., Billack, B., Smith, P.J.S. & Heck, D.E. 2001, "Proteins and Lipids Define the Diffusional Field of Nitric Oxide", *American Journal of Physiology: Lung Cellular and Molecular Physiology,* vol. 281, pp. 904.

Privett, K., Kunert, M.P. & Lombard, J.H. 2004, *Vascular Phenotypes: High throughput characterization of vascular reactivity in rats conditioned on 0.4% and 4.0 % NaCl diet.* Medical College of Wisconsin (User manual for vascular tension studies)

Radomski, M.W., Palmer, R.M.J. & Moncada, S. 1987, "Endogenous Nitric Oxide Inhibits Human Platelet Adhesion to Vascular Endothelium", *The Lancet,* pp. 1057-1058.

Resnick, N., Yahav, H., Shay-Salit, A., Shushy, M., Schubert, S., Zilberman, L.C.M. & Wofovitz, E. 2003, "Fluid shear stress and the vascular endothelium: for better and for worse", *Progress in Biophysics & Molecular Biology,* vol. 81, pp. 177.

Rhoades, R.A. 2003, *Human Physiology 4th Edition.* Brooks/Cole Publishing Company.

Russell, R. 2006*, The Nitric Oxide Molecule.* Available: http://www.windows2universe.org.

Santiago, E., Contreras, C., Sacrista´, A., Sánchez, A., Rivera, L., Climent, B. & Prieto, D. 2013, "Signaling pathways involved in the H_2O_2-induced vasoconstriction of rat coronary arteries", *Free Radical Biology and Medicine,* vol. 60, pp. 136.

Schmidt, H.H.H.W., Hofmann, H., Schindler, U., Shutenko, Z.S., Cunningham, D.D. & Feelisch, M. 1996, "No NO From NO Synthase", *Proceedings of the National Academy of Sciences of the United States of America,* vol. 93, pp. 14492.

Schulz, K., Kerber, S. & Kelm, M. 1999, "Reevaluation of the Griess Method for Determining NO/NO$_2^-$ in Aqueous and Protein-Containing Samples", *Nitric Oxide: Biology and Chemistry,* vol. 3, pp. 225.

Severinghaus, J.W. 2002, "The Invention and Development of Blood Gas Analysis Apparatus", *Anesthesiology,* vol. 97, pp. 253.

Sonta, T., Inoguchi, T., Tsubouchi, H., Sekiguchi, N., Kobayashi, K., Matsumoto, S., Utsumi, H. & Nawata, H. 2004, "Evidence for Contribution of Vascular NAD(P)H Oxidase to Increased Oxidative Stress in Animal Models of Diabetes and Obesity", *Free Radical Biology & Medicine,* vol. 37, pp. 115.

Spark, J.I., Delaney, C.L., Allan, R.B., Ho, M.H.L. & Miller, M.D. 2013, "Can fish oil supplementation improve endothelial function in asymptomatic offspring of patients with peripheral arterial disease?", *Open Access Journal of Clinical Trials,* vol. 5, pp. 83.

Steinberg, D. & Witztum, J.L. 2002, "Is the Oxidative Modification Hypothesis Relevant to Human Atherosclerosis?", *Circulation,* vol. 105, pp. 2107.

Streefkerk, J.O., de Groot, A.A., Pfaffendorf, M. & van Zwieten, P.A. 2002, "Influence of the nature of pre-contraction on the responses to commonly employed vasodilator agents in rat-isolated aortic rings", *Fundamental & Clinical Pharmacology,* vol. 16, pp. 485.

Strijdom, H., Jacobs, S., Hattingh, S., Page, C. & Lochner, A. 2006, "Nitric Oxide production is higher in rat cardiac microvascular endothelial cells than ventricular cardiomyocytes in baseline and hypoxic conditions: A comparative study. ", *FASEB Journal,* vol. 20, pp. 314.

Strijdom, H., Muller, C. & Lochner, A. 2004, "Direct intracellular nitric oxide detection in isolated adult cardiomyocytes: flow cytometric analysis using the fluorescent probe, diaminofluorescein", *Journal of Molecular and Cellular Cardiology,* vol. 37, pp. 897.

Szasz, T., Bomfim, G.F. & Webb, R.C. 2013, "The influence of perivascular adipose tissue on vascular homeostasis", *Vascular Health and Risk Management,* vol. 9, pp. 105.

Szasz, T. & Webb, R.C. 2012, "Perivascular adipose tissue: more than just structural support", *Clinical Science,* vol. 122, pp. 1.

Tang, Y., Jiang, H. & Bryan, N.S. 2011, "Nitrite and Nitrate: Cardiovascular Risk–Benefit and Metabolic Effect", *Current Opinion in Lipidology,* vol. 22, pp. 11.

Tarpey, M.M., Wink, D.A. & Grisham, M.B. 2004, "Methods for detection of reactive metabolites of oxygen and nitrogen: in vitro and in vivo considerations", *American Journal of Physiology - Regulatory, Integrative and Comparative Physiology,* vol. 286, pp. 431.

Vallance, P. & Chan, N. 2001, "Endothelial function and nitric oxide: clinical relevance", *Heart,* vol. 85, pp. 342.

Visser, M., Bouter, L.M., McQuillan, G.M., Wener, M.H. & Harris, T.B. 1999, "Elevated C-Reactive Protein Levels in Overweight and Obese Adults.", *Journal of the American Medical Association,* vol. 282, pp. 2131.

Xian, Y., Zhang, W., Xue, J., Ying, X., Jin, L. & Jin, J. 2000, "Measurement of nitric oxide released in the rat heart with an amperometric microsensor", *Analyst,* vol. 125, pp. 1435.

Yudkin, J.S. 2003, "Adipose tissue, insulin action and vascular disease: inflammatory signals", *International Journal of Obesity,* vol. 27, pp. 25.

Yudkin, J.S., Kumari, M., Humphries, S.E. & Mohamed-Ali, V. 2000, "Inflammation, obesity, stress and coronary heart disease: is interleukin-6 the link?", *Atherosclerosis,* vol. 148, pp. 209.

Zhang, X. 2004, "Real Time and In Vivo Monitoring of Nitric Oxide by Electrochemical Sensors - From Dream to Reality", *Frontiers in Bioscience,* vol. 9, pp. 3434.

Zhao, W., Zhang, J., Lu, Y. & Wang, R. 2001, "The vasorelaxant effect of H_2S as a novel endogenous gaseous KATP channel opener", *The EMBO Journal,* vol. 20, pp. 6008.